UNIVERSITÀ DI PARMA

UNIVERSITÀ DEGLI STUDI DI PARMA

PhD COURSE IN

"Drugs, Biomolecules and Health Products"

XXXI CYCLE

INHALABLE DRY POWDERS FOR PULMONARY VACCINATION

Coordinator:

Chiar.mo Prof. Marco Mor

Tutor:

Chiar.mo Prof. Ruggero Bettini

PhD Candidate: Irene Rossi

Years 2015/2018

Index

Abbreviations

DPI = Dry Powder Inhalers

EM = Emitted Mass

EF = Emitted Fraction

RM = Respirable Mass

RF = Respirable Fraction

FSI = Fast Screening Impactor

ACI = Andersen Cascade Impactor

DoE = Design of Experiment

SDS-PAGE = Sodium Dodecyl Sulfate–Polyacrylamide Gel Electrophoresis

ELISA = Enzyme-Linked Immunosorbent Assay

SEM = Scanning Electron Microscopy

TEM = Transmission Electron Microscopy

RIF = Rifampicin

VER = Verapamil HCl

INH = Isoniazid

HA = Sodium Hyaluronate

LMW = Low Molecular Weight

HMW = High Molecular Weight

Mtb = *Mycobacterium tuberculosis*

NTM = nontuberculous mycobacteria

TB = Tuberculosis

AMs = Alveolar Macrophages

MOI = Multiplicity of Infection

M. smeg. = Mycobacterium smegmatis

1. INTRODUCTION

1.1 Vaccination and standard vaccination programs

According to World Health Organization (WHO) active immunization, i.e. vaccination, is defined as "the process whereby a person is made immune or resistant to an infectious disease, typically by the administration of a vaccine. Vaccines stimulate the body's own immune system to protect the person against subsequent infection or disease. Immunization is a proven tool for controlling and eliminating life-threatening infectious diseases and is estimated to avert between 2 and 3 million deaths each year. It is one of the most cost-effective health investments, with proven strategies that make it accessible to even the most hard-to-reach and vulnerable populations. It has clearly defined target groups; it can be delivered effectively through outreach activities; and vaccination does not require any major lifestyle change."

The vaccination is the most important cost-effective choice to treat or prevent infectious diseases by the stimulation of the immune system against the selected microbe. The finalities of vaccination are: protection of people susceptible to infection, increase of herd immunity and to vanquish a specific infection in one country or in the world [1]. Hence, active immunization determines the production of antibodies, and in some cases also cellular responses mediated by lymphocytes and macrophages, against the infective agent or its toxic products [2].

Standard vaccination programs are usually addressed to children and are financed by government. In many countries, included USA [3], proof of vaccination is required as a condition for school entry. During history, vaccination programs permitted to eradicate many infections and the disease conditions associated. Routine immunization schedules are very expensive and, frequently, require several administrations to boost the coverage. For example, based on what reported by WHO 85% of children, globally, have been vaccinated, at the age of one year, with the first dose of measles vaccine and 67% of them receive a second dose.

Although, 167 countries have added a second dose of measles vaccine as part of their routine vaccination schedule, coverage levels remain very low and the WHO recommended a coverage of at least 95% to prevent outbreaks [4]. Another example is the Human papillomavirus (HPV) vaccine. HPV can cause cervical cancer and other types of cancer in both men and women. While, initially, HPV vaccine was addressed only towards girls, now, it is extended to male. In 2017, the HPV vaccine was introduced in 80 countries. The vaccination schedule for HPV establishes different number of doses scheduled for females based on their ages: 2-schedule doses under 15 years old and 3-schedule doses from 15 years on [5].

Traditional vaccines are of different types according to the characteristics of the injected antigen: attenuated live viral vaccines (Poliomyelitis, Mumps, Measles, Rubella, Yellow fever), inactivated viral vaccine (Influenza), viral subunit vaccine (Hepatitis B), killed bacterial vaccines (Pertussis, Typhoid fever and Tuberculosis) and inactivated bacterial toxins, toxoids (Diphteria, Tetanus). Recombinant DNA techniques can be used to produce, in a safe organism such as *E. coli* or yeast, protective antigens in order to provide a specific immunity [6].

In standard vaccination programs, the vaccines are usually given as an intramuscular (i.m.) or subcutaneous (s.c.) injection, except for polio vaccine, which is also administered as oral solution. So, currently vaccines are almost exclusively administered via parenteral routes. Parenteral administration is typically required for antigens which are macromolecules, i.e. polypeptides, proteins and polysaccharides, hence unable to penetrate into the systemic circulation via other less-invasive routes, as the oral and transdermal ones [7]. These types of formulations and modes of administration presents different disadvantages, especially when used in developing countries. Major drawbacks are the need of specialised healthcare workers, the natural diffidence of patients (especially children and/or belonging to specific ethnic or religious groups), the use of needles which increase the risk of injuries and transmission of pathogens like Hepatitis B virus and Human Immunodeficiency virus (HIV), as well as the requirement of refrigerated storage/distribution (“cold chain”). This cold chain requirement

imposes significant practical difficulties in the implementation of immunization campaigns in low- and middle-income countries.

Therefore, there is a strong need for alternative way of administration, more patient friendly and less expensive [8].

1.2 Pulmonary vaccination

The route of administration is key for determining a successful vaccination. For this reason, especially for nonreplicating immunogens, immunization through aerosol or intranasally can give rise to a more successful coverage stimulating also the mucosal immunity [2]. Immunization by aerosol has not to be intended only for prevention in case of viral or bacterial respiratory infections.

Taking into account what previously explained, delivery of vaccines through a pulmonary way represents an attractive and alternative target. Pulmonary vaccination would offer many advantages. The respirable airways located in the lower lungs are characterized by a large surface area, thin mucosal membrane, and highly dense blood vasculature, allowing rapid absorption [9]. Moreover, the possibility to reach an elaborate mucosal network of antigen presenting cells, APCs (alveolar macrophages, AMs; dendritic cells, DCs; B cells) is a fundamental additional advantage. By presenting the vaccine to the pulmonary mucosa it is possible to induce the production of local antibodies (secretory Immunoglobulins A, IgA), determining a wider protection than the exclusive production of IgG inducted by the systemic administration. From a physiological point of view, the lung can be divided into two parts: the conducting and transitional airways and the lung parenchyma. The conducting airways have a dense mucus layer with DCs, that can entrap pathogens or vaccines particles. Local antibodies can be produced by the lamina propria. Furthermore, the lung parenchyma, is covered with epithelial cells, contains APCs like DCs and AMs too [8]. When antigens enter the lung, they can be taken up by AMs or DCs. After antigen uptake, the DCs migrate to draining lymph nodes

where antigens are presented to naive T cells. The T cells differentiate into memory or effector T cells. Via efferent lymphatics, T cells can provide help to B cells in the systemic germinal centres resulting in production of systemic antibodies [10].

Accessibility, ease of administration and no invasiveness are others important features of pulmonary needle-free vaccination. The lungs present also limited proteolytic activity and a very large surface area for absorption, that are very important factors for the trigger of the immune response [10].

Despite all these advantages, some technical issues need to be overcome. In the last ten years the integrations between nanotechnology and particles engineering permitted to address some physico-chemical and biological problems to increase targeting, delivery and therapeutic efficiency of pulmonary vaccination. However, different issues still remain to be addressed. Mistakes in inhalation manoeuvres can occur, for this reason trained healthcare workers may be necessary; local irritation, inflammatory responses and exacerbation in patients with lung-associated diseases (i.e. asthma) can represent possible risks for this type of vaccination.

The pulmonary administration of vaccines could be performed using two types of devices/formulations: dry powder inhaler (DPI) and nebulizers. Pressurized metered dose inhaler (pMDI) are definitely less studied in pulmonary vaccine delivery, because they add extra formulation issues connected with antigen stability in propellant and damage of DNA structures during nebulization, as well as with the issue of synchronization between actuation and inhalation [9]. DPIs proposed in the scientific literature present the vaccine in a powder formulation, which permits a high payload and higher physicochemical stability of the formulation. Most of them are passive devices and therefore no external power source is needed, which increases flexibility of use and reduces the production costs. Single dose DPIs could be also offered in a disposable version and, hence, would not require cleaning. Contrary, liquid for nebulization require a longer time for their administration coupled to an energy power source. For these reasons they are less recommended for their use in developing countries [10].

Although presently there are no pulmonary vaccine in the market, there are many formulations, liquids and powders, which have been studied or which are in preclinical or clinical research. These studies regard many types of pathogen or toxins: *Influenza virus*, *Measles virus*, *Mycobacterium tuberculosis*, Ricin [10].

The most extensively studied vaccine for pulmonary administration in humans is measles. Pulmonary administration of this vaccine induces more intense local and systemic immune response. Compared to injection forms, aerosol immunisation showed to increase the immune response in HIV-positive individuals and it was not blocked by maternal antibodies. Seroconversion rate was of 80%, even in children younger than 9 months of age. *In vivo* study on Macaques have shown that a single intranasal dose of the DPI vaccine induces durable, fully protective immunity. Two devices were tested: Puffhaler® (Aktiv-Dry) and Solovent (BD, Technologies) loaded with a powder produced with a supercritical fluid drying process [11].

1.3 DPI vaccines

In general, proteins in aqueous medium can undergo to degradations reactions (oxidation, hydrolysis, deamidation). Solid state vaccines are more stable and, without any doubt, more attractive, considering also the commonly accepted benefits of dry powder inhalers [12]. Techniques for production of powders for inhalation are: freeze drying, spray drying and spray freeze drying.

Freeze drying is a multi-steps process: freezing, primary and secondary drying [9]. Proteins are potentially unstable in all these steps, incurring into denaturation for ice crystal formation and change of pH due to crystallization of buffers [13]. So, they need stabilizers or cryoprotectants. Freeze drying product is a cake-like structure that need others process to obtain an inhalable form. For this reason, is not the most suitable technique for the production of DPI vaccines.

On the other hand, spray drying permits to produce respirable dry powders containing biopharmaceuticals in a single-step and, by monitoring the process parameters (inlet

temperature, air flow rate, aspiration and feed rate), it is possible to achieve the desirable characteristics of shape, density and particle size, in order to produce highly respirable vaccines (particle size < 5 μm) able to reach the respirable airways and induce an immunogenic response. However, proteins are very sensible to drying. Thermal, mechanical and dehydration stress can occur with the consequent loose of the native conformation and capability to be bound by the specific antibodies. It is well known that sugars (e.g. trehalose), polyols (e.g. mannitol), organic acids (e.g. aspartic acid) and amino acids (e.g. L-leucine) can protect proteins from these stresses by acting as stabilizing agents [8,14].

Finally, spray freeze drying is a combination of the two previous techniques: solution is sprayed into a cryogenic medium. For this reason, proteins are protected to the stress caused by heating [15]. Nevertheless, the stress imparted by freezing is still present.

Dry powder aerosol vaccination has been extensively used in preclinical immunization studies on animals. Influenza vaccine was the most investigated on mice and rats, but only for nasal delivery [13,16,17]. While BCG and a novel hepatitis B vaccine were administered on guinea pigs by pulmonary route, inducing an immune response comparable to the parental route and superior local mucosal immunity, respectively [18,19].

Another example of a dry powder inhaler for vaccine administration is a live attenuated vaccine against *Francisella tularensis* that proved to be stable up to 6 months when stored in a desiccator at 4 °C [20].

1.4 *Human papilloma virus*

Human papilloma virus (HPV) belongs to a family of more than 100 double stranded DNA virus types; it is globally the second pathogen responsible of cancer cases (30% of global cancer cases), following *Helicobacter pylori* [21]. So far, two vaccines against HPV are available on the market: Gardasil® and Cervarix®. They are both administered by intramuscular injections and are made up of L1 major capsid protein virus-like particle (VLP), presenting a highly HPV

type specificity. Cervarix® is a bivalent vaccine against the high cancer risk associated HPV types (16, 18), whereas Gardasil® covers against 4 different HPV types (6, 11, 16, 18). In December 2014, FDA has approved a new version of the latter, Gardasil® 9, able to protect against the nine HPV types globally more associated with HPV-caused cancers (6, 11, 16, 18, 31, 33, 45, 52, 58). In spite of the great advancement in preventing HPV infection achieved with the introduction of these two vaccines, they still present some limitations. Beside the limited HPV types coverage, they require multiple immunization schedules of i.m. injections and, as all parental administered vaccines, cold-chain storage determining high costs of production and distribution.

A vaccine against *human papilloma virus* (HPV16) administered by inhalation is currently under clinical investigation. It consists in a suspension of the antigen in saline solution, nebulised as liquid using a jet nebulizer. The aerosol vaccinations are well tolerated, with serum antibodies secretion comparable to the intramuscular immunisation. A mucosal immune response (anti-HPV16 VLP IgA) has been also induced [22].

Canali et al. have recently demonstrated that an immunization with the minor capsid protein L2 induces broadly protective responses and a robust cross protection also *in vivo* [23,24].

Furthermore, the minor capsid L2 was inserted in VLPs by Tumban et al. and formulated in DPI by spray drying with sugars and amino acids [25]. *In vivo* study reported highly immunogenic response. After one year at 37°C the L2 VLP DPI reconstituted determined high anti-L2 IgG antibody titers [26], however, after 14 months at room temperature a single dose in mice demonstrated only partial coverage against HPV16. Whereas, two doses after storage for 34 months at room temperature determined high titer of anti-HPV antibodies [27].

1.5 Bacille Calmette-Guèrin

Bacille Calmette-Guèrin (BCG) is a nonpathogenic mycobacterium approved to be used as live vaccine against *Mycobacterium tuberculosis* (Mtb). Tuberculosis (TB), caused by Mtb, is a

major communicable infectious disease. According to the World Health Organization (WHO), in 2016, there were an estimation of 10.4 million new TB cases [28]. BCG is usually administered to all children in the countries where risk of getting TB is high. BCG is prepared form a live attenuated form of *Mycobacterium bovis*, discovered in cows, but able to case the disease also in human. Vaccine preparation is quite cheap, it only requires the subculture of the bacillus in an appropriate medium. BCG is recognized as safe upon inoculation in the arm by intradermal injection [29]. Many research groups studied the possibility to administer this vaccine by inhalation, taking also into accounts that the lungs are the primary way of entrance of Mtb. Some of these works are about spray drying of BCG vaccine, in order to obtain a more stable vaccine to be easily spread in developing countries. Garcia-Contreras et al. developed a low cost and technically simple spray dried nanomicroparticles BCG vaccine (leucine : BCG, 95:5) [19]. The administration of this DPI to guinea pigs, followed by subsequent challenged with virulent Mtb, determined reduced bacterial burden and lung pathology. Also the spray dried vaccine formulated by Wong et al. [30] employed leucine as excipient. BCG was inserted in a leucine matrix and the system proved to be stable for 4 months at 4 and 25 °C, reporting a better viability of the bacillus than the same freeze-dried formulation and a commercial version. Despite these achievements, BCG presents many limits connected to erratic efficacy (from 0 to 80%) of the antigen itself [31]. First of all, it shows low efficacy in adults, hence BCG vaccination is usually given at birth. It is also contraindicated in HIV-infected people, although in Tb-endemic countries, where often both infections are associated, BCG vaccination in HIV-exposed neonatal is still continued [32]. Moreover, there are some evidences of coverage for only up to 10 years [33] as well as of influence environmental and genetic factors on the immune response and effectiveness of the vaccine [31]. Finally, the most critical point is that BCG is not effective against TB drug resistant strains, which are every year more common among all reported TB cases all over the world, as well as against nontuberculous mycobacteria

(NTM), cause of superinfections in immunocompromised patients. For this reasons, new safe, effective and affordable vaccine candidates are strongly needed [31].

1.6 DPIs to treat mycobacteria

More than 600,000 of all TB new infections in 2016 were estimated to be multi drug resistant (MDR) and rifampicin resistant (RR) TB [28]. In addition, apart from Mtb, different species of *Mycobacterium* (MB) are getting a great deal of interest, as cause of superinfections. Limits of BCG vaccine for these cases, focused the attention of research groups more on pulmonary delivery of antibiotics for mycobacteria infections treatment than to develop of BCG formulations for inhalation. Few information about the immune response against these nontuberculous mycobacteria (NTM) are available [34], whereas MTB interactions with alveolar macrophages (AMs) have been extensively studied [35]. *Mycobacterium* bacilli enter the lungs and proliferate inside alveolar macrophages (AMs) [36]. Therefore, pulmonary delivery of first and/or second-line antibiotics still has a continuously growing interest [37]. This delivery strategy offers the many advantages typical of this route of administration and can be easily transferred to specific benefits for mycobacteria infection treatment. The needle-free route is suitable to reach high drugs concentration at the site of action, especially for poorly water-soluble drugs, preventing gastrointestinal decomposition and first-pass metabolization effect after oral administration and reducing the risk of drug resistance. In this respect, also doses and frequency of administration can be reduced, as well as toxicity, improving the patient compliance [37]. Hence, the possibility to increase drugs concentration directly targeting infected AMs is a fundamental advantage, reachable through antibiotics inhalation, in the case of TB treatment.

High dose delivery can only be reached by increasing the loading in microparticles. This may be achieved by spray drying of drugs alone [38] or with a minimal amount of excipient, e.g. 1% w/w of magnesium stearate [37,39].

In order to be effective, aerodynamic size of microparticles intended to be pulmonary administrated has to be lower than 5 μm, however particles with a too small diameter (< 0.5 μm) are destined to be exhaled [40]. On the other hand, to increase the amount of antibiotics penetrating the infected AMs, it is generally accepted that particles with a small size distribution, in the range of 200-550 nm, are likelihood to be subjected to phagocytosis by AMs [41,42]. Particles of these nano-dimensions could not be handled in a dosage form nor efficiently deposited into the lungs, so they need further manipulation to be efficiently inhaled. Another strategy to increase the macrophages uptake is the use of specific material for particle construction. Poly Lactic-co-Glycolic Acid (PLGA) microparticles loaded with first-line antibiotics, such as rifampicin, have been proposed as a promising approach for a macrophages targeted delivery [43]. Maretti et al. demonstrated by confocal microscopy images the presence of inhaled solid lipid microparticles comprising sodium taurocholate inside macrophages cytoplasm [44]. Moreover, alveolar macrophages specific ligands, such as mannan, were employed in different type of formulations (liposomes, solid lipid nanoparticles and microparticles) to improve uptake of antibiotics [45-47]. Also, di palmitoyl phosphatidylcholine (DPPC) particles reported an improved peripheral lung deposition [48].

In addition, peculiar chemical signals related to the nature of the material employed in the formulation [49,50] can determine a higher AMs uptake. In this respect it has been reported that low molecular weight hyaluronic acid sodium salt (HA), an endogenous compound, is capable to be efficiently internalized inside the macrophages via binding CD44 receptor on the AM surface [51]. Furthermore, low molecular weight HA is able to polarize macrophages at M1 phenotype [52], that encourage inflammation, so this activation of macrophages could be exploited to further improve MB treatment [53].

TB treatment is required for long periods. So, extended release is indispensable to reduce the number of administrations. All first and second-line drugs, alone and in combination, were comprised in slow release formulation. In this respect, proliposomal and solid lipid

nanoparticles (SLN), the latter administered mainly via nebulisers, are the most interesting examples. Proliposomal dry powder formulations were loaded with isoniazid and their efficacy against Mtb was higher than free isoniazid [54]. Intratracheal administration of hydrogenated soy phosphatidylcholine (HSPC) spray dried proliposomes, loaded with rifapentine, increased the antibiotic residence time and half-life in the lungs compared to lipid-free dry powder [55]. Moreover, rifampicin, isoniazid and pyrazinamide loaded in sodium alginate nanoparticles determined concentrations above MIC for two weeks [56].

Finally, the use efflux pumps inhibitors [57] such as verapamil or thioridazine [58], along with first line antituberculars, may lead to an increase of the intracellular concentration, a decrease of the duration of treatment [59], and a reduction of the onset of drug resistance. However, the systemic administration of these “adjuvant” drugs is largely hindered by their side effects.

PART I

2. AIM

Needle-free noninvasive alternative routes of administration for vaccines acquired a considerable interest in the last decades. Among them, pulmonary vaccination represents a great option for the many advantages that it can convey. The lungs are the primary entrance of external agents, pathogens or not, so they are physiologically predisposed to generate immune reactions. For this reason, the lungs contain local antigen presenting cells able to induce mucosal and systemic immunity. Moreover, the word wide distribution of the presently available vaccines is limited by the need of "cold chain" for storage and distribution. In this respect, a formulation in form of dry powder inhaler that do not require continuous refrigeration and target directly the lungs represent attractive alternatives to liquid dosage forms administered parenterally.

The aim of the part one of this project was to develop a platform for pulmonary administration of antigen-based vaccines.

In specific, the goal was to design highly respirable dry powder produced by spray drying, through a particle engineering approach. To achieve this goal a deep know-out on spray drying of biomacromolecules and a careful evaluating of the critical points of the production process had to be develop in order to conserve the activity of the antigen proteins.

The macromolecule selected as model was a novel antigen against human papilloma virus (HPV) [24,60]. The primary objective of this first section was to obtain dry engineered antigen particles for inhalation via spray drying by molecular deposition of a lubricant on the particle surface [39]. However, all vaccines on the market include adjuvants to enhance, sustain and prolong the immune response. Hence, a further aim was the assessment of the suitability of substituting the surfactant with a well-known adjuvant amphiphilic in nature, already used in many commercial vaccine formulations.

Beside the investigation of the method and conditions for keeping the protein activity after spray drying, the produced powders were characterized for structure, particle size distribution, aerodynamic behavior upon aerosolization *in vitro*. Furthermore *in vivo* deposition and immunization experiments were performed.

3. MATERIALS AND METHODS

3.1 Materials

Antigen *Pf*Trx HPV16 L2 [24] as well as its update version *Pf*Trx HPV16 L2 OVX313 [60] was produced and provided by the Department of Chemistry, Life Sciences and Environmental Sustainability of the University of Parma. Buffers TBS (tris-buffered saline, Tris 25 mM, NaCl 30 mM, pH 7.4) and KP (phosphate buffered saline, potassium phosphate 25 mM, pH 7.4) were used to store the protein after expression. Mannitol, Pearlitol® SD 200 batch no. E556G, was a kind gift by Roquette Freres, France. Sodium stearate (batch no. 170641) was bought from Magnesia GmbH, Germany. Glycopyranoside Lipid A (GLA, PHAD®, batch no. 699800-03-028), synthetic version of Monophosphoryl Lipid A (MPLA), was supplied by Avanti Polar Lipids (Alabama, USA). All solvents were at analytical grade and ultrapure water (0.055 µS/cm, TOC 1 ppb) was produced by reverse osmosis (Purelab Pulse + Flex ultrapure water, Elga-Veolia, Italy).

3.2 Methods

3.2.1 Spray drying

Dried engineered powders for inhalation (DPI) containing the antigen were produced by spray drying employing a mini Spray Dryer Büchi B-290 (Büchi Laboratoriums-Technik, Switzerland) in aspiration and open mode. Dried powders containing E2-Crimson were, instead, spray dried with a mini Spray Dryer Büchi B-191 (Büchi Laboratoriums-Technik, Switzerland). The feed solution was prepared by dissolving the balking agent in ultrapure water whereas the amphiphilic compound was dissolved in ethanol (95% v/v). Protein was, then, added to the water fraction and ethanol portion was added drop wise to the aqueous one (water:

ethanol=70:30 v/v) under continuous magnetic stirring, at 200 rpm. Total solid concentration was always 0.6% w/v, only in the case of the Alexa 750 labelled-antigen formulation, due to the limited labelling yield, it was reduced to 0.2% w/v, corresponding to 0.59% w/w of the total solid of labelled-protein. Alexa 750 labelled-antigen was produced incubating for 1 hour at room temperature, under continuous stirring at 250 rpm, a PBS solution comprising Alexa 750 (Life Technologies, California, USA) and *Pf*Trx HPV16 L2 antigen (molar ratio 1:10). Then, free Alexa 750 was removed employing a size exclusion column (MicroBio spin size exclusion spin columns, Bio-Rad, California, USA). Finally, quantity of labelled-antigen was evaluated comparing absorbance at λ 280 nm (OD280) of processed antigen and native antigen.

Bulking agent concentration in the solution was adjusted for each formulation on the bases of protein concentration and amphiphilic compound tested (Figure 3.1), to reach 100% of weight of the total solid in the solution. The final water:ethanol mixture was 70:30 v/v, except for starting formulations prepared with 5% v/v of ethanol and 95% v/v of water. The drying parameters were set as follow: inlet temperature (125 °C), drying air flow rate (601 L/h), aspiration (35 m^3/h), solution feed rate (3.5 mL/min) and nozzle diameter 0.7 mm. Figure 3.2 illustrates schematic of the theoretical re-distribution of the amphiphilic compound in the vaccine particles during the spray drying process, based on what reported by Parlati et al. [39]. Finally, for solid state and flowability characterization two blank spray dried powders, without the antigen, were prepared following the usual composition and process parameters, but containing the different amphiphilic compounds (sodium stearate or GLA). In order to simulate the characteristics of vaccine-containing powder 1 mL of 25 mM KP buffer was added to the feed solution.

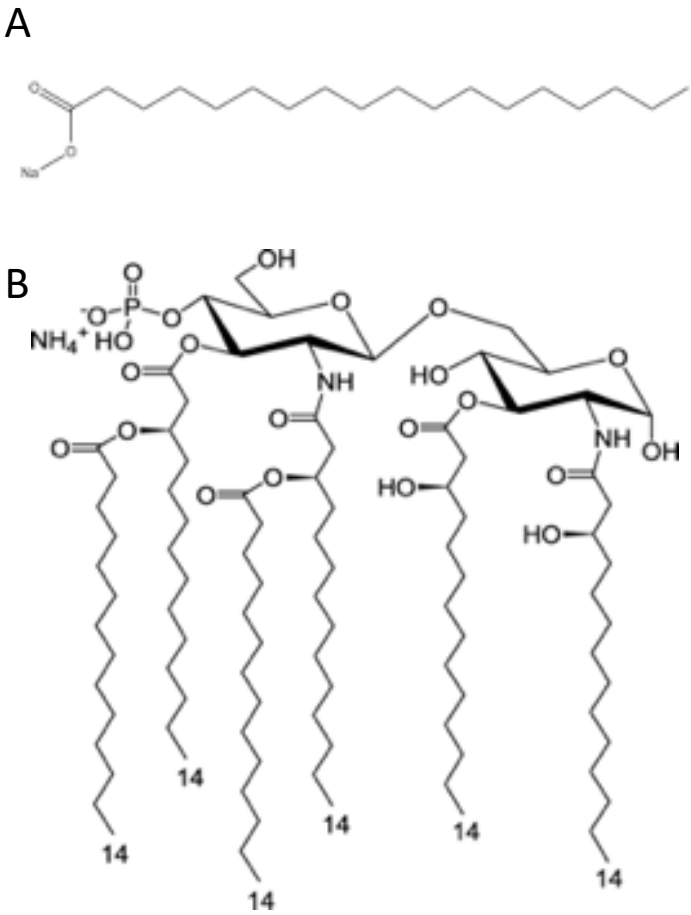

Figure 3.1. Molecular structure of the different surfactants employed: sodium stearate (panel A) and GLA (panel B).

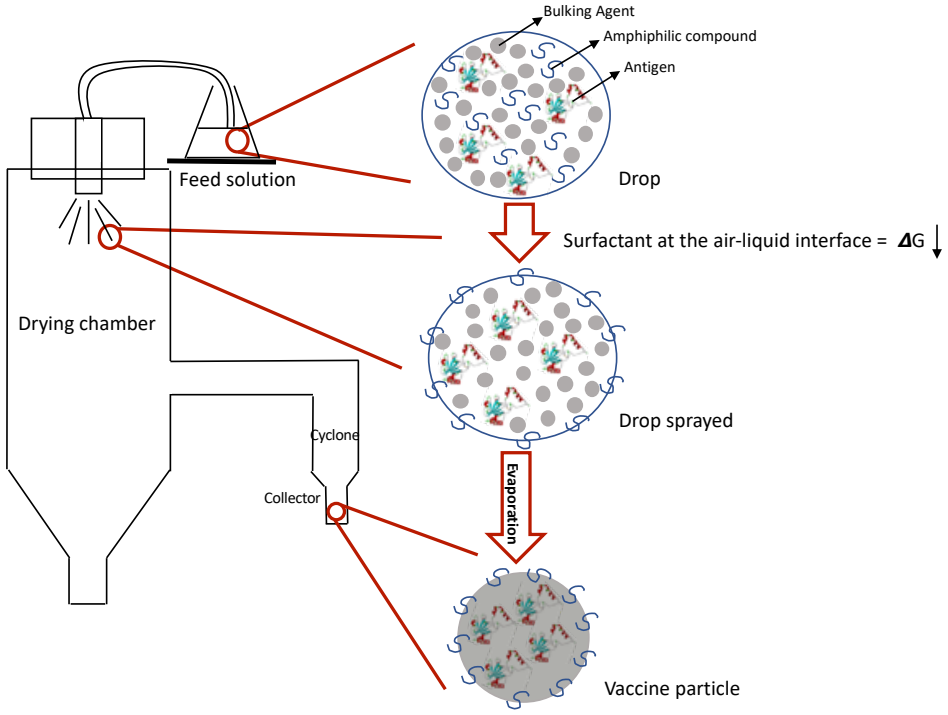

Figure 3.2. Schematic of the proposed particle formation process during spray drying.

3.2.2 Particle size distribution by laser diffraction

The particle size distribution (PSD) of spray dried powders was measured by laser light scattering (Spraytec®, Malvern Instruments Ltd., United Kingdom). The diffractometer was equipped with a 300 mm focal lens, which measures particle size in the range 0.1-900 μm. Samples were prepared by suspending 10 mg of powders in 10 mL of cyclohexane containing 0.1% w/v of Span 85 (Honeywell Fluka™, New Jersey, USA). To improve homogeneity, the dispersion was put in an ultrasonic bath (Branson Ultrasonics Corporation 8510, Connecticut, USA) for 5 minutes before PSD measurements that was carried out in triplicate for each sample with an obscuration threshold of about 10%. Data were expressed as volume diameter of 10^{th} ($D_{v,10}$), 50^{th} ($D_{v,50}$) and 90^{th} ($D_{v,90}$) percentile of the particle population and as Span value $[(D_{v,90}-D_{v,10})/D_{v,50}]$.

3.2.3 Scanning Electron Microscopy

Scanning Electron Microscopy (FESEM-FIB Zeiss Auriga Compact, Germany) was employed to investigate particles morphology, shape and surface characteristics of the spray dried powders. Powders were deposited on adhesive black carbon tabs pre-mounted on aluminum stubs, powder in excess was removed with a gentle nitrogen flow, and samples imaged without any metallization process. The microscope was operated after 30 min of depressurization under high vacuum conditions ($1.87\ 10^{-4}$ Pa) with an accelerating voltage of 1.0 kV and a working distance of 4.9 mm. Images were taken at different magnification.

3.2.4 Mannitol HPLC analysis

A Shimadzu VP (Shimadzu Corp., Japan) high performance liquid chromatographic (HPLC) system coupled with refractive index detector set at 40 °C (RID-10A, Shimadzu Corp, Japan) was used for quantification of mannitol, readapting the analytical method reported in the

specific monography by United States Pharmacopeia (USP 41). Ultrapure water was employed as mobile phase at a flow rate of 1 mL/min and injection volume was set at 100 µL on a Waters 717 plus autosampler (Waters Corporation, Massachusetts, USA). As a stationary phase an Aminex® HPX-87H Ion Exclusion, 300 mm x 7.8 mm (Bio-Rad, California, USA) column was used. The column was equilibrated at 80°C for 2 hours with a mobile phase flow rate of 0.2 mL/min and, then, maintained at that temperature during the chromatographic runs. Finally, Shimadzu Class VP software was used for data acquisition and analysis. Each sample was injected 6 times and the 3 closer value were used to calculate mean and standard deviation. Linearity of the responses was assessed between 0.01 mg/mL and 1 mg/mL (R^2= 0.999) (Figure 3.3). The limit of detection (LOD) and the limit of quantification (LOQ) were 0.0026 mg/mL and 0.008 mg/mL, respectively.

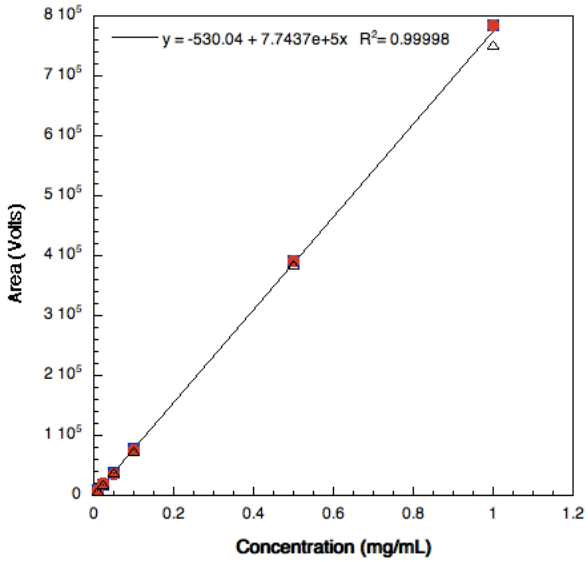

Figure 3.3 Relationship between mannitol concentration and detector response in the concentration range 0.01 mg/mL and 1 mg/mL of mannitol in ultrapure water.

3.2.5 *In vitro* aerodynamic performance assessment

The aerodynamic performance of powders was investigated using a Fast Screening Impactor (FSI, Copley scientific Ltd, United Kingdom). This is an abbreviated impactor that permits to divide the powder emitted from a device in two fractions: the first one composed of particles

with an aerodynamic diameter > 5 μm, which is collected inside the Coarse Fraction Collector (CFC), and the second one constituted of particles with an aerodynamic diameter < 5 μm, collected in the Fine Fraction Collector (FFC), where a filter is placed (glass filter type A/E, diameter 76 mm, Pall Corporation, New York, USA). Moreover, an Induction Port (IP) was placed on the top of the CFC and a mouthpiece adaptor attached to the IP to produce an airtight seal between the inhaler mouthpiece and the induction port 10 mg (or 5 mg in the case of the powders collected after dynamic vapor sorption analysis) of powder were loaded manually in a hypromellose Quali-V-I capsule size 3 (Qualicaps®, Spain) and one single capsule for each test was aerosolized using a high resistance (HR) RS01® device (RPC, Plastiape, Italy). The entire system was connected to a vacuum pump (Mod. 1000, Erweka GmbH, Germany) which created the air flow to aerosolize the powder and distribute it in the FSI. The flow rate used during each test was adjusted, according to current USP monograph, with a Critical Flow Controller TPK (Copley Scientific, Nottingham, United Kingdom) in order to produce a pressure drop of 4 kPa over the inhaler. Thus, flow rate was set at 60 L/min before each experiment using a Flow Meter DFM 2000 (Copley Scientific, Nottingham, United Kingdom): The flow activation time (in seconds) was calculated according to equation (3.1):

$$Activation\ time\ = 240/Q \quad (3.1)$$

where Q is the test flow rate.

Therefore, the pump was activated for 4 seconds for each test so that a volume of 4 L of air was withdrawn from the inhaler. The aerodynamic performance was tested in triplicate.

The following aerodynamic parameters were calculated: the emitted mass (EM) was the amount of powder that was emitted from the device; the emitted fraction (EF) was calculated as the ratio between the EM and the amount of powder loaded in the capsule. The respirable mass (RM) was the mass of powder with aerodynamic diameter lower than 5 μm, i.e. the amount deposited on the FFC filter; the respirable mass (RF) was calculated as the ratio between RM and the amount of powder loaded in the capsule. EM and RM were calculated from the weight

of the device loaded with the filled capsule and the filter before and after the aerosolization of the powder.

Andersen Cascade Impactor (ACI, Apparatus 3, USP 41, Copley scientific Ltd, United Kingdom) was employed to determine aerodynamic distribution of mannitol in the two powders produced for the *in vivo* study. ACI is an 8-stage cascade impactor, including an IP and a filter. Cut-offs diameters of the stages -1, -0, 1, 2, 3, 4, 5, 6 are the following: 8.60, 6.50, 4.40, 3.20, 1.90, 1.20, 0.55 and 0.26 μm. A glass microfiber filter of diameter 82.6 mm (Whatman plc, United Kingdom) was placed right below stage six in order to collect particles with a diameter lower than that of the stage 6 cut-off. 20 mg of each powder were loaded in Quali-V-I size 3 capsules and RS01® device was always employed for aerosolization. Before running the experiment, 2 mL of a solution of Tween® 1% w/v in ethanol was applied on the particle collection surface of each stage; after complete solvent evaporation a thin layer of surfactant was obtained on the stage surfaces that ensured efficient particle capture (avoided particle bouncing). Flow rate generated by a vacuum pump (SCP5, Copley scientific Ltd, United Kingdom) was set at 60 L/min, using a Flow Meter DFM 2000, and activated for 4 seconds through a Critical Flow Controller TPK. After the powder aerosolization, samples were collected with ultrapure water in 50 mL volumetric flasks for device plus capsule and induction port samples. Powder deposited on stages -1, -0 and 1 was solubilized with 25 mL of ultrapure water, while for all the other stages 10 mL were used. Filter was removed from the system and put in a crystallizer, 10 mL of ultrapure water were added, and the crystallizer was put 5 minutes in an ultrasonic bath. The solutions obtained from filter and device plus capsule were filtered with 0.45 μm cellulose acetate syringe filters (Labservice Analytica Srl, Italy), before injection in HPLC. Different aerodynamic parameters were calculated: EM, as the mannitol mass collected from the induction port to the filter; EF as percentage ratio between the EM and amount of powder loaded in the capsule; RM, the mass of the aerosolized mannitol with an aerodynamic diameter < 5 μm; RF was determined as percentage of the RM with respect to the

EM. Moreover, Mass Median Aerodynamic Diameter (MMAD) defined as the diameter which separates the powder in two populations with equal weight was determined by plotting the cumulative percentage of mass less than the cut-off diameter for each stage on a probability scale versus the aerodynamic diameter of the stage on a logarithmic scale. MMAD is the slope of the line obtained by linear regression of the experimental points. Finally, Geometrical Standard Deviation (GSD), a parameter indicating how wide particle size distribution was, calculated as reported in USP 41 chapter 601 (equation 3.2)

$$GSD = \sqrt{\frac{size\ X}{size\ Y}} \tag{3.2}$$

where size X is the aerodynamic diameter at 84.13% of the particle population and size Y is the aerodynamic diameter at 15.87% of the particle population.

3.2.6 Fluorescence determination

Fluorescence protein E2-Crimson was studied employing fluorometers. Its stability at different pH was investigated with Spark 10M fluorometer (Tecan, Switzerland). Initially a calibration curve was prepared using a solution 9.5 mg/mL of E2-Crimson in 25 mM buffer phosphate pH 7.4. Linearity was assessed between 5 and 700 μg/mL. Samples were read on a Corning® Costar flat black plate (Corning Costar, Massachusetts, USA) exciting at λ 611 nm and collecting emission signals at λ 665 nm with an optimization gain of 82%. To the values obtained were, then, subtracted the value of the blank (25 mM phosphate buffer) and plotted (Figure 3.4). Two different lines were identified: for protein concentrations between 5 and 500 μg/mL (line α) R^2 was 0.997, while for concentrations between 500 and 700 μg/mL (line β) R^2 was 0.998.

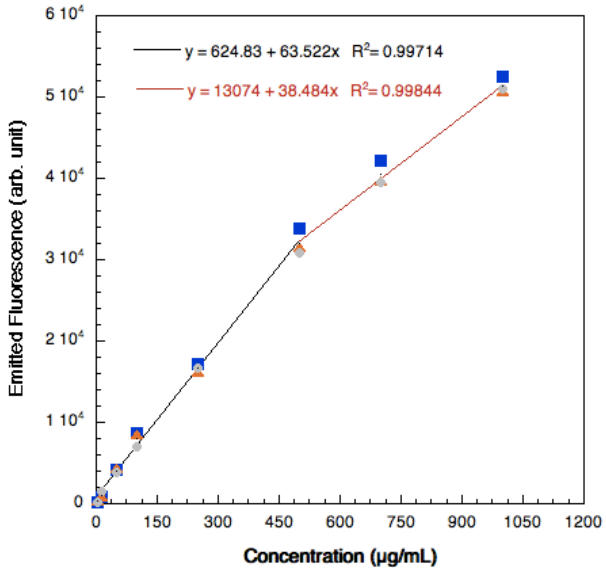

Figure 3.4 Linearity of the responses studied between 5 µg/mL and 0.7 mg/mL of E2-Crimson concentration.

The limit of detection (LOD) was 7.84 µg/mL (line α) or 23.74 µg/mL (line β); the limit of quantification (LOQ) was 1121.08 µg/mL (line α) or 3397.20 µg/mL (line β). Accuracy was calculated for each point of the two lines: for line α it ranged between 1.05 and 57.58%, while for line β values were around 1%.

Stability of E2-Crimson at different pH (1.4, 4.3, 5.2, 5.8, 6, 7.7, 8, 10.6 and 11) was studied reading its fluorescence. A 15% v/v phosphoric acid solution and potassium hydroxide 5M were used to change the pH of 1 mL (9.5 mg of E2-Crimson) of the starting buffer solution. pH was measured with a digital pHmeter (GLP21, Crison Instrument, Spain). Residual fluorescence of 200 µL of the samples was read on a Corning® Costar flat black plate exciting at λ 611 nm and collecting emission signals at λ 665 nm. Analysis was done in triplicate and data were, then, analyzed using values collected for sample at pH 7.7 (starting protein buffer solution) as reference standard (100% of residual activity).

Stability of E2-Crimson in different ethanol aqueous solutions (5-50% v/v) and residual fluorescence in powders produced by spray drying was determined by employing a

Luminescent Spectrometer Ls50B (Perkin Elmer Massachusetts, USA). 120 μL, comprising 6 μM of protein, were read exciting at λ 611 nm and collecting emission signals at λ 646 nm.

3.2.7 Far-UV circular dichroism

Circular dichroism (CD) is a type of spectroscopy able to give structurally information on macromolecules. It involved different absorption of left and right handed circularly polarized light. Far-UV (< 240 nm) CD spectrum of protein gives information about their secondary structure, so it was employed to evaluate structurally changes in *Pf*Trx HPV16 L2 antigen (7 μM in 10mM phosphate buffer pH 7.4) after exposure to different hydro-alcoholic solutions, from 5% up to 70% v/v of ethanol (95% v/v). Far-UV CD spectra (200–260 nm) were acquired with a Jasco J715 Spectropolarimeter (Mariland, USA) equipped with a Peltier temperature controller, using a 0.2 cm path-length cuvette, a bandwidth of 1 nm, a data pitch of 0.5 nm, and a response time of 4 s; CD spectra were averaged from 4 scans. Following baseline correction, the measured ellipticity, h (mdeg), was converted to the molar mean residue ellipticity [Θ] (deg cm^2 $dmol^{-1}$), using [Θ] 5 $h/cn_{res}l$, where Θ is ellipticity, c is the molar concentration of the protein, n_{res} is the number of amino acid residues in the protein and l is the optical path length in centimeters. Samples were analyzed after 10 minutes and after 30 minutes from preparation of the different protein hydro-alcoholic solutions.

3.2.8 Design of experiment

A design of experiment (DoE) was set to investigate the influence of the type and concentration of buffer, in which the antigen was dissolved, on the characteristics of spray dried powders produced. The DoE developed was a half fractional factorial design (FFD) with 2^{4-1} experiments, namely 4 factors (Critical Process Parameters. CPPs) studied and 2 levels each. The design space (Table 3.1) was built up with two different software, in order to compare their

results: The Unscrambler® (X- version 10.3 (32-bit), 2013; Camo software, Oslo, Norway) and Minitab® (17.1, 2013; Minitab Ltd., United Kingdom). The total number of experiments carried out was 11: 8 variations of the factors studied and 2 central points (#4U-7M and #2U-6M); the layout of the experiments reported by the two software was different, so it was decided to follow the one of The Unscrambler®.

The 4 factors were:

- Type of buffer: TBS, tris-buffered saline, Tris 25 mM and NaCl 30 mM, pH 7.4 or KP, phosphate buffered solution, potassium phosphate 25 mM, pH 7.4;

  and 3 parameters of the spray drying process
- Drying inlet temperature: 110°C or 125°C;
- Aspiration: 30 m^3/h or 35 m^3/h;
- Feed rate: 3.5 mL/min or 4.5 mL/min.

The Critical Quality Attributes (CQAs) used as reference of the quality of the product were: yield of the spray drying, emitted fraction (EF) from the aerosolization device, respirable fraction (RF) and mean volume diameter ($D_{v,50}$) of the powder.

Due to the high production cost, the DoE was carried out on solutions without the antigen, but containing only blank buffers.

Table 3.1 Design matrices obtained with the software The Unscrambler® (U) and Minitab® (M) and values set for each experiment, in bold phase are reported the central points with the two different buffers, but same process parameters.

#The Unscambler®	#Minitab®	Buffer	Inlet Temperature (°C)	Aspiration (m^3/h)	Feed Rate (mL/min)
1U	3M	KP	125.0	30.0	3.5
2U	4M	KP	110.0	35.0	3.5
3U	9M	KP	110.0	30.0	4.5
4U	**2M**	**TBS**	**117.5**	**32.5**	**4.0**
5U	10M	KP	125.0	35.0	4.5
6U	5M	TBS	110.0	30.0	3.5
7U	**6M**	**KP**	**117.5**	**32.5**	**4.0**
8U	1M	TBS	125.0	30.0	4.5
9U	7M	TBS	110.0	35.0	4.5
10U	8M	TBS	125.0	35.0	3.5

3.2.9 Solid state characterization and thermal analysis

Differential scanning calorimetry (DSC) profiles were determined using a Mettler DSC model 821e (Mettler Toledo, Ohio, USA) driven by a STARe software (Mettler Toledo, Ohio, USA). Measurements were preceded by a calibration with Indium (onset of melting T_m = 157.1°C, enthalpy of melting ΔH_m = 27.84 J g-1). DSC traces were recorded by placing accurately weighed quantities (4–6 mg) of powder in a 40 µL aluminum pan which was then sealed and double pierced. Scans were performed between 25 and 280 °C at heating rate of 10 °C min^{-1} under a flux of dried nitrogen (100 mL/min).

Thermo-gravimetric analysis was performed employing a TGA/DSC1 (Mettler Toledo, Ohio, USA). 3-6 mg of spray dried powders were placed in 100 µL alumina pan and heated at a rate of 10 °C min^{-1} from 25 °C to 125 °C under a flux of dried nitrogen (80 mL/min). The mass loss, attributed to residual moisture of the spray dried powders, was determined directly by TGA.

TGA operated through a STARe software (Mettler Toledo, Ohio, USA), that was also for data analysis.

DPIs crystallinity was assessed through X-ray powder diffraction (PXRD, Miniflex X-ray diffractomer, Rigaku, Japan) using a radiation CuKα of 30 kV, a scan speed of 0.05°/min and a range of scan between 2° and 35° on powder sample (about 300 mg) placed in a sample holder and flattened using a glass slide.

Dynamic vapor sorption (DVS) analysis was performed with an Aquadyne DVS-2 (Quantachrome Instruments, Florida, USA) using a gravimetric method. The instrument was calibrated in 0–90% Relative Humidity, RH, range at 25 °C with a certificated standard of microcrystalline cellulose (Microcrystalline cellulose for water sorption isotherm measurements, CRM no. 302, individual identification no. 0441, E.U. Bureau of reference). The balances of the instrument were calibrated at 25 °C, 50% RH using a 200 mg standard weight prior to the measurement of each specimen. The transition from one step to the next occurred automatically when the rate of weight variation was lower than 0.001% min^{-1} and in any case not earlier than 30 min from the beginning of the step.

The samples of vaccine DPIs containing the different surfactants (about 50 mg) were analyzed in isothermal mode at 25°C and 40°C measuring the water vapor sorption in the 0–95% RH range (step size = 5% RH). The analysis was cycled (from RH 0 to 95% and back from 95 to 0%).

3.2.10 Bulk and tapped density determination

Bulk and tapped density were determined following Ph. Eur. 9th ed. prescriptions. For bulk density, 450 mg of spray dried powder was gently introduced, without compacting, into a 10 mL graduate cylinder (readable to 0.1 mL). Powder was carefully level and the unsettle apparent volume was read. Density was, finally, calculate as ratio between mass (g) on volume (mL). This test was carried out in triplicate.

Tapped density was, instead, evaluated employing a tapped density tester (model SVM 122, Erweka GmbH, Germany). 450 mg of powder was poured in a 10 mL graduate cylinder and 10, 500 and 1250 taps were applied. After every tap step volume was read. According to the Pharmacopoeia requirements, since the difference between V_{500} and V_{1250} was > 0.2 mL, others 1250 were performed until the volume read was stable.

3.2.11 True density measure through a gas pycnometer

Real density of spray dried powder was measured with AccuPyc II 1340 gas pycnometer (Micromeritics Instrument Corporation, Georgia, USA) driven by an AccuPyc II 1340 V.109 software. Helium (purity 5.0) was used as measuring gas.

The measurements were conducted at ambient temperature nearly 30 minutes after the equipment switch on and the saturation of the pipelines with the gas.

A cell of 3.5 cm^3 was used. Before the sample measurements the equipment was calibrated using a stainless steel sphere (volume 2.421764, Instrumental kit n. 133-34905-00).

To perform the density determination, an amount corresponding to about 100 mg of each sample was accurately weighted (balance E154, Gibertini, Italy, sensitivity 0.1 mg). Then, the specimen was inserted in the measuring cell; the sample occupied around the ¾ of the cell volume.

The instrument was operated and the density computed on the base of the volume of gas in the cell.

Five measurements were performed for each sample.

3.2.12 Powders Flow

Dynamic angle of repose is commonly used to characterize flow properties of powder, according to Ph. Eur. 9^{th} ed. Dynamic angle of repose was determined employing a Friability tester (model TA3R, Erweka GmbH, Germany), where the drum had been removed and

replaced with a transparent glass vial (volume 10 mL). The powder (about 50 mg) was gently introduced in the vial. The vial was, then, attached to the tester arm and was rotated for 60 seconds at 20 rpm. A video was recorded, and frames were analyzed with the software Image J64 (NIH, USA). 6 different measures were used to determine the dynamic angle of repose of the two powders.

3.2.13 Contact angle determination

The measure of the contact angle between a liquid and a solid surface is commonly used for determining the wettability of solids [61]. The approach is based on the capability of a liquid to spread spontaneously over the surface of a solid reaching a thermodynamic equilibrium. According to the relative affinity between the liquid and the solid surface the measured angle assumes a value that results from the balance between solid/liquid and the solid/gas surface tensions Contact angle can be determined with various methods that are essentially based on goniometric or tensiometric measurement. A particularly useful approach is the sessile or static drop method which is carried out by depositing a liquid drop onto the surface of a disk which in the case of pharmaceutical powders is obtained by compaction [62]. The compressed disc (about 40 mg of spray dried powders, 1.6 mm height x 6 mm of diameter) was prepared with a tablet press machine with 7 mm punch (EKO Korsch Maschinenfabrik, Germany). Then the compressed disc was placed on a plate of a surface wettability tester (app. 28, type 4-1, AB Lorentzen & Wettre, Sweden) and a water drop of about 10 μL was deposited on the surface of the disc by means of a microsyringe (Hamilton, USA). The picture of the contact between the liquid drop and the solid surface was taken and the angle was measured using the software Image J64 (NIH and University of Wisconsin, USA). Three discs and 6 drops were analyzed for each sample.

The measure of the contact angle was used to determine the extent of surface of the microparticles produced coated with the different; The fraction of surface coated was calculated by applying the relationship known in the literature as Cassie and Baxter equation (3.3) [63]:

$$cos\vartheta_{powder=}f_{surfactant}cos\vartheta_{surfactant} + f_{bulking\ agent}cos\vartheta_{bulking\ agent} \quad (3.3)$$

where $f_{surfactant}$ and $f_{bulking\ agent}$ are the fractions of surface area of the compressed disk occupied by the surfactant and the bulking agent respectively; $\vartheta_{surfactant}$ and $\vartheta_{buking\ agent}$ are the water contact angle experimentally determined on a compressed disk of surfactant and bulking agent, respectively; ϑ_{powder} the experimental contact angle determined on a compressed disk of the spray dried powder.

3.2.14 Sodium dodecyl sulfate–polyacrylamide gel electrophoresis

Sodium dodecyl sulfate–polyacrylamide gel electrophoresis (SDS-PAGE) is used in biochemistry for the separation of a protein mixture based on the molecular weight of the components. SDS-PAGE was used in order to identify and quantify the antigen *Pf*Trx HPV16 L2 in the spray dried powders. Samples were, first of all, boiled at 100°C for 10 minutes with sodium dodecyl sulfate, which binds proteins denaturing and charging them, and with β-mercaptoethanol, which breaks disulfide bridges. An anionic dye, bromophenol blue, to follow the electrophoretic run through colored bands, and glycerol to impart an adequate density, were added. The analysis is based on the application of a different voltage at the far ends of the gel, which causes a migration of negatively charged protein-SDS complex towards the positively charged anode. The gel acts as a sieve: small molecular weight molecules are able to migrate through the gel mesh easily and faster than larger molecules. When the dye reaches the bottom of the gel and before proteins reach the electrodes, the voltage is removed, and the gel is stained with a Coomassie staining dissolved in ethanol, water and glacial acetic acid solution. The gel is, then, decolored and the banding pattern pictured.

The protein content in the spray dried powder (20 mg dissolved in 100 μL of ultrapure water) was determined by SDS-PAGE analysis, using predetermined amounts of the native (not processed) *Pf*Trx HPV16 L2 antigen as reference (molecular weight = 18 kDa) and a molecular weight marker at known concentrations of bovine serum albumin (BSA, 60 kDa), carbonic anhydrase (30, kDa) and lysozyme (14.4 kDa).

3.2.15 Enzyme-linked immunosorbent assay

Enzyme-linked immunosorbent assay (ELISA) is an immune-enzymatic assay commonly used to evaluate the presence of a ligand (a protein) in a sample, using a single or a pair of antibodies. In this work, ELISA was used to determine whether the antigen contained in the spray dried powders kept its integrity and activity, by assessing its capability to be bound by specific antibodies. ELISA was carried out on 100 μL of resuspended powders in phosphate buffer, PBS, (5 μg/mL). The plate was put at 4 °C overnight to allow coating, fix of the protein to the well. Thereafter, wells were washed with PBS/Tween 20 0.3% v/v three times and, to avoid nonspecific reaction, 200 μL of 2% v/v skim milk was included for 1 hour at 37°C. Wells were washed other three times, then, a dilution 1:2 of the L2 epitope-specific monoclonal antibody (K4) and polyclonal antibody directed against the *Pf*Trx scaffold in PBS were added to the wells, starting from concentration of 1:5000 and 1:2000 of the two antibodies, respectively. After incubation for 1 hour at 37 °C and three washes, horseradish peroxidase-conjugated goat anti-mouse secondary antibody (Sigma Aldrich, Missouri, USA), previously diluted 1:5000 in PBS was added and the system incubated for another hour at 37°C. Plate was washed three times and developed by adding the ABTS [2,29-azino-bis(3-ethylbenz-thiazoline-6-sulfonic acid)] staining solution (1 mg/ml in 100 mM sodium acetate-phosphate buffer pH 4.2, plus 0.015% H_2O_2; 100 μL/well). Absorbance at 415 nm was measured, after 30 minutes of incubation at 30°C, with an automated plate reader (iMark™ Microplate Absorbance Reader Bio-Rad, California, USA). The analysis of the data was carried out on the base of the cut-off,

namely the baseline on which it could be evaluated at what dilution the values obtained were positive.

Native *Pf*Trx HPV16 L2 antigen was used as positive and negative control: positive adding both antibodies and negative in the wells where was not added neither antibodies (baseline).

3.2.16 *In vivo* and *ex vivo* imaging

In vivo lung deposition of the antigen-containing spray dried powder was assessed by imaging techniques, employing three different instruments: *in vivo* imaging system (IVIS® Spectrum, Perking Elmer Inc., USA), fluorescent molecular tomography (FTM, 2500 Fluorescence Tomography System, Perking Elmer Inc., USA) and micro-computed tomography (μCT, Quantum FX Micro-CT scanner, Perking Elmer Inc., USA) [64].

Alexa Fluor 750, excitation at λ 749 nm and emission at λ 775 nm (Molecular Probes, ThermoFischer Scientific, Massachusetts, USA), conjugated *Pf*Trx HPV16 L2 antigen was prepared according to the manufacturer's instructions and incorporated into a DPI at the maximum affordable level of labelled protein concentration (0.59% w/w of the total solid in the feed solution). The experiment was initially performed with a solution of labelled antigen (40 μg labelled protein in 20 μL of KP buffer + 30 μL water for injection): 50 μL were loaded in a readapted version of Penn Century (Dry Powder Insufflator™-Model DP-4M) to permit intratracheal administration of liquids in one female BALB/c mouse [64,65]. The protocol established visualization at 5, 10, 15 and 30 minutes after the administration, sacrifice of the mouse after 35 minutes and *ex vivo* imaging of lungs, liver, kidneys and spleen with IVIS® Spectrum. Proteins were extracted from frozen tissues and an SDS-PAGE was performed to evaluate the presence of the labelled antigen, reading the gel at λ 800 nm. μCT was performed with 4 minutes of acquisition, at high resolution and no gating strategy.

Later, the same experiment was carried out with the DPI containing the labelled protein on two Balb/c female mice. 2 mg of powder were administered to each animal using a Penn Century device. Visualization was carried out after 5 and 10 minutes from administration and sacrifice after 15 minutes for *ex vivo* IVIS® Spectrum imaging. Lungs and trachea were always frozen for SDS-PAGE. μCT was performed at 15 minutes after administration with the same parameters of the previous experiment.

3.2.17 *In vivo* immune response evaluation

Six- to eight-weeks-old female BALB/c mice (Envigo RMS Inc., United Kingdom) were immunized three times at weekly intervals. Mice were divided in five different groups:

- 3S (7 mice) received subcutaneous administration of 0.05 mL (12 mg/mL, containing 20 μg of antigen) of a saline solution containing *Pf*Trx HPV16 L2 + Alum (50 μg) + GLA (10 μg), (positive control);
- 4S (7 mice) received subcutaneous administration of powder E (1 mg), containing *Pf*Trx HPV16 L2 and GLA, solubilized in 50 μL PBS;
- 5S (5 mice) received subcutaneous administration of a blank spray dried powder (1 mg), containing only mannitol and GLA, solubilized in 50 μL PBS;
- 1T (13 mice) received intratracheal administration of about 2 mg of powder E, containing *Pf*Trx HPV16 L2 and GLA;
- 2T (13 mice) received intratracheal administration of about 2 mg of powder F, containing *Pf*Trx HPV16 L2 OVX313 and GLA.

Intratracheal administration was performed with Penn Century (Dry Powder Insufflator™-Model DP-4M). Before the experiment, the amount emitted from the device was evaluated by weighting the device before and after insufflation, of the vaccine-containing powders. It resulted that about 50% of the loaded powder dose was emitted from the devise. Taking into account this data, 4 mg of each powder (E or F) was loaded in the device during the *in vivo*

immunization. The protocol followed established the collection of pre-immunization serum by submandibular blood sample. After 28 days mice were sacrificed, and sera collected analyzed through GST-L2 ELISA.

GST–L2 ELISA was carried out in 96-well plates pre-coated with coating buffer (1 sodium carbonate 50 mM: 4 sodium bicarbonate 50 mM) added of glutathione-casein (1:500) and incubated overnight at 4 °C protected from light. Then, wells were washed three times with PBS/Tween 20 0.3% v/v and subsequently blocked with 100 μL for each well of casein buffer (PBS/casein 0.2% w/v) and incubated for 1 hour at 37 °C. Glutathione-casein-coated plates were again washed and serial dilution (starting from 1:50) of 100 μL of sera collected from mice were added in the wells and incubated for another hour at 37 °C. Plates were washed again three times, as above, and incubated at 37 °C with 100 μL/well of a horseradish peroxidase-conjugated goat anti-mouse secondary antibody (Sigma Aldrich, Missouri, USA) previously diluted 1:5000 in PBS. After 1 hour, plates were washed three times and developed by adding the ABTS [2,29-azino-bis(3-ethylbenz-thiazoline-6-sulfonic acid)] staining solution (1 mg/ml in 100 mM sodium acetate-phosphate buffer pH 4.2, plus 0.015% H_2O_2; 100 μL/well). Absorbance at λ 415 nm was measured, after 30 minutes of incubation at 30 °C, with an automated plate reader (iMark™ Microplate Absorbance Reader Bio-Rad, California, USA).

Finally, immunoglobulin subclasses in sera from immunized mice were determined by ELISA using a mouse antibody isotyping kit (Pierce Rapid ELISA mouse mAb isotyping Kit; Invitrogen, Thermo Scientific, Massachusetts, USA) following manufacturer's instructions. Absorbance at λ 415 nm was read with a microtiter plate reader (Bio-Rad, California, USA).

3.2.18 Statistical analysis

Values were expressed as mean ± standard deviation. Statistical significance of differences was examined using two-tailed unpaired t-test with significance level fixed at p-value ≤ 0.05.

Statistical analysis was performed with Microsoft Excel version 16.18 (Microsoft Corporation, Washington, USA) and Prism 7 software version 7.0d (GraphPad Software, California, USA).

4. RESULTS AND DISCUSSION

4.1 Choice of a bulk agent employing a fluorescent model protein

The general objective of this PhD project was to develop a platform for pulmonary administration of vaccines. In detail, the aim was to develop a dry powder vaccine formulation to be delivered to the lungs against *human papillomavirus* taken as model pathogen. The development of a vaccine against HPV was conducted in collaboration with the Department of Chemistry, Life Sciences and Environmental Sustainability of the University of Parma, which has the expertise for the production of antigens using recombinant DNA techniques.

The drying of a solution containing a vaccine, or in general every macromolecules of proteinaceous nature, is highly challenging process [66]. First of all, the risk to lose the structure and, consequently, often, the activity, due to drying conditions and especially high temperatures involved in the process [67]. In general, spray drying is a relative aggressive process (air flow rate, high temperature) with high possibilities of denaturation for proteins (degradation, loss of third structure, oxidation etc.), most of them not easily predictable. The risk using proteins are greater compared to small molecules of synthetic origin. A further element to be considered is the fact that, macromolecules are very expensive to obtain and purify. So, they are produced in small quantities, usually too small to implement an effective spray drying process.

The general idea beyond this project was to design and produce vaccine-containing engineered particles for inhalation, via spray-drying, by exploiting a molecular deposition of a lubricant (fatty acids, surfactants, amino acids) on microparticles surface during the particle formation process. To date this technique has been used with aminoglycoside antibiotics (tobramycin and amikacin) [39]. These authors produced highly respirable powders containing a high drug content (99% w/w) with the goal to reduce the amount of powder to be inhaled for each administration and, consequently, the associated side effects. All these characteristics may

result in an increased patient convenience and therapeutic efficacy. However, several issues have to be addressed in order to apply such a technique to the production of a vaccine-containing powder. The first issue refers to the need to use a water-ethanol solution in order to dissolve the lubricant which is lipophilic in nature.

The second issue is the amount of solid content in the feed solution to obtain a powder at the end of the spray drying process. As a matter of facts, in the common case of a vaccine constituted by an antigenic protein, the increase of the concentration of the antigen-containing solution after the protein expression or after post-translational modifications very often results in protein aggregation and precipitation. For this reason and, overall to avoid the protein aggregation/denaturation during the solid particle formations, a bulking agent has to be added to the feed solution.

Both these issues were addressed in a preliminary study using a fluorescent protein, cheaper, easier and faster to produce. For this purpose, the E2-Crimson protein was selected. This is a basic far red fluorescent protein derived from *Discosoma sp*., a family of marine cnidarian related to sea anemones. This protein is reported to be noncytotoxic in bacterial and mammalian cells [68] with an excitation maximum at λ 611 nm and emission at a λ of 646 nm. E2-Crimson is commonly employed in flowcytometry and, in general, in the microscopy field.

First of all, the effect of the pH of the solution on the protein stability was assessed. Table 4.1 shows the residual percentage of active protein as a function of the pH of the dissolving buffer (Figure 4.1). These values were calculated from emitted fluorescence measurements. It can be appreciated that the protein was stable only at neutral or slightly basic pH (from about pH 6 to about pH 8).

Table 4.1. Emitted fluorescence and relevant residual activity of E2-Crimson solution at different pH. Mean value and standard deviation in parenthesis (n=3).

pH	Emitted fluorescence	Active protein (%)
1.4	2.00 (0.00)	-1.01
4.3	2.00 (0.00)	-1.01
5.2	23.00 (1.73)	-0.98
5.8	50223.33 (182.38)	99.90
6.6	50320.00 (36.43)	100.00
7.7	50259.67 (119.30)	100.00
8	50259.67 (547.51)	100.00
10.6	10970.67 (547.51)	16.86
11	20.67(0.58)	-0.98

Figure 4.1 E2-Crimson solutions in buffer KP at different pH. From left to right: pH 1.4; 4.3; 5.2; 5.8; 6.6; 8; 10.6; 11.

Before starting the investigation of the effect of the bulking agent on the obtained powder characteristics a study on the denaturation of E2-Crimson in solution containing different percentage of ethanol (from 5 to 50% v/v), was carried out by fluorometry (Figure 2, panel A). The figure evidenced a progressive decrease of the protein fluorescence as a function of the

ethanol concentration in the solution. Taking into consideration these results and the need to have at least a limited amount of ethanol in solution to allow the lubricant (sodium stearate) dissolution, 5% v/v of the organic solvent was selected to prepare the feed solution; consequently, taking into consideration the sodium stearate solubility in this water-ethanol solution, a 0.002% w/v solution was prepared. This solution contained an amount of sodium stearate corresponding to 0.33% w/w of the solid in the feed solution (slightly soluble, [69]). A first approximation of protein concentration equal to that of sodium stearate was selected for the preparation of the feed solutions. These resulted in a balking agent concentration of 0.595% w/v (99.34 % on the weight of the solid).

Three different bulking agents, two sugars and a polyalcohol, namely lactose, trehalose and mannitol were chosen and tested in terms of their capability to maintain the protein stability, to afford suitable yield and *in vitro* aerodynamic performance. Taking into account the finding reported in Table 4.1, namely the fact that the pH value of the solution might be a possible cause of protein degradation, the pH of the three solutions before and after the spray drying process was measured. In all the cases pH values between 7.2 and 8 were obtained.

As for the yield of the process, the highest value was obtained for the powder containing mannitol (54.7%), being 42.6% and 38.7% the values obtained for the powder containing lactose and trehalose respectively. Compared to available literature, the yield of the mannitol-containing powder could be considered relatively good [70].

However, E2-Crimson was highly degraded in all the powders produced, with the minimum fluorescence value reported for the powders containing mannitol (Figure 2, panel B). Anyway, the florescence peak at 640 nm was not present also in the other two formulations, indicating that E2-Crimson was not fluorescent anymore after the spray drying process.

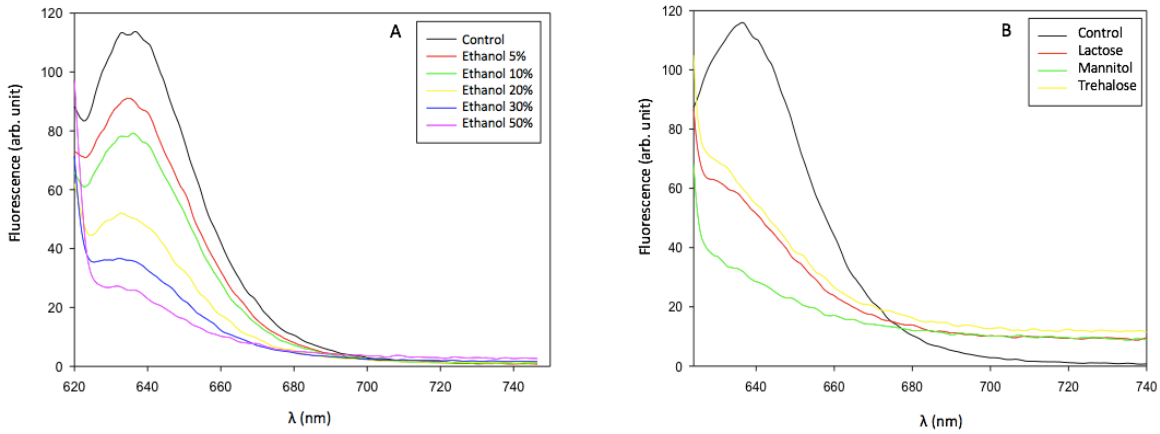

Figure 4.2. Fluorescence (λ=640 nm) of E2-Crimson in presence of different percentage of ethanol (panel A) and in the spray dried powders produced with different bulking agents (panel B).

Nevertheless, the powders produced were also studied for their aerodynamic performances. Table 4.3 reports the values obtained. The Emitted Fraction (EF) was high (> 80%) for all the spray dried powders, indicating that microparticles had a good flowability and were well emitted from the device used for the test. On the contrary, a big difference among the three formulation as to amount of powder deposited on the filter (mg of powder < 5 μm, Respirable Mass, RM) was noticed: the values were very low for lactose and trehalose with a Respirable Fraction (RF) even < 5%; in these cases all the microparticles were trapped in the Induction Port or in the Coarse Fraction Collector. For the powders containing the two sugars, the device was not able to deagglomerate the particles. These data, along with those relevant to the emitted fraction, may indicate that the powder was likely constituted by aggregates of microparticles or particles with relatively large dimensions. This assumption is supported by the particle size distribution analysis (Figure 4.3): lactose and trehalose undersize cumulative curves presented many inflection points, that pointed out the presence of different particle populations (average span values: 3.01 ± 0.22 and 3.81 ± 1.37 for lactose and trehalose powders respectively). A completely different RF value (57.55%) was obtained for the powder containing mannitol. For this formulation the volume diameters were: $D_{v,10}$ 2.24 ± 0.02 μm, $D_{v,50}$ 8.45 ± 1.74 μm and

$D_{v,90}$ 16.56 ± 2.07 μm with a span value of 1.71 ± 0.11. The distribution was narrower and monomodal, with a median volume diameter < 10 μm.

Table 4.3. Aerodynamic parameters for the powders containing the three bulking agents. Data were determined by weighting. Mean value and standard deviation in parenthesis (n=3).

Powder	Emitted mass (mg)	Emitted fraction (%)	Rspirable mass (mg)	Respirable fraction (%)*
E2-Crimson/lactose	8.65 (1.34)	85.96 (13.53)	0.35 (0.21)	3.48 (2.11)
E2-Crimson/mannitol	8.17 (0.75)	80.98 (7.23)	5.80 (1.04)	57.55 (12.22)
E2-Crimson/trehalose	9.85 (0.07)	97.57 (0.91)	0.15 (0.07)	1.49 (0.70)

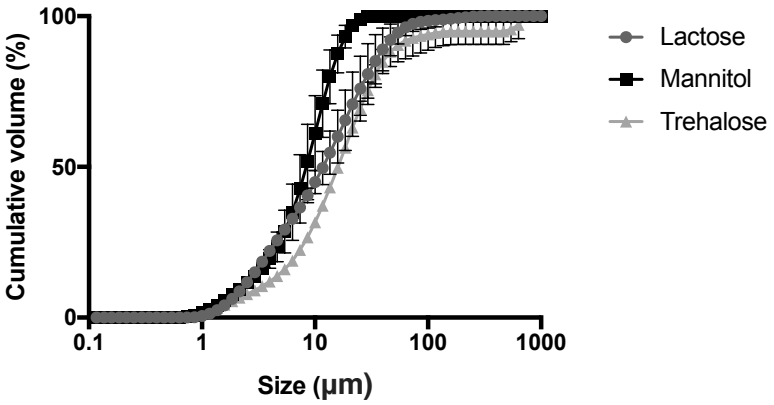

Figure 4.3. Cumulative undersize particle distribution evaluated by laser light diffraction of the E2-Crimson spray dried powders containing lactose (circle), mannitol (square) and trehalose (triangle). The bars represent the standard deviation (n=3).

Thus, mannitol was pre-selected as the best bulking agent for further developments because the powder produced with mannitol was the one reporting the highest yield and the best aerodynamic characteristics whereas the protein chemical stability was poor for all the tested bulking agents, likely due to the protein was extremely sensitive to the drying process.

4.2 *Pf*Trx HPV16-L2 stability in hydro-alcoholic solutions

Then, we moved to the following part of this work handling directly the vaccine against HPV. The novel vaccine studied was described in the papers of Rubio et al. and Canali et al. [24,71]. These authors developed a new molecule starting from *human papillomavirus* minor capsid protein L2. This capsid protein contains polypeptides regions more conserved among the 15 carcinogenic mucosal HPV types, but it is less immunogenic compared to the major capsid protein L1. Nevertheless, it has been investigated as a valuable antigen by many research groups for the development of a broadly protective HPV vaccine [72-78].

Rubio I. et al. [71], using the Thioredoxin Displayed Multipeptide Immunogens (TDMI), scanned the N-terminal (amino acids residues 1–120) region of HPV16 L2 and identified a 19 amino acids L2 peptide (segment 20–38) that, upon tandem multimerization within the display site of *Escherichia coli* thierodoxin A (*Ec*Trx), acquired strong immunogenicity and elicited the production of polyclonal as well as monoclonal antibodies capable of cross-neutralizing multiple high-risk HPV types. In a following work, Canali et al. [24] reported the production of a > 90% pure form of the same antigen type in a *Pyrococcus furiosus* thierodoxin A (*Pf*Trx) scaffold with a one-step thermal purification procedure, developing a safer and more effective immunogenic protein, highly thermostable (the protein resisted unmodified at a temperature of about 95°C), less cross-reactive and, last but not the least at low cost. The predicted 3D structure of this antigen (*Pf*Trx HPV16 L2), is shown in Figure 4.4: the HPV16 L2 (20-38) peptide (the epitope which binds the antibody) repeated three times and the *Pf*Trx scaffold can be appreciated.

*Pf*Trx HPV16 L2 was the antigen employed for the development of the formulation in form of dry powder for inhalation in this work.

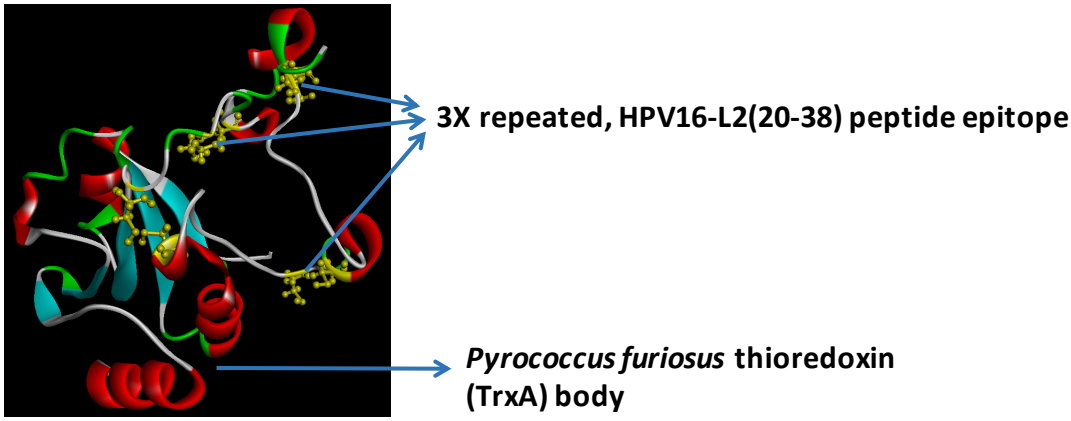

Figure 4.4. 3D predicted structure of the vaccine *Pf*Trx HPV16 L2 (courtesy of S. Ottonello and G. Spagnoli, University of Parma).

As already done for the E2 Crimson protein, the stability of the antigen in water-ethanol solutions was firstly studied by employing far-UV circular dichroism, in order to identify whether there was a change in the secondary structure of the protein as a consequence of the contact with ethanol. Figure 4.5 illustrates the obtained curves after 10 minutes from the addition of ethanol. The protein secondary structure was completely conserved (overlay of the curves) in solutions containing up to 15% v/v of ethanol; from 20 to 50% v/v the protein presented very light, and likely reversible, changes in the structure; after 10 min in 70% v/v ethanol some secondary structures changed, but the protein was not denatured. In fact, the curve presented the same trend of the others, but with lower values of absorption: it was hypothesized a loss of some hydrogen bonds, due to a less competition with water, and/or α-helices or β-sheets structures already present, which determined a more constrained structure in a more hydrophobic environment [79]. The analysis was repeated for the same samples after 30 min and the results were comparable to the previous analysis. Moreover, the process was reversible, because diluting hydroalcoholic solution from 50% to 25% v/v it was possible to reobtain a curve completely overlaid to the others. So, it was possible to conclude that the protein was substantially stable in solutions containing ethanol up to 70% v/v.

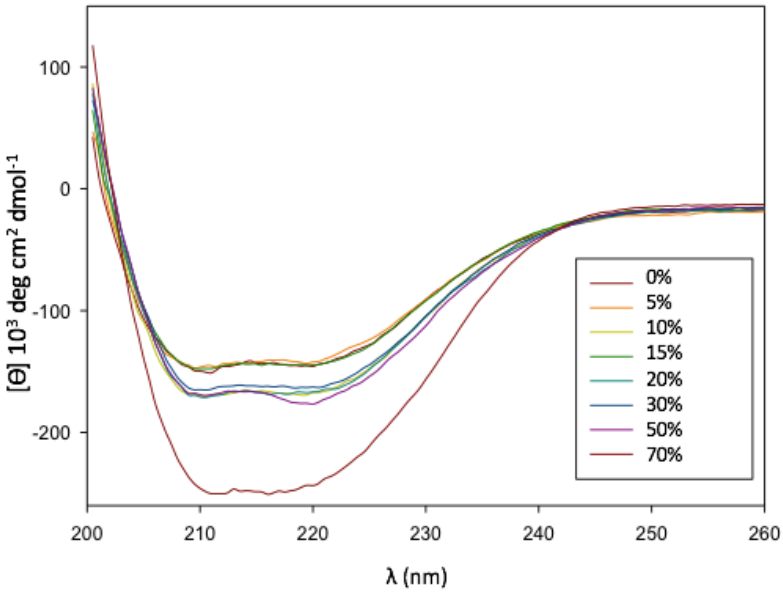

Figure 4.5. Far-UV circular dichroism curves, for the antigen *Pf*Trx HPV 16 L2 in hydro-alcoholic solutions at different ethanol percentages.

Typically, but not always, the loss of the secondary structure is correlated to the loss of the activity [80].

To evaluate the maintenance of the activity of the antigen after exposure to hydro-alcoholic solutions, an ELISA test was performed in order to assess whether the antigen was still recognized by the specific antibodies. The test was executed using two different antibodies, able to recognize and bind the scaffold (anti-*Pf*Trx) and the epitope (K4, anti-L2 (20-38) respectively.

The suitability of the method was preliminarily assessed by testing the capability of the ELISA to put into evidence the reduction of the protein activity as a consequence of protein modification (either physical or chemical) induced by heating at 98 °C and exposure to 10 mM of β-mercaptoethanol for 24 hours. Figure 4.6 reports the binding of the native and heat-treated vaccine with the two antibodies. Changes were better evident for the scaffold portion whereas the epitope was still able to be bound by the specific monoclonal antibody K4.

The solution tested for the circular dichroism analysis were submitted to the ELISA as well. The Figure 4.7 shows that the protein was stable in all the tested solutions as indicated by the fact that the bind of both antibodies was comparable to the control (the antigen not treated). These data indicated that the antigen *Pf*Trx HPV16 L2 was perfectly stable in hydroalcoholic solutions, up to 50% v/v of ethanol. Therefore, a water:ethanol 70:30 v/v solution was selected to be utilizes as solvent for the production of the respirable microparticles containing the *Pf*Trx HPV16 L2 antigen. Incidentally this was in complete agreement with the prescription of Parlati et al. [39].

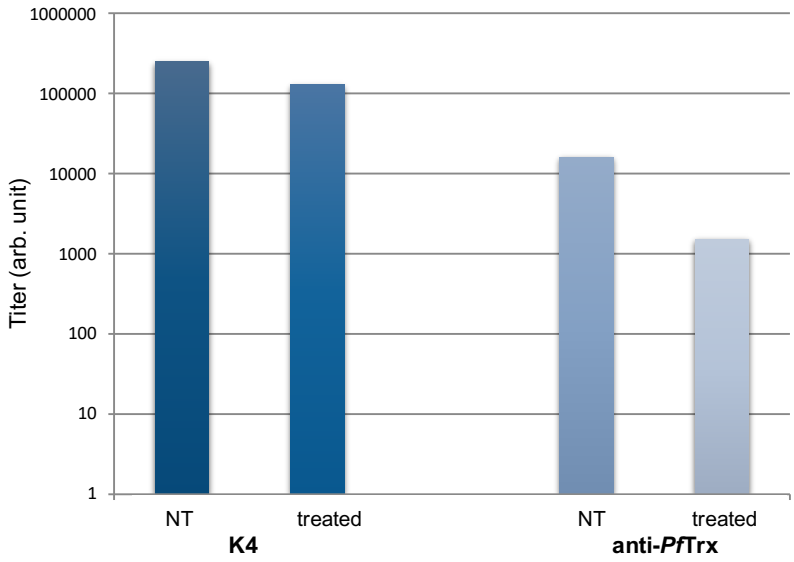

Figure 4.6. Binding capability between the native (NT) and heat-treated antigen with the two antibodies (Anti-*Pf*Trx and K4).

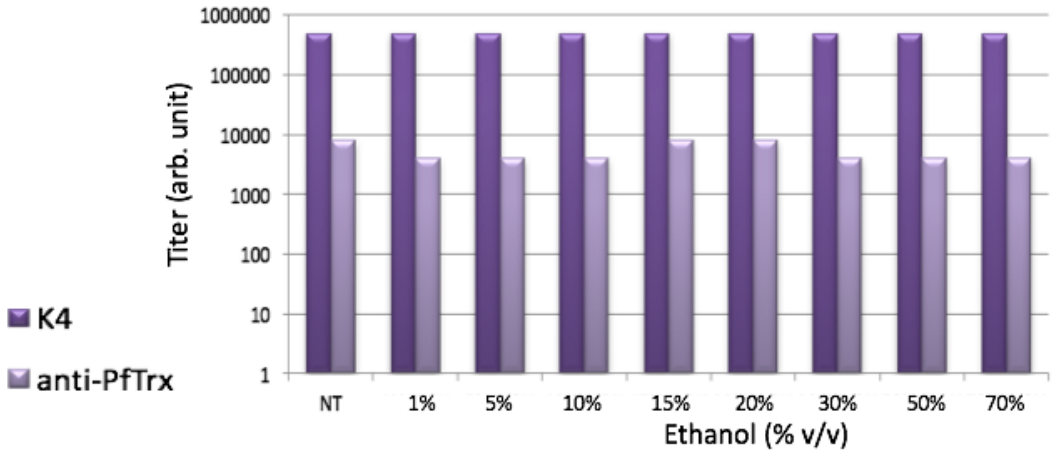

Figure 4.7. Binding capability of the antigen *Pf*Trx HPV16 to the two antibodies (anti-*Pf*Trx and K4) after exposure to hydro-alcoholic solutions at different ethanol percentages.

4.3 Production and characterization of spray dried powders with different percentages of surfactant

Thus, four new formulations of the antigen, with mannitol as bulking agent, were produced by spray drying (Table 4.4). In this second formulation study the best percentage of surfactant, sodium stearate was investigated, in order to obtain respirable microparticles. All the feed solutions (100 mL) contained 2 mg of *Pf*Trx HPV16 L2 (0.33% by weight of solid content of the solution) and increasing amounts of sodium stearate. Thus, 2 mL of a heat purified 1 mg/mL antigen solution in tris-buffered saline (TBS, Tris 25 mM, NaCl 30 mM) were added to the water fraction of the feed solution. Ethanol content was kept constant at 30% v/v, except for the powder without the surfactant, which was produced from an aqueous solution. The powder with a ratio 1:1 between the antigen and the surfactant afforded the lowest yield (31.53%), while the highest yield (59.46%) was obtained using 2% (of the weight solid content of the solution) of sodium stearate, indicating that an increased amount of surfactant, improved the deposition of the powder in the spray dryer collector, likely due to the formation of a lower amount of extra-fine particles escaping the cyclone. In the formulation without sodium stearate the yield was good, about 55%, although it should be underlined that this condition (absence of the component with high vapor pressure) somehow modified the evaporation rate of the solvent and the consequent particle formation. The pH of the solution before the spray drying ranged from slightly acid to slightly basic and so was pH of the solution obtained by dissolving the spray dried powder in ultrapure water (6.44-7.51). According to Talley et al. this pH values are suitable for guaranteeing the activity and stability of the protein [81].

Table 4.4. Composition (% of the weighted solid content of the solution), production yield and pH of the feed solutions.

Powder #	Sodium Stearate	Concentration of mannitol	pH of feed solution	Yield (%)
1	-	99.67	5.89	54.63
2	0.33	99.34	5.88	3.53
3	1	98.67	7.94	43.72
4	2	97.67	8.14	59.46

The aerodynamic performance of these powders was studied with the Fast Screening Impactor (Figure 4.8). The amount of the surfactant influenced the RF: in particular, with 0.33% (powder 2) and 2% w/w (powder 4) of sodium stearate RF was only 8-14% of the loaded mass. However, the flowability of the powders, as indicated by the EF (75%, 90%, 94% for powders 2, 3 and 4 respectively), increased with the amount of surfactant. As previously reported by Parlati et al. and Buttini et al. [39,82], the best performing powder was the one with 1% w/w of sodium stearate (number 3) (RF = 48.10% ± 9.39). Parlati et al. reported that the *in vitro* deposition correlated with the sodium stearate content following a parabolic behavior with the maximum value around 1% w/w of surfactant. At 1% w/w the hydrophobic chains of sodium stearate were preferentially distributed at the air/water interface.

Figure 4.9 shows the relation between RF and the percentage of sodium stearate in the powder. The profile obtained for the powders prepared from the ethanol containing solutions could be described with a quadratic equation (parabolic) in agreement with the findings of Parlati et al. Interestingly and differently from what reported by Parlati at al. the values collected for the powder spray dried without surfactant did not fall into the parabolic interpolation. This can be explained by considering that the solution used for the production of this powder did not contain ethanol, thus confirming what previously stated with respect to the change of the drying rate and conditions in this specific case.

The particle size distribution analysis (Figure 4.10) reported the lowest median volume diameter for powder number 3 (3.41 ± 0.73 μm). $D_{v,50}$ for formulation 1 was, instead, > 5 μm (6.16 ± 0.78 μm). However, this value was much lower than those showed by powders 2 and 4, that presented particle size distributions shifted toward higher values.

The process parameters set allowed for to producing a good respirable *Pf*Trx HPV16 L2-mannitol powder (particles < 5 μm and RF around 48% of the loaded dose).

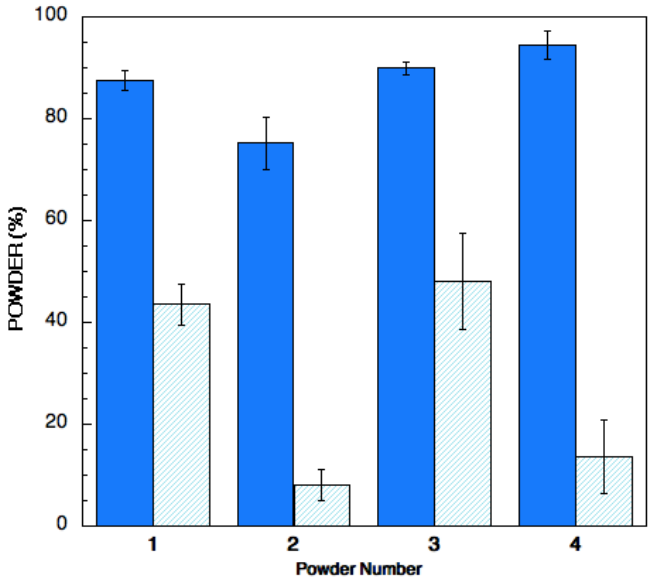

Figure 4.8. Aerodynamic parameters, Emitted (EF, blue bar) and Respirable Fraction (RF, light blue bar), of the four powders prepared with increasing amount of sodium stearate. The bars represent the standard deviation (n=3).

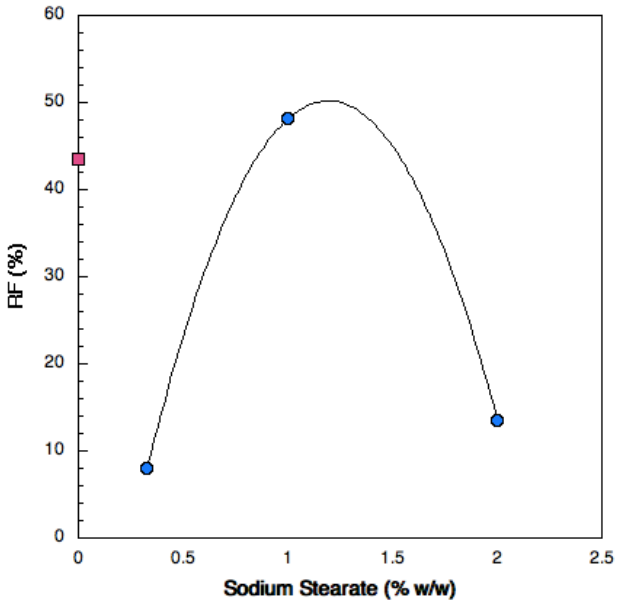

Figure 4.9 Relationship between initial sodium stearate concentrations (% of the weighted solid content of the solution) and respirable fraction (RF %) of the powders.

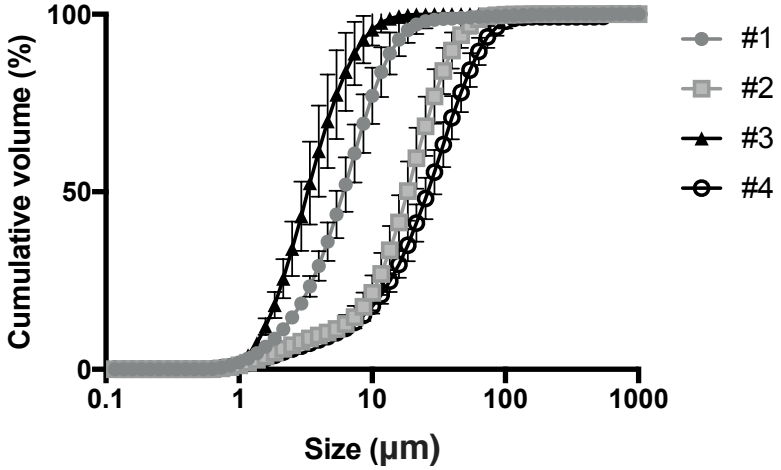

Figure 4.10. Particle cumulative undersize distribution evaluated by laser light diffraction of the spray dried powders produced number 1 (full circle); number 2 (square); number 3 (triangle) and number 4 (empty circle). The bars represent the standard deviation (n=3).

These four powders were analyzed using SDS-PAGE to visualize the presence of the protein in the spray dried powders and its content. The powders were compared with the protein not treated tested in an amount equal to the theoretical value of the antigen in the spray dryed powders (0.33% w/w). The intensity of the bands was the same of the control, as shown in Figure 4.11. Moreover, the protein was in its native conformation, as indicated by the fact that

the bands were at the same height of the control sample, corresponding to the antigen molecular weight (18 kDa).

The capability of the antigen in the products to be recognized by the specific monoclonal (anti-L2, K4) and polyclonal (anti-*Pf*Trx) antibodies was tested using ELISA. The samples reported the same titer of the control (Figure 4.12).

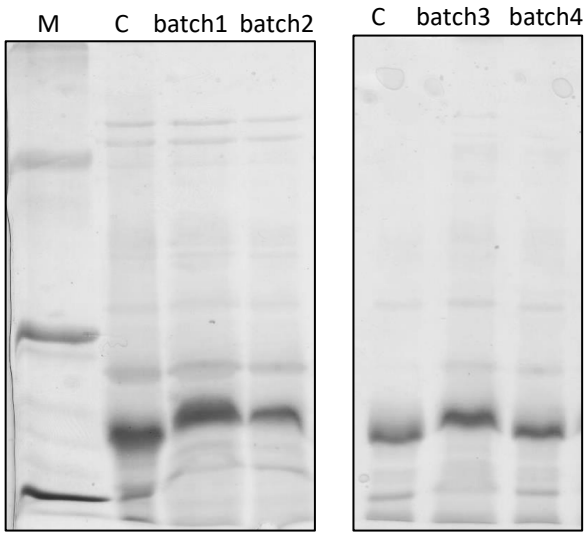

Figure 4.11. Picture of SDS-PAGE gels used to identify and quantify *Pf*Trx HPV16 L2 antigen in different batches (1-4) of the spray dried powder #1 (5 µg of antigen was loaded for the control (C) and for powders; M = marker of different molecular weights).

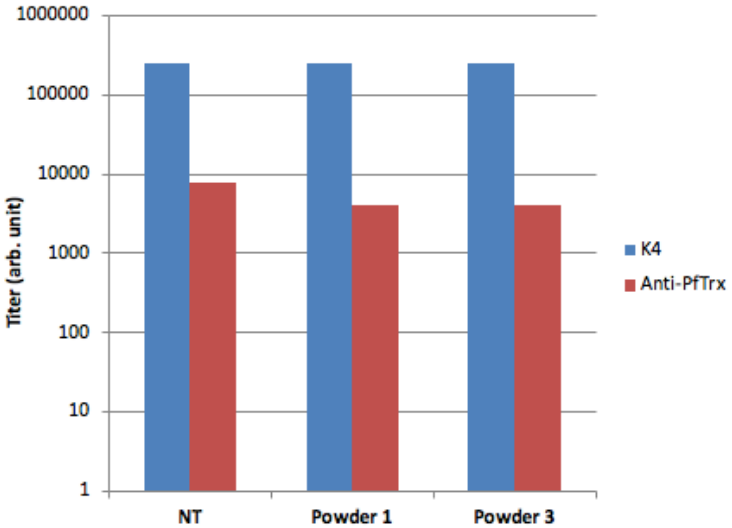

Figure 4.12. Binding capability of PfTrx HPV16 L2 antigen contained in the spray dried powders 1 and 3 to the monoclonal antibody K4 and polyclonal antibody anti-scaffold (anti-*Pf*Trx) in comparison to the untreated antigen (NT).

4.4 Design of experiment to investigate the influence of the type of protein buffer on the spray drying process

The subsequent step was to increase the content of antigen in the dried formulation. Therefore, four other powders were produced, taking the previous best formulation (number 3) as model. These powders contained 0.5, 0.83 or 1.33% w/w of protein, respectively, and were prepared from the same starting antigen solution in TBS. However, a dramatic decrease of the production yield was obtained (Table 4.5), with almost nothing deposited in the spray dryer collector (0.13%) for the powder with a protein concentration of 1.33% of the weighted solid content of the solution (#3C). The dried powders were completely deposited in the cyclone or in the drying chamber (Figure 4.13). The *in vitro* aerodynamic performance (Table 4.5) evidenced that also the respirable fraction decreased by loading a higher amount of antigen.

However, the explanation of this behavior was not the higher content of protein, but the type and higher volume of buffer, stabilizing the protein, added to the feed solution, which increased the total amount of salts in the latter (from 1.59% w/w of the total solid added to the feed solution in the powders #1 and 3 to 6.38% w/w in #3C). The small amount of the dried product deposited in the collector may be ascribed to the crystallization of salts, in particular to sodium chloride, during the process [83,84].

Table 4.5. Composition, production yield and aerodynamic parameters for the powders with loading amount of antigen (n=3, * 1 run with powder collected from the spray drier collector and 2 runs with powder from the cyclone) (** n=2, with only powder collected from the cyclone). Mean value and standard deviation in parenthesis.

Powder #	**Antigen content (% w/w)**	**Yield in the collector (%)**	**Yield in the cyclone (%)**	**EF (%)**	**RF (%)**
3A	0.5	55.72	-	89.72 (9.02)	59.55 (16.11)
3B	0.83	4.34	34.9	89.53 (5.04)*	40.38 (5.55)*
3C	1.33	0.13	7.29	87.80 (11.25)**	13.40 (0.81)**
1B	0.83	5.10	28.56	87.69 (12.92)*	34.37 (34.01)*

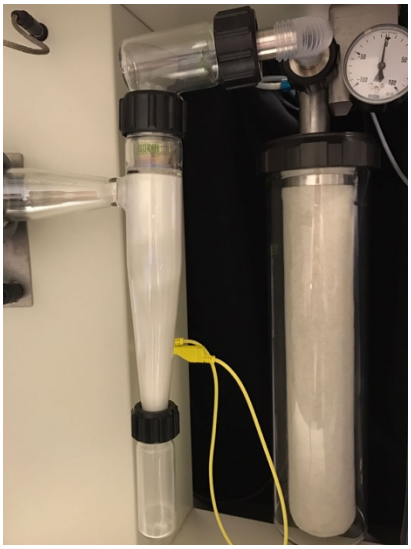

Figure 4.13. Spray drier B-290 collector and cyclone after drying of formulation with a protein content of 0.83% of the weighted solid content of the feed solution (Powder 3B).

To better investigate the influence of the type of buffer used on the spray drying process a half-Fractional Factorial Design (FFD) of experiment was performed. The design matrix (Table 4.6) was constructed and analyzed with two different software The Unscrambler® and Minitab® and reported 10 experiments. The design space was built up by investigating 4 Critical Process Parameters (CPPs): 1) type of buffer, namely TBS (tris-buffered saline, Tris 25 mM, NaCl 30 mM pH 7.4) or KP (phosphate buffered saline, potassium phosphate 25 mM, pH 7.4); 2) drying inlet temperature (110°C or 125°C); 3) aspiration (30 m^3/h or 35 m^3/h) and 4) feed rate (3.5 mL/min or 4.5 mL/min). The values were chosen based on the process parameters used for the powders already dried and on their usually influence on the product characteristic [85]. The Critical Quality Attributes (CQAs) used as indicators of quality of the product were: yield of the spray drying, emitted fraction from the device (EF), respirable fraction (RF) and mean volume diameter ($D_{v,50}$). All the 10 experiments were performed using only buffer without the antigen, due to its significant production cost.

Table 4.6. Design matrices obtained with the software The Unscrambler® and Minitab® and values set for each experiment; in bold the central points with the two different buffers, but same process parameters are reported.

#The Unscambler®	#Minitab®	Buffer	Inlet Temperature (°C)	Aspiration (m^3/h)	Feed Rate (mL/min)
1U	3M	KP	125.0	30.0	3.5
2U	4M	KP	110.0	35.0	3.5
3U	9M	KP	110.0	30.0	4.5
4U	**2M**	**TBS**	**117.5**	**32.5**	**4.0**
5U	10M	KP	125.0	35.0	4.5
6U	5M	TBS	110.0	30.0	3.5
7U	**6M**	**KP**	**117.5**	**32.5**	**4.0**
8U	1M	TBS	125.0	30.0	4.5
9U	7M	TBS	110.0	35.0	4.5
10U	8M	TBS	125.0	35.0	3.5

The yield of the spray drying process was taken as the first quality attribute, due to the outcome of the staring study. The yield was evaluated in the collector and in the cyclone (Table 4.7). The powder with the highest total yield was #8U-1M (70.16%); despite, most of the powder was collected in the cyclone (55.20%). #8U-1M contained TBS; the lowest total yield was obtained in experiment #4U-2M (57.79%), despite the difference between the two fractions collected was less pronounced. The amount of powder deposited in the cyclone or in the collector of the spray dryer was different in the 10 experiments. The results are mostly associated to the type of buffer (Figure 4.14). The experiments #4U-2M, 6U-5M, 8U-1M, 9U-7M, 10U-8M reported the highest amount in the cyclone fraction (> 35%). They were all powders containing TBS; so, this type deposition can be ascribed to the presence of sodium chloride in the buffer. Among TBS powders, #4U-2M, gave rise to the lowest yield in the cyclone, non the less it did not report the highest yield in the collector. The latter was obtained with #9U-7M (25.25%). For this experiments the parameters used were the lowest drying

temperature (110°C), higher aspiration (35 m^3/h) and feed rate (4.5 mL/min), suggesting that these conditions were able to minimize salts crystallization.

As to the experiments carried out with KP as buffer, the yield in the collector was between 16.75% (#3U-9M) and 61.28% (#1U-3M), this value was also the highest obtained between all powders produced. #1U-3M presented the smallest yield in the cyclone (2.36%). It is wort underlying that the process parameters were the same adopted for TBS-containing powders, thus the observed differences in the obtained yield were, evidently only then consequence of the different composition of the buffer.

Table 4.7. Yield of the production processes of the 10 experiments expressed as total and yields of the cyclone and of the collector.

#Unscrambler® #Minitab®	**Total yield (%)**	**Yield in the cyclone (%)**	**Yield in the collector (%)**
1U-3M	63.65	2.36	61.28
2U-4M	61.81	7.52	54.29
3U-9M	66.74	16.75	49.98
4U-2M	57.79	36.04	21.74
5U-10M	63.06	7.25	55.83
6U-5M	66.05	53.52	12.52
7U-6M	61.90	6.02	55.87
8U-1M	70.16	55.20	14.94
9U-7M	68.58	43.31	25.25
10U-8M	62.08	49.55	12.53

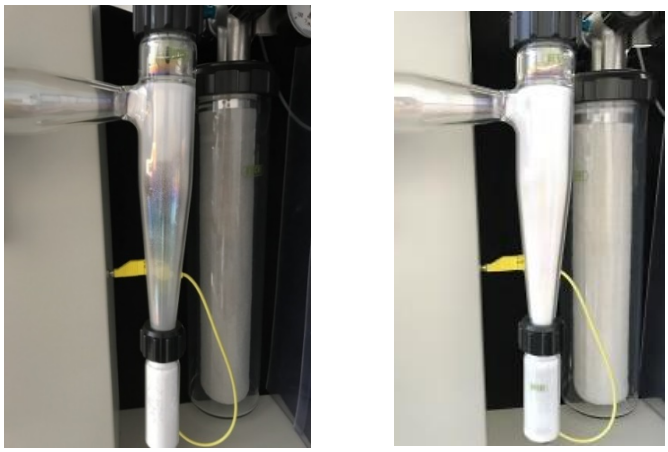

Figure 4.14. Images of the deposition in the cyclone and in the collector for the experiment 1U-3M, on the left, and 8U-1M, on the right.

The mean volume diameters obtained for the fraction of powder deposited in the collector were smaller those of the powder in the cyclone. Except for #8U-1M and #3U-9M, $D_{v,50}$ was always smaller than 5 μm, whereas, $D_{v,90}$ of all the experiments was highly variable (7.40-27.76 μm). This characteristic was not always connected to the type of buffer employed, but more to the process parameters (i.e. #2U-4M, 1U-3M and 3U-9M, all produced with KP, presented $D_{v,90}$ of 7.40, 11.00 and 27.76 μm, respectively). The drying aspiration influences the particle size values obtained: the use of 35 m^3/h aspiration allowed to drag the dried particles faster, reducing aggregation phenomena [85]. #2U-4M was also the powder with the lowest volume diameters for the cyclone-deposited fraction and presented a distribution closer to be monodispersion, showing the smallest span values (1.61).

Finally, powders #9U-7M and #10U-8M were the only ones presenting similar volume diameters between the two fractions. Moreover, experiment #9U-7M, even though it was produced with TBS, had the smallest $D_{v,50}$ for the cyclone-fractions. Oppositely, #4U-2M exhibited completely different particle distributions between the two fractions ($D_{v,50}$ = 18.02 μm in the cyclone fraction vs 3.88 μm in the collector fraction). This result is not surprising as according to Mosèn et al., the smallest particle distribution deposit in the collector [86].

Table 4.8. Volume diameters of 10th ($D_{v,10}$), 50th ($D_{v,50}$) and 90th ($D_{v,90}$) percentile of the particle population for the 10 experiments analyzed by laser diffraction. Mean value and standard deviation in parenthesis (n=3).

#Unscrambler® #Minitab®	Volume diameters of cyclone-deposited powder (μm)			Volume diameters of collector-deposited powder (μm)		
	$D_{v,10}$	$D_{v,50}$	$D_{v,90}$	$D_{v,10}$	$D_{v,50}$	$D_{v,90}$
1U-3M	2.34 (0.05)	7.99 (0.35)	43.84 (18.03)	1.66 (0.13)	4.12 (0.80)	11.00 (0.98)
2U-4M	2.11 (0.01)	5.21 (0.22)	9.29 (0.43)	1.63 (0.06)	3.74 (0.10)	7.40 (0.31)
3U-9M	3.17 (0.15)	14.34 (0.75)	50.71 (14.20)	2.34 (0.09)	9.82 (0.35)	27.76 (1.40)
4U-2M	2.33 (0.01)	18.02 (1.12)	55.71 (0.36)	1.47 (0.09)	3.88 (0.26)	7.06 (0.68)
5U-10M	2.04 (0.01)	6.12 (0.02)	16.81 (0.84)	1.77 (0.01)	4.70 (0.08)	20.18 (0.88)
6U-5M	2.00 (0.05)	5.21 (0.09)	10.64 (0.45)	1.66 (0.00)	4.50 (0.04)	10.10 (0.10)
7U-6M	2.36 (0.01)	7.46 (0.03)	22.56 (0.78)	1.66 (0.01)	4.07 (0.03)	7.99 (0.07)
8U-1M	2.13 (0.12)	6.29 (0.61)	15.65 (2.54)	1.97 (0.25)	7.63 (0.54)	19.62 (0.51)
9U-7M	2.01 (0.12)	5.74 (0.40)	13.80 (1.54)	1.62 (0.01)	3.39 (0.01)	12.56 (0.63)
10U-8M	1.81 (0.07)	4.84 (0.18)	11.18 (0.17)	1.78 (0.03)	4.78 (0.24)	11.63 (0.83)

The last feature investigated was the aerodynamic performance (Table 4.9). The emitted mass was higher for all the experiments, with EF between 75-90% being the #7U-6M collector-deposited powder the one with the lower value (EM = 7.77 mg). The fine particle fraction exhibited quite a large variability (Figure 4.15). RF was higher for the powders in the collector (ranging from 50 to 90%) compared to the powders in the cyclone (from 35 to 60%). In this study, RF was calculated on the emitted and not on the loaded mass, otherwise some of the values collected would have been too close to zero. #3U-9M was the powder with the lowest RM in both the fractions (for the cyclone = 3.00 mg and for the collector = 4.47 mg). The best performing powder for the cyclone fraction, in terms of RF, as already seen for the yield, was #1U-3M (8.23 mg corresponding to 92.52% of the emitted mass).

Table 4.9. Emitted (EM) and Respirable Mass (RM) measured by weight of the powder collected in the cyclone or in the collector, separately (n=3, mean value and standard deviation in parenthesis). For #1U-3M it was not possible to perform the test for the cyclone-deposited fraction, because the amount collected was not enough.

	Cyclone		**Collector**	
#Unscrambler® #Minitab®	**EM (mg)**	**RM (mg)**	**EM (mg)**	**RM (mg)**
1U-3M	-	-	8.90 (0.10)	8.23 (0.15)
2U-4M	9.27 (0.83)	4.47 (0.25)	9.17 (1.20)	5.30 (1.00)
3U-9M	8.63 (1.20)	3.00 (0.46)	8.77 (1.01)	4.47 (1.59)
4U-2M	8.00 (1.92)	3.60 (1.95)	8.07 (0.47)	4.80 (2.57)
5U-10M	9.13 (1.19)	5.57 (1.50)	8.60 (0.10)	6.40 (1.15)
6U-5M	9.60 (0.00)	5.43 (1.01)	8.97 (0.55)	5.03 (0.92)
7U-6M	8.40 (0.30)	4.83 (0.25)	7.77 (1.67)	6.27 (1.66)
8U-1M	8.37 (1.19)	5.03 (1.55)	8.07 (0.64)	4.73 (0.06)
9U-7M	8.70 (0.44)	4.57 (0.80)	8.63 (1.06)	6.60 (2.36)
10U-8M	8.37 (0.46)	4.97 (0.57)	8.60 (1.06)	4.70 (0.10)

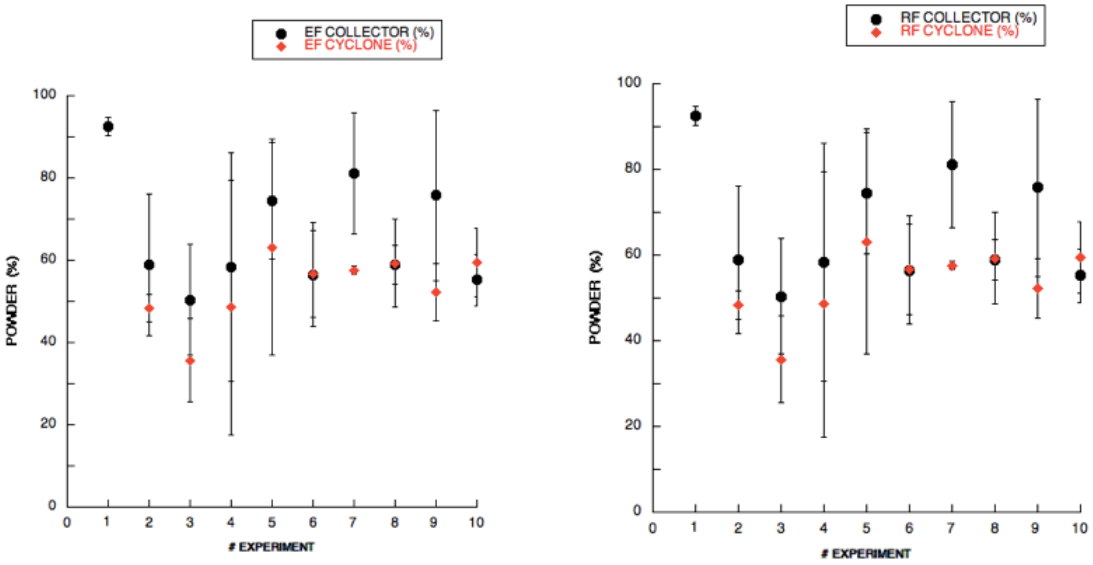

Figure 4.15. Emitted (EF) and Respirable Fraction (RF) of the 10 experiments (numeration for Unscrambler®). The bars represent standard deviation (n=3).

The data collected were successively analyzed with the two software The Unscrambler® and Minitab®. The Unscrambler® reported the statistical significance levels, through analysis of variance (ANOVA), for each CQAs varying the process parameters studied individually or as 2-way interaction (i.e. how the quality attribute depended on the contemporary variation of two the parameters). Significant values (p-values ≤ 0.05) were registered only for yield and RF of the collector fraction. Regarding the yield, there was a significant correlation with the type of buffer ($p = 0.05$; F calculated >> F table). For the RF, the variation of all CPPs (buffer salts, drying temperature, aspiration and feed rate) was significant ($p = 0.03$). Moreover, three different 2-way interactions were significant: buffer type-inlet temperature ($p = 0.03$); buffer type-aspiration ($p = 0.03$) and inlet temperature-aspiration ($p = 0.03$).

Figures 4.16 and 4.17 show the correlation between inlet temperature and aspiration on RF variation, employing KP or TBS respectively. The best RF (red zone) was associated with high inlet temperature (125°C) and low aspiration (30 m^3/h) for KP, on the contrary, with TBS lower drying temperature (110°C) and higher aspiration maximum (35 m^3/h) were required to maximize the RF. The presence of sodium chloride in TBS influenced the RF of the collector powder: low inlet temperature, maximum aspiration and high feed rate (experiment #9U-7M), decreased the crystal growth of salts [83,84].

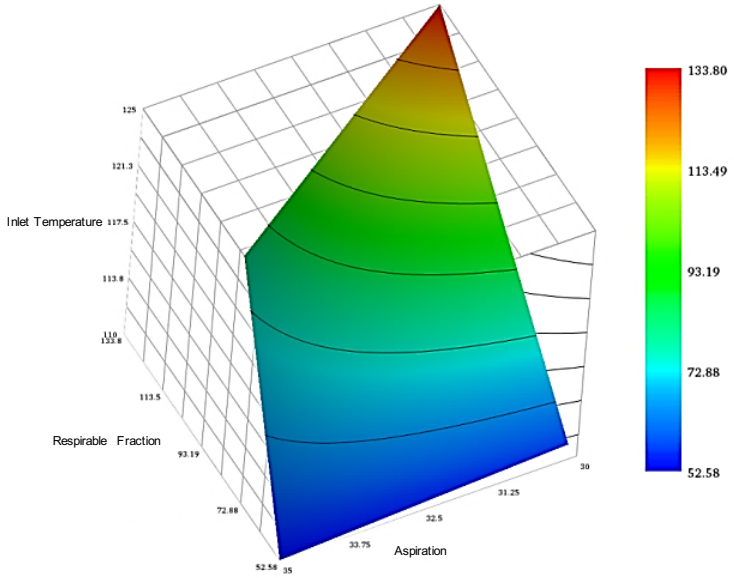

Figure 4.16. 3D plot for the Respirable Fractions as a function of aspiration and Inlet temperature for the collector-deposited powders employing buffer KP: higher values (red zone) were observed with high inlet temperature (125°C) and low aspiration (30 m^3/h).

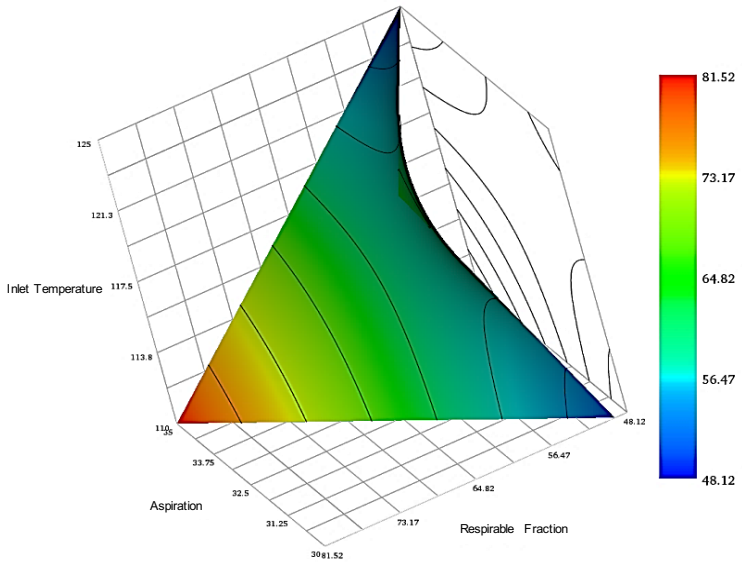

Figure 4.17. 3D plot for the Respirable Fractions as a function of aspiration and Inlet temperature for of the collector-deposited powders employing buffer TBS: higher values (red zone) were observed with low inlet temperature (110°C) and high aspiration (35 m^3/h).

Minitab® software identified more significant correlations than Unscrambler®. Yield in both collected fractions was significantly related to the type of buffer used ($p < 0.001$). Figure 4.18 illustrates this correlation: the slope of the line linking the values obtained with the two buffers was significantly different from 0.

Contour plots (Figure 4.19) shows the not significant correlation between the inlet temperature and feed rate, taking the two buffers separately, on the yield in the collector. Using TBS (Figure 4.19, plot on the left), the yield was maximized (dark green zone) with low temperature (110°C) and high feed rate (4.5 mL/min); with KP (Figure 4.19, plot on the right), high temperature (125°C) and low feed rate (3.5 mL/min) afforded a better yield (dark blue zone), in agreement with Unscrambler® results.

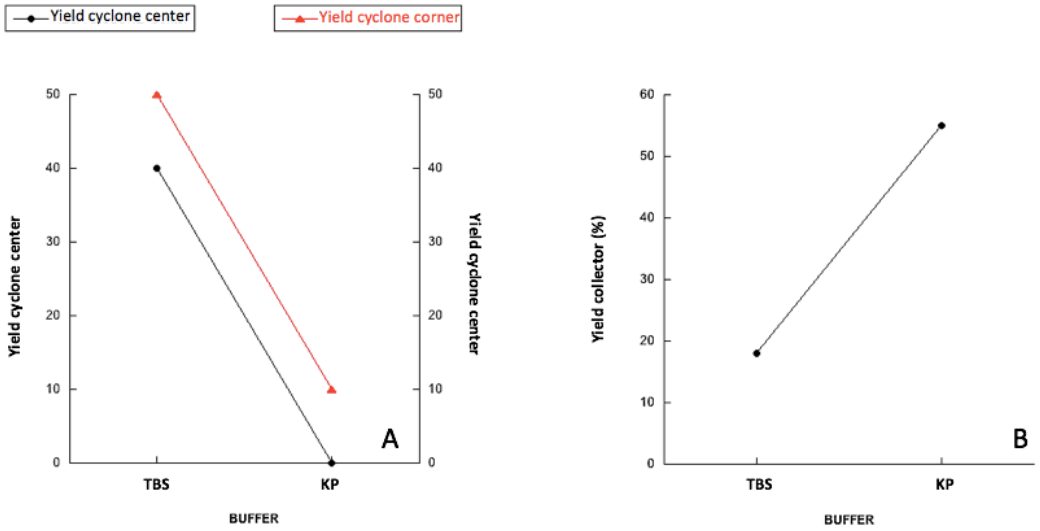

Figure 4.18. Yield for the cyclone-deposited powders (A) as function of the type of buffer (center point = central point corresponding to a mean value between the two levels of the parameter investigated; corner point = best point obtained). Yield for the collector-deposited powders (B) as a function of the type of buffer.

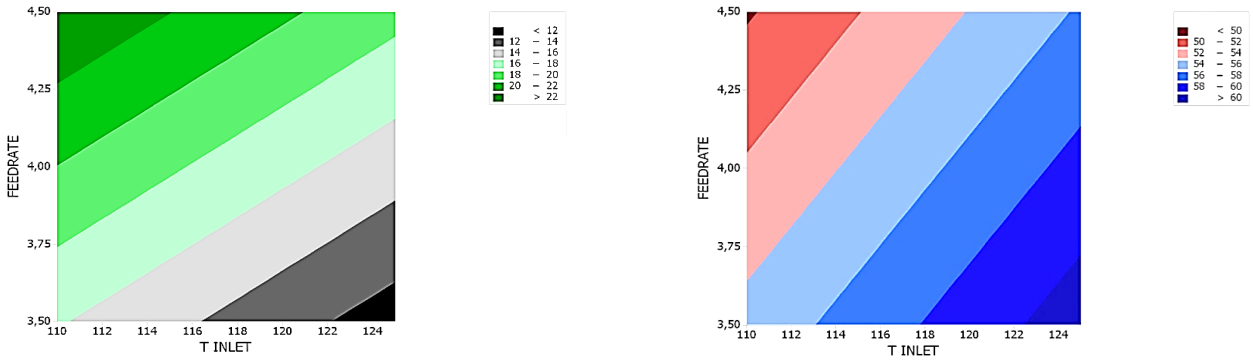

Figure 4.19. Contour plots for the two different type of buffer (TBS, on the left hand-side and KP, on the right-hand side) showing the 2-way interaction between feed rate and drying temperature on the yield in the collector.

The variation of the EM of the collector-deposited powder was significantly affected by inlet temperature and feed rate. For this attribute, a 2-way interaction, although not significant, between the type of buffer and inlet temperature was pointed out. EM of the collector presented a significant 3-way interaction with inlet temperature, aspiration and feed rate.

RF of the collector was statistically connected to the drying temperature (Figure 4.20): a higher temperature led to powders with higher RF. Figure 4.20 illustrates, for the RF of the collector fraction, a significant ($p < 0.05$) 2-way interaction between inlet temperature and buffer type and a not significant correlation between feed rate and buffer type. In the case of TBS solution (Figure 4.21, plot on the left), RF increased with feed rate and decreasing the drying temperature (dark green zone); on the other hand, with KP (Figure 4.21, plot on the right) RF was higher when powders were produced with a high temperature and a low feed rate (dark blue zone). The same relations were observed for the RF of the cyclone-deposited powder.

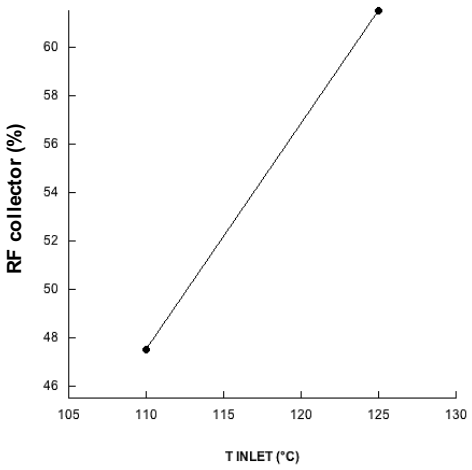

Figure 4.20. Relation between RF of the collector-deposited powder and drying temperature.

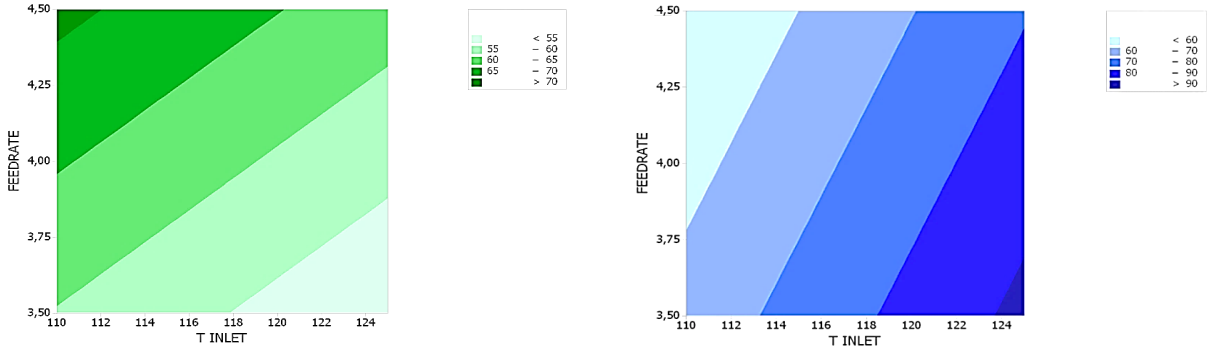

Figure 4.21. Contour plots for the two different type of buffer (TBS, on the left and KP, on the right) showing the 2-way interaction between feed rate and drying temperature on the RF of the collector-deposited powders.

A final correlation, although not significant, was evidenced between the $D_{v,50}$ of the collector-deposited fraction and aspiration rate.

Minitab® software allowed optimizing the CPPs studied, in order to obtain the best quality attributes: maximum yield in the collector, minimum in the cyclone, small mean volume diameter of the collector fraction, maximum emitted and fine particle fractions. The best CPP for the parameters reported were:

- KP buffer;
- Inlet temperature: 125°C;
- Aspiration: 30 m^3/h;
- Feed rate: 3.5 mL/min.

Those were the same parameters employed to produce the previous dried powders containing *Pf*Trx HPV16 L2, except for the buffer type and aspiration rate; the latter, however was not identify as significant parameter from both software. Therefore, it was decided to keep the previously used the spray drying parameters and to change only the type of buffer for the subsequent production of powders containing the antigen.

4.5 Production and characterization of spray dried powders with higher antigen content

Three new powders were produced with increasing amount of antigen (0.83%, 1.33%, 2.00% of weight of the solute content) (Table 4.10), in KP 25 mM buffer solution. The pH of the feed solutions was checked to avoid protein precipitation (7.90-8.32). The yield of the production process increased with the percentage of the loaded protein (39.38-64.62%). As a matter of fact, the yield was connected with the volume of KP used: powders A and B were spray dried with a higher volume of buffer (5 and 8 mL, respectively) and the yield was < 45%, whereas for powder C the feed solution contained only 1.5 mL of KP and the yield was > 60%. This confirms the fact that the type and volume of buffer influenced the yield and the characteristics of the powder produced.

Table 4.10. Composition (% of the weighted solute), production yield and pH of the feed solutions of the spray dried powders with loading of the antigen content.

Powder	Antigen	Mannitol	Sodium stearate	Buffer phosphate (% v/v)	Yield (%)
A	0.83	98.17	1	5	39.38
B	1.33	97.67	1	8	44.23
C	2	97.00	1	1.5	64.62

* Powder number 1 was added as formulation produced with the smallest amount of antigen and renamed powder A.

The aerosolization from the device was high for all the powders > 75% (Figure 4.22), indicating that air flow generated by the RS01® device was able to efficiently deagglomerate the particles. A difference in the performance was noticed for the Respirable Mass. Indeed, the worst FPM (3.53 ± 2.01 mg) was reported for the formulation prepared with the highest amount of KP

buffer (powder B), compared to a value of 7.30 ± 0.62 mg reached by powder C (RF = 70.86% ± 5.59).

This evaluation was supported by particle size distribution analysis (Figure 4.23): powder C was the one with a monomodal distribution (span = 1.28 ± 0.04) shifted to the left.

The aerodynamic performance was related to the total volume of buffer used in the feed solution: the respirability of the dried powders decreased with the increase of the buffer concentration. In detail, the use of a less concentrated buffered solution (1.5% v/v) to feed the spray dryer, favored the formation of smaller and less cohesive particles: the resulting powder (powder C, containing antigen at 2.00% of the weight of the total solute) showed the highest RF value. On the contrary, the powder containing the protein at 1.33% of the weight of the total solute (powder B, produced by adding 8% v/v of potassium phosphate buffer to the feed solution) presented the lowest RF value with a high standard deviation (34.49% ± 19.89).

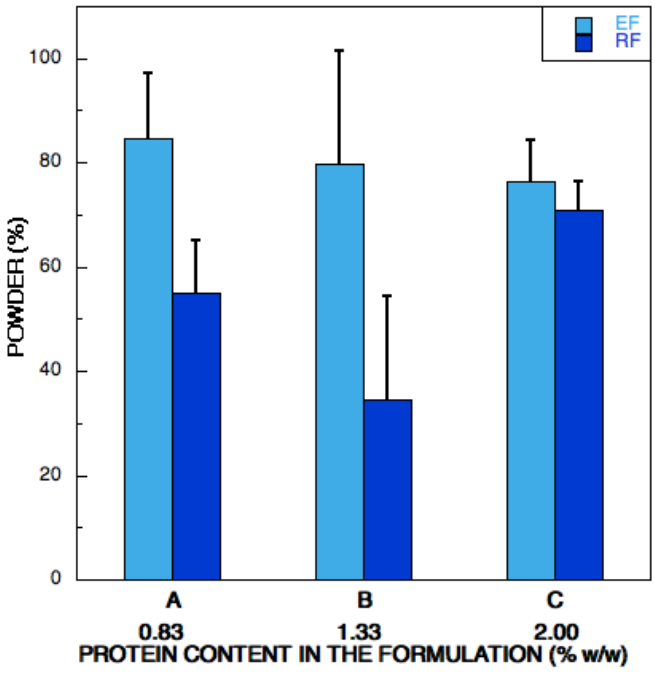

Figure 4.22. Aerodynamic parameters, Emitted (EF) and Respirable Fraction (RF), of the three powders with different antigen loading. The bars represent the standard deviation (n=3).

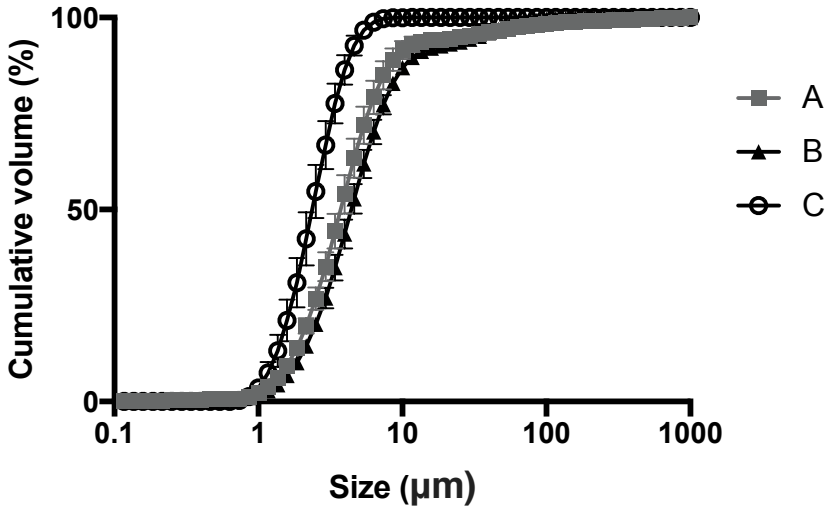

Figure 4.23. Particle cumulative undersize distribution evaluated by laser light diffraction of the spray dried powders with loading of the antigen: 0.83% w/w powder A (square), 1.33% w/w powder B (triangle), 2.00% w/w powder C (empty circle). The bars represent the standard deviation (n=3).

Microparticles morphology was visualized by SEM (Figure 4.24). Particles incorporating antigen at 0.83% (powders A) appeared less spherical than microparticles loaded at higher amount of protein antigen. In all cases, the particles appeared partially sintered with the smaller ones coalesced onto the bigger. This characteristic, however, seemed not to particularly influence the dispersibility of the powders from the device employed.

SDS-PAGE analysis allowed quantifying in specific manner the *Pf*Trx HPV16 L2 antigen in each formulation on the base of its molecular weight (18 kDa) (Figure 4.25). All powders were found to contain an amount of protein very close to the nominal content. Furthermore, ELISA tests did not reveal any appreciable difference in immunoreactivity among the different powders and the control (non-spray dried) antigen in terms of recognition by a monoclonal anti-L2 antibody (K4) and of a polyclonal anti-*Pf*Trx antibody (Figure 4.26).

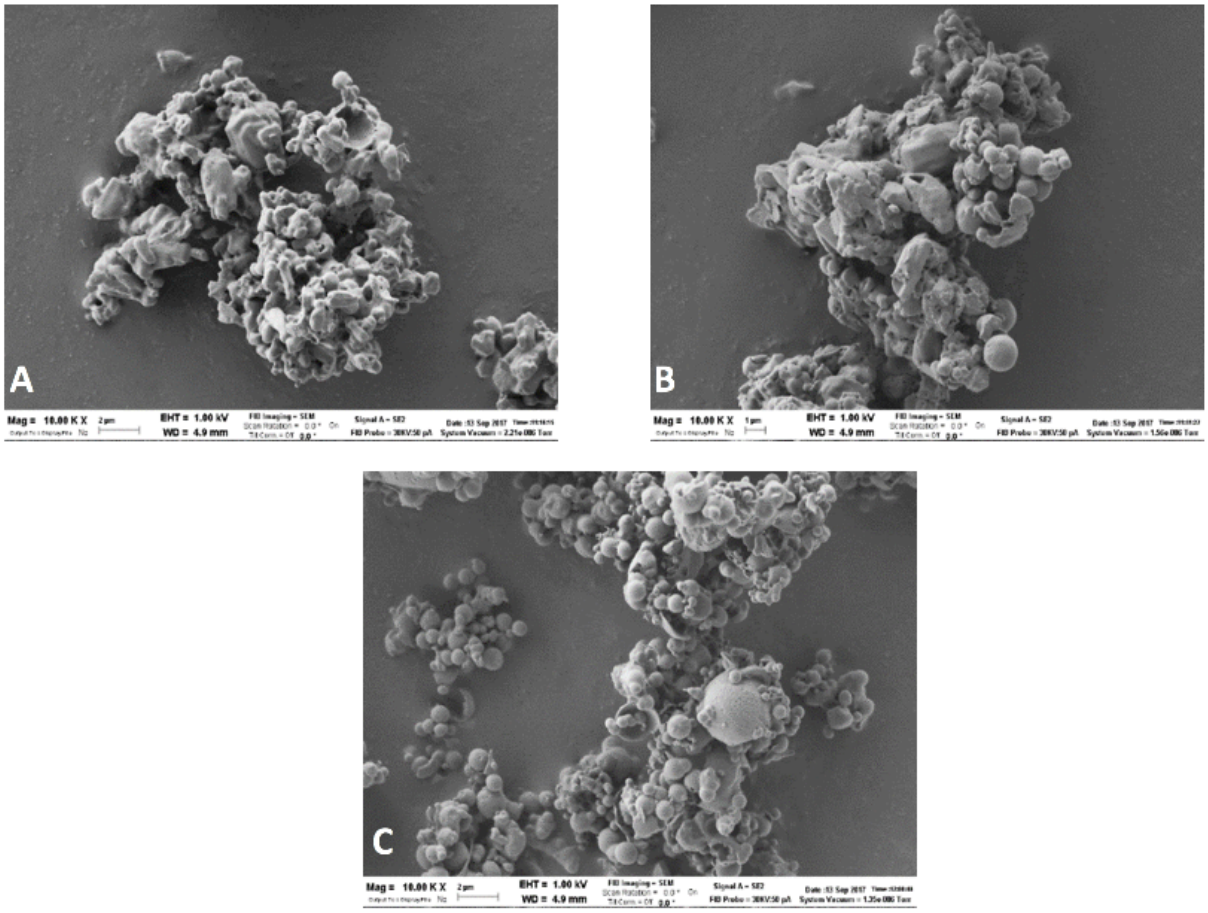

Figure 4.24. SEM images of powders, containing *Pf*Trx HPV16 L2 antigen 0.83% (A), 1.33% (B) and 2.00% (C) of weight of the total solid in the solution. Magnification 10.000x.

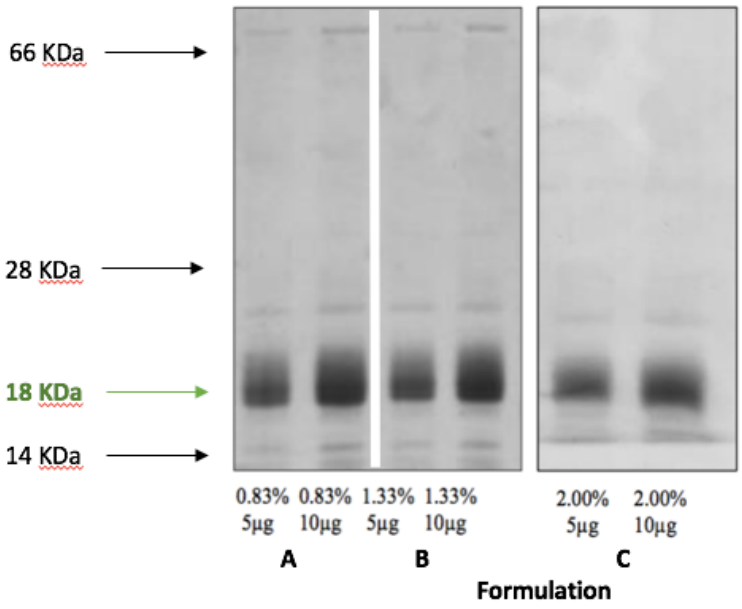

Figure 4.25. Pictures of SDS-PAGE gels used to identify and quantify the PfTrx HPV16 L2 antigen in the spray dried powders containing 0.83% (A), 1.33% (B) and 2.00% (C).

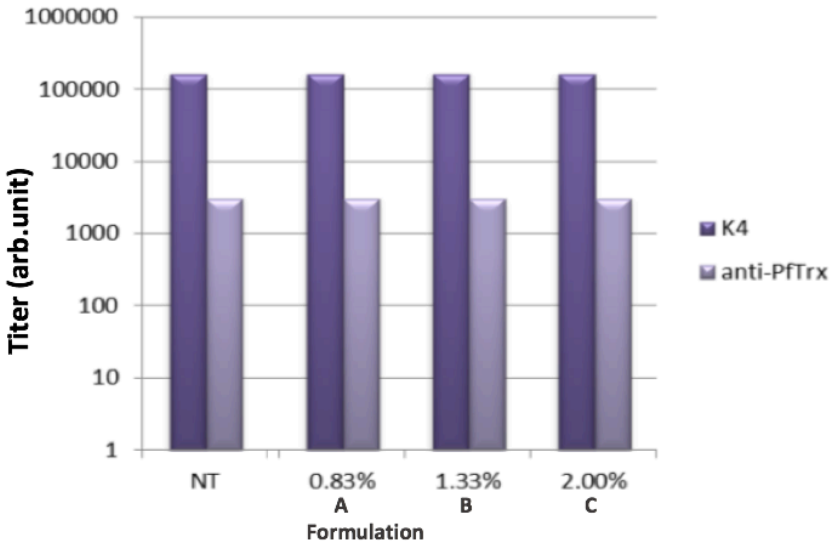

Figure 4.26. Binding capability of *Pf*Trx HPV16 L2 antigen contained in the spray dried powders at 0.83% (A), 1.33% (B) and 2.00% (C) to be recognized by the two specific antibodies.

4.6 Replacement of the amphiphilic compound

The phase of the project was substantially devoted to the evaluation of whether the technology of molecular deposition as described by Parlati et al. [39] for large doses of small molecules, such as antibiotics, could be successfully translated to the production of respirable particles containing a protein antigen, as proposed in Figure 3.2. The data above reported, clearly indicate that this translation was efficaciously achieved. However, a suitable immune response often requires the contemporary administration of an adjuvant. The adjuvant according to the definition of the National Institute of Allergies and Infectious Diseases of the National Institute of Health of Bethesda, MD, USA, is "a substance that is formulated as part of a vaccine to enhance its ability to induce protection against infection…Adjuvants are important for activating the innate immune response, resulting in improved adaptive immunity with enhanced activation of T and B cells." [87]. Alum, is the mostly used adjuvant in marketed vaccines, is also comprised in the HPV vaccine Cervarix® in combination with monophosphoryl lipid A which is amphiphilic immune stimulant agonist of a toll-like receptor (TLR4). The amphiphilic nature of this adjuvant has suggested and prompted us to evaluate the possibility to replace the surfactant, sodium stearate, with monophosphoryl lipid A (MPLA) [88], in order to prepare

respirable coated with this compound to improve both the technological (flow, de-aggregation, respirability) and immune properties of the mannitol/*Pf*Trx HPV16 L2 microparticles. The synthetic version of MPLA, also called glucopyranosyl lipid adjuvant or GLA, was employed to coat mannitol/*Pf*Trx HPV16 L2 microparticles.

As a first approximation the amount of GLA to be employed was calculated by considering the ratio between GLA and sodium stearate molecular weight (1763.47 and 306.46 g/mol, respectively), to achieve the same level of coating. From this calculation it turned out that 1% by weight of sodium stearate corresponds to about 0.17% by weight of GLA.

The theoretical amount of GLA necessary to entirely coat the total surface of the particles can be computed by knowing the average diameter of the particles constituting the powder and the surface molecular area of the surfactant from the following sets of equations.

The surface area (SA) occupied by 1 g of surfactant is:

$$SA_{1g\ surfactant} = \left(\frac{1}{MW_{surfactant}} \times N_A\right) \times\ MSA_{surfactant} \qquad (4.1)$$

where $MW_{surfactant}$ is the molecular weight of the surfactant, N_A Avogadro Constant ($6.022\ 10^{23}$ /mol) and $MSA_{surfactant}$ the molecular surface area of the surfactant: 0.401 nm^2/molecule for sodium stearate [69] and 1.16 nm^2/molecule for GLA [89].

The amount of surfactant ($g_{surfactant\ in\ 100g\ powder}$) to be used for the complete coating with a molecular monolayer 100 g of powder constituted by perfectly spherical particles, can be calculated from the following proportion:

$$1\ g_{surfactant} : SA_{1g\ surfactant} = g_{surfactant\ in\ 100g\ powder} : SA_{surfactant\ in\ 100g\ powder} \qquad (4.2)$$

If we assume a perfect spherical shape, the SA of a single particle of the spray dried powder can be calculated as:

$$SA_{particle} = 4\pi r^2 \qquad (4.3)$$

where r^2 is $\frac{1}{2}$ $D_{v,50}$.

The volume (V) of a single spherical particle is:

$$V_{particle} = \frac{4}{3}\pi r^3 \quad (4.4)$$

From the real density (d) of the powder, that was measured via a gas pycnometry (1.5 g/mL), it the V of 1 g of powder can be calculated:

$$V_{1g\ powder} = \frac{1}{d} \quad (4.5)$$

So, the V of 100 g of powder is:

$$V_{100g\ powder} = V_{1g\ powder} \times 100 \quad (4.6)$$

The ratio between V of 100 g of powder and V of a particle gives the number (n) of particles in 100 g of powder (7):

$$n_{particles\ in\ 100g\ powder} = {V_{100g\ powder}}/{V_{particle}} \quad (4.7)$$

Thus, the SA of 100 g of powder is:

$$SA_{100g\ powder} = SA_{particle} \times n_{particles\ in\ 100g\ powder} \quad (4.8)$$

Finally, by combining eq. 4.1, 4.2 and 4.8 the theoretical amount, of surfactant necessary to completely coat 100 g of powder constituted of perfectly spherical particles can be computed. The values calculated for the two amphiphilic compounds were very 0.13 grams for sodium stearate and 0.34 grams for GLA. These fully theoretical values indicate that in the case of sodium stearate coated particles, the approach adopted according to Parlati et al. [39] would result in a largely overestimated amount of coating agent in the formulation (considering the relevant surface values, 1% of surfactant would cover nearly 780 grams of powder), suggesting that a large part of sodium stearate would position within the particle core. In the case of GLA the amount selected based on the simple scaling down of the amount for sodium stearate considering the relent molecular weights, at maximum would afford nearly 50% of the total particle surface area coated.

To support or reject these assumptions, contact angle measurements were carried out with the aim to determine experimentally the percentage of particle surface coating of mannitol/antigen microparticles by sodium stearate. Unfortunately, the same measurements could not be carried out with GLA, due to the too large amount of compound necessary for such type of measurements. Contact angle measured on powders B was 26.66° ± 3.01. Using the Cassie and Baxter relationship (equation 3.3) the coating percentage for powder B was determined by using as reference angles for the surfactant sodium stearate 104.6° (experimentally determined) and for mannitol 2.8° (experimentally determined). The obtained result was 8.7%, a figure nearly two order of magnitude lower than the theoretical value determined with equation 2. This may be surprising with respect to the calculated theoretical value above mentioned. However, it should be taken into account the reliability of this determination is largely affected by the fact that the particle shape (Figure 4.24, panel B) is characterized by the presence of a large amount of empty spaces among collapsed small subunits. Therefore the interface with the liquid during the contact angle measurements is not only solid but it is at least in part represented by gas (air) with a specific interfacial tension likely different from the solid liquid interface tension.

A spray dried powder D (yield 79.32%) contained antigen at 1.33%, starting from a more concentrated KP buffer solution of the protein (4 mg/mL vs 1 mg/mL employed to produce powder B with the same antigen content). Taking into consideration the above reported calculation for the maximum theoretical coating for GLA, it was decided to keep the GLA at 0.17% w/w of the solid content of the spray dried solution as it was evaluated that 50% area coated would be a suitable figure both from the technological and immunological point of view, taking also into account the high cost of this immune stimulant.

Powder D, once dissolved in ultrapure water, afforded a slightly basic, pH (8.00).

The aerodynamic performance was compared to that of powder B (Figure 4.27). RS01® device efficiently emitted the powder (EM = 8.60 ± 0.78 mg), as for all other formulations. RF was,

however, higher for powder D compared to powder B: 61.24% ± 8.58 and 34.49% ± 19.89, respectively. These data suggest the strong effect of the adjuvant and the total volume of buffer added to the feed solution on the aerodynamic performance of the two powders.

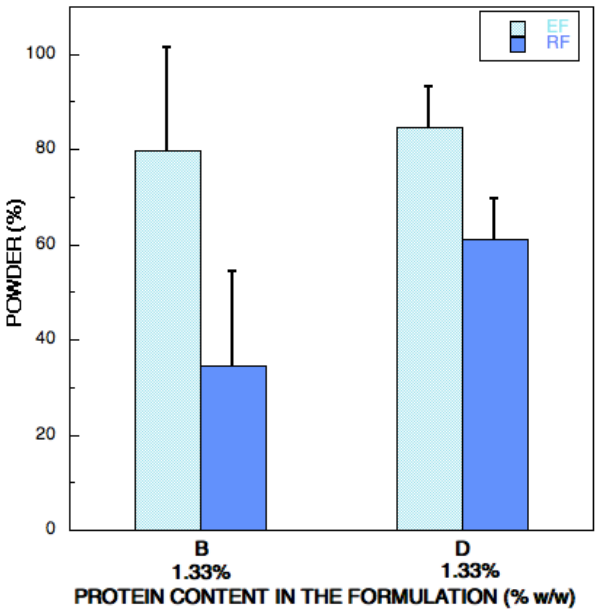

Figure 4.27. Aerodynamic performance, Emitted (EF) and Respirable Fraction (RF), of powders with sodium stearate (B) or with GLA (D) produced with equal content of antigen (1.33% w/w of the total solid of the feed solution). The bars represent the standard deviation (n=3).

The mean volume diameter was 2.93 ± 0.24 μm for powder D and 4.43 ± 0.29 μm of powder B. Moreover, particle morphology of powder D evidenced a better similarity with powder C than B: particles were more regular and spherical (Figure 4.28). Indeed, both were spray dried from a feed solution with a quite similar buffer concentration. The characteristic of sintered particles was conserved also here.

The content of antigen in the powder was still close to the nominal dose. However, *Pf*Trx HPV16 L2 was recognized and bonded by the monoclonal and polyclonal antibodies with a titer lower than the control (54000 vs 100000 for K4 and 1000 vs 5000 for the anti-scaffold antibody), comparable to Figure 4.26. The decrease seemed to be not particularly significant, because the values were still high, the antigen was still able to bind both of the antibodies.

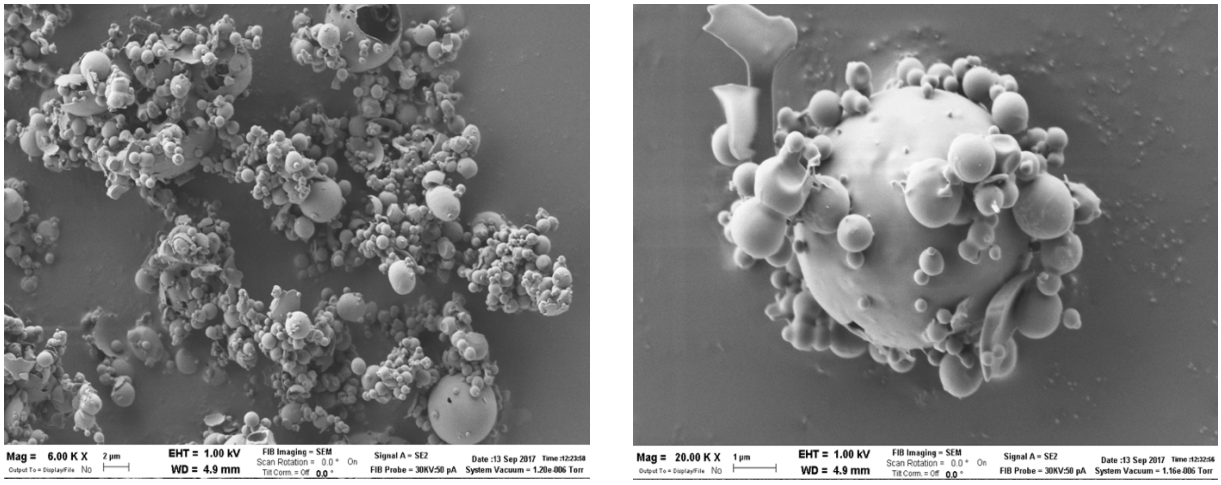

Figure 4.28. SEM images of GLA powder D containing 1.33% w/w of PfTrx HPV16 L2 antigen. Magnification 6.000x (on the left-hand side) and 20.000x (on the right-hand side).

4.7 *In vivo* and *ex vivo* imaging

An imaging technique was adopted to observe the deposition of the powder in the lungs of mice. A preliminary experiment was conducted through intratracheal administration in a BALB/c mice of an Alexa Fluor 750-labeled antigen saline solution, by employing version of PennCentury (Dry Powder Insufflator™-Model DP-4M) adapted for solution [65]. This first experiment was carried out as control. The protocol established bioluminescence, IVIS® Spectrum, Florescence Tomography System, FTM, and/or micro Computer Tomography, μCT, imaging at three different time points (5, 15 and 30 minutes after the administration).

The results obtained *in vivo* and on the *ex vivo* specimens (Table 4.11 and Figure 4.29) showed that the signal of fluorescence was significant in the lungs. The localization was more evident after 15 minutes from the administration. However, the highest fluorescence was reported for the liver. In order to understand whether this signal was due to the labeled antigen or only to the free fluorophore, an SDS-PAGE was performed (Figure 4.30). The band corresponding to the labelled protein was not present in the gel for the samples extracted from the liver, thus indicating that the relevant signal observed in the ex vivo IVIS® sample was due to the free fluorophore, which had a molecular weight too small to be retained in the gel. The main localization in the lungs was also confirmed by FMT and μCT (Table 4.12 and Figure 4.31).

FMT showed a higher signal in the lungs after 30 minutes from the administration. Interesting the μCT data showed a clear different density between the two lobes of the lungs: Figure 4.31 indicate that intratracheal liquid treatment went preferentially in the left lobe of lungs.

Table 4.11 IVIS® results: emission values (arb. unit) of Alexa Fluor 750-labelled antigen saline solution *in vivo* after 5 or 15 minutes from the intratracheal administration and *ex vivo* for lungs, liver, kidneys and spleen.

	Spot	**In vivo**		**Ex vivo**			
Ex-Em	**1μL protein + 9 μL saline**	**5 min**	**15 min**	**Lungs**	**Liver**	**Kidneys**	**Spleen**
710-780	$3.07x10^7$	$4.64x10^8$	-	-	-	-	-
745-800	$6.97x10^7$	$8.47x10^8$	$1.03x10^9$	$4.65x10^9$	$2.53x10^{10}$	$8.47x10^8$	$1.31x10^9$
745-820	-	$4.10x10^8$	-	-	-	-	-

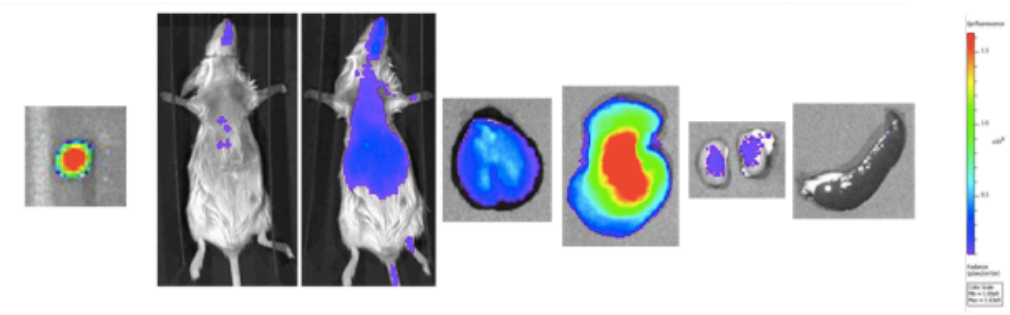

Figure 4.29. IVIS® results. From left to right: spot, *in vivo* images after 5 or 15 minutes from the intratracheal administration and *ex vivo* images of lungs, liver, kidneys and spleen, respectively.

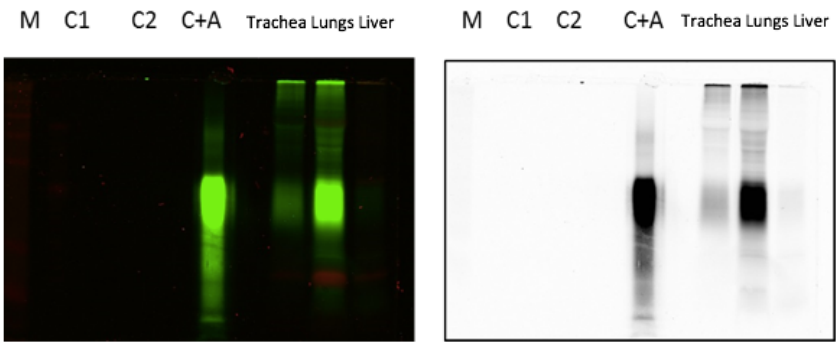

Figure 4.30. SDS-PAGE gels of the proteins extracted from different organs (trachea, lungs, liver) of the mouse after intratracheal administration of a saline solution containing the Alexa Fluor 750-labelled antigen (controls: M = marker; C1 and C2 protein not labelled; C+A labelled protein).

Table 4.12 FMT results: emission values (pmol) of Alexa Fluor 750-labelled antigen saline solution *in vivo* after 5, 15 and 30 minutes from the intratracheal administration.

	***In vivo* (pmol fluorescence)**		
Laser	**5 min**	**15 min**	**30 min**
750	22.7	86.2	59.5
790	111.9	111.9	182

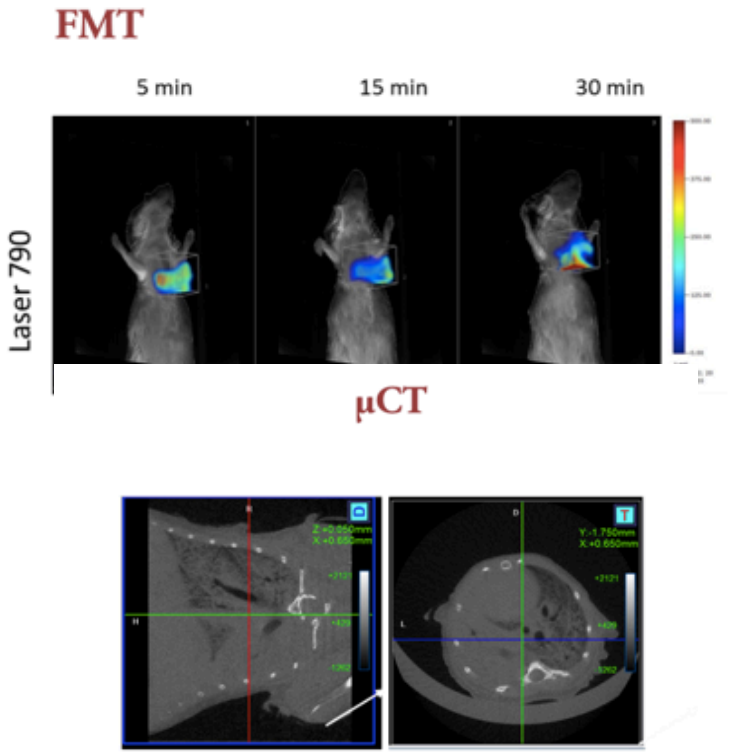

Figure 4.31. FMT imaging (on the top) of the Alexa Fluor 750-labeled protein after 5, 15 or 30 minutes from intratracheal administration and µCT imaging (on the bottom).

These encouraging preliminary results with the liquid formulation prompted us to perform the same experiment with the spray dried powder containing the Alexa Fluor 750-labeled *Pf*Trx HPV16 L2 antigen (0.59% of the weight of the total solid in the feed solution) administered intratracheally. The spray dried powder (yield = 57.79%) was previously checked in terms of aerodynamic characteristics (EF = 87.24% ± 6.12 and RF = 67.03% ± 4.95). A protocol was set establishing to administer the powder intratracheally through a PennCentury powder insufflator in two BALB/c female mice and imaged with IVIS® and FMT after 5 and 10

minutes. After 15 minutes the mice were sacrificed, *ex vivo* IVIS® imaged and, finally, lungs and liver frozen for a subsequent SDS-PAGE. The insufflator was loaded with 1.7 mg (10 μg of labelled antigen) and 2 mg (12 μg of labelled antigen) of powder for the two mice, respectively.

Figures 4.32 (IVIS®) and 4.33 (FMT) and Tables 4.13 (IVIS®) and 4.14 (FMT) show a fairly even powder distribution in the mice respiratory tract, with a consistent deposition in the lungs. This was confirmed by *ex vivo* lung fluorescence detection (Table 4.13 and Figure 4.32). μCT analysis (Figure 4.33) evidenced that differently from solution, the powder did not afford a difference in the density of the images of the lobes, indicating absence of preferential distribution in one lobe rather than the other.

The presence of the labelled protein was also confirmed by SDS-PAGE on trachea and lungs collected from the two mice (Figure 4.34).

Table 4.13 IVIS® results: table with emission values (arb. unit) of Alexa Fluor 750-labelled antigen powder *in vivo* after 5 or 10 minutes from the intratracheal administration and *ex vivo* after 15 minutes.

Mouse 1	***In vivo***		***Ex vivo***
Ex-Em (745-800)	**5 min**	**10 min**	**15 min**
Trachea	6.63×10^8	7.86×10^8	1.15×10^{10}
Lungs	3.71×10^8	4.31×10^8	

Mouse 2	***In vivo***		***Ex vivo***
Ex-Em (745-800)	**5 min**	**10 min**	**15 min**
Trachea	1.03×10^9	7.86×10^8	5.86×10^9
Lungs	3.53×10^8	4.31×10^8	

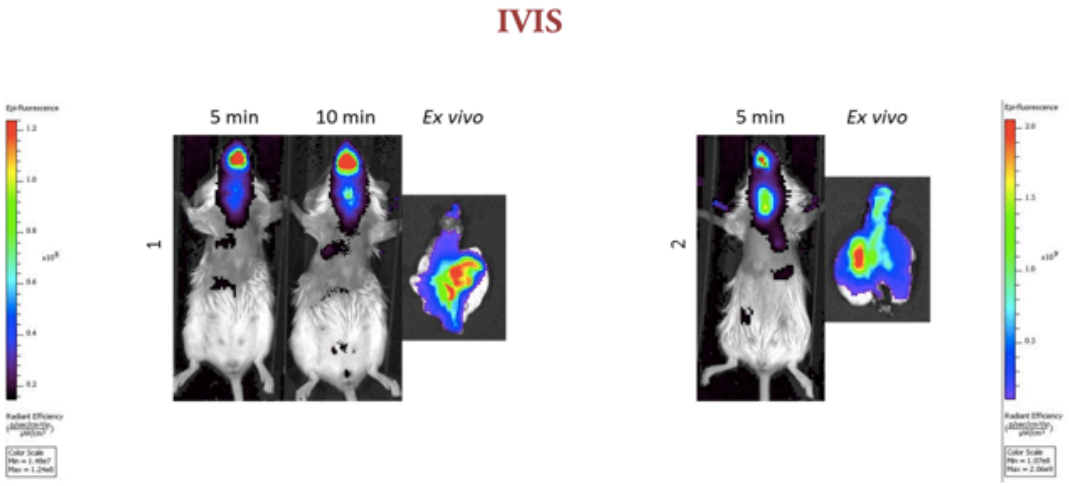

Figure 4.32. IVIS® results. Images collected *in vivo* after 5 or 10 minutes from the intratracheal administration and *ex vivo* for lungs after 15 minutes.

Table 4.14 FMT results: emission values (pmol) of Alexa Fluor 750-labelled antigen powder *in vivo* after 5 or 10 minutes from intratracheal administration.

Mouse 1	***In vivo* (pmol fluorescence)**	
Laser 790	**5 min**	**10 min**
ROI Lungs	38.56	34.22

Mouse 2	***In vivo* (pmol fluorescence)**	
Laser 790	**5 min**	**10 min**
ROI Lungs	21.06	-

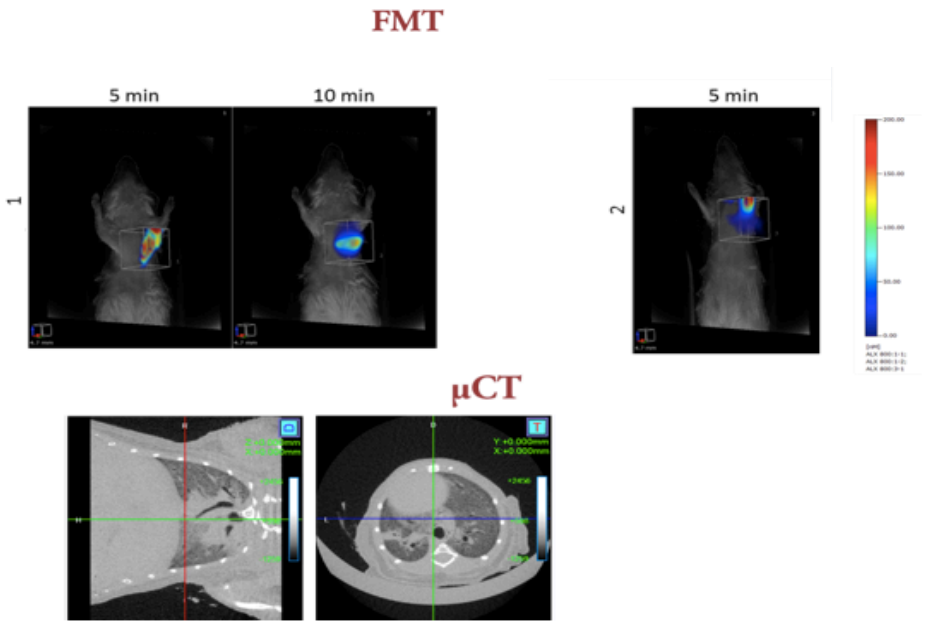

Figure 4.33. FMT imaging (on the top) of the Alexa Fluor 750-labeled antigen powder after 5 or 10 minutes from intratracheal administration and µCT imaging (on the bottom).

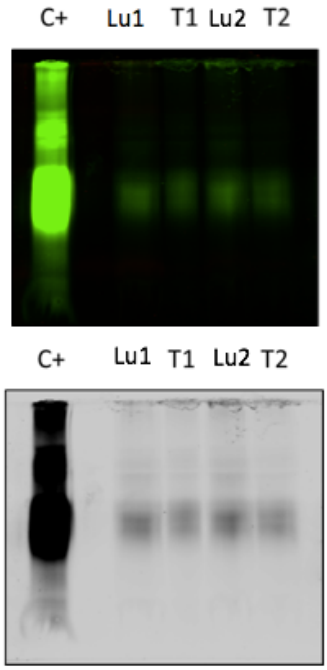

Figure 4.34. SDS-PAGE gels of the proteins extracted from trachea and lungs of the two mice after intratracheal administration of a powder containing Alexa Fluor 750-labeled protein (control: C+ = labelled protein, Lu1 and Lu2 signal emitted by lung of mouse 1 and 2 respectively, T1 and T2 signal emitted by trachea of mouse 1 and 2 respectively,).

4.8 *In vivo* immunization study

Once determined the ability of the DPI containing *Pf*Trx HPV16 L2 antigen to efficiently deposit into the lungs, an immunization study in BALB/c female mice was performed.

In order to perform the study two new powders (E and F) were produced and characterized (Table 4.11), both containing GLA as adjuvant, and two different type of antigen (*Pf*Trx HPV16 L2 for powder E and *Pf*Trx HPV16 L2 OVX313 for powder F) highly purified, detoxified and sterilized by filtration, staring from a 12 mg/mL KP buffer solution. The second antigen *Pf*Trx HPV16 L2 OVX313 was an updated version of the *Pf*Trx HPV16 L2 antigen. The epitope was the same (3x HPV16 L2 (20-38)), although this protein had a heptameric structure spontaneously forming a nanoparticle by the modified domain C4bp (OVX313), which is more recognized by the immune system, giving a higher immune response compared to the monomer [60].

Process yields were the highest ever obtained, due to the highest concentration of vaccines in the smallest volume of buffer added to the feed solution. Powders resolubilized in ultrapure

water presented neutral/slightly basic pH. A different particle size distribution of E and F (Figure 4.35) was obtained ($D_{v,50}$ = 2.65 ± 0.18 μm and 7.15 ± 1.48 μm E and F, respectively). Moreover, powder F presented visible aggregates and particles morphology was different to powder E, with non-spherical, irregular and sintered particles (Figure 4.36). All these data may be connected to the presence of 6 exposed positive surface charges in *Pf*Trx HPV16 L2 OVX313 nanoparticle antigen. The charged antigen determined a precipitation of the system during the production, indeed a suspension was spray dried. The evident particle diversity was attenuated ($p >> 0.05$) as to the aerosolization performance by the device RS01® (Figure 4.37): the device was able to emit and deagglomerate the powders with a similar efficiency (EF = 81.35 vs 81.29% and RF = 60.01% ± 2.02 for E and 56.03 ± 6.78% for F).

To obtain more information on the aerodynamic diameter distribution of the powders their aerodynamic performance was also assessed with Andersen Cascade Impactor (ACI) by detecting and quantifying the mannitol in the impactor stages with a HPLC/RID method. Due to the fact that the antigen was embedded in the GLA coated mannitol particles, it was assumed that this latter could be taken as a reliable indicator of the antigen emission from the device and distribution in the different stages of the impactor. Emitted mannitol from RS01® was 12.55 mg for E (EF = 64.17%) and 15.37 mg for F (EF = 78.18%); these figures were close to the values obtained by weight with FSI.

Mannitol FPM was about 9 mg for both powders (RF = 72.29% and 60.48% for E and F, respectively). Furthermore, MMAD was 2.5 μm for both formulations. The major difference between E and F was observed in the amount of mannitol deposited in the induction port (IP) that was significantly higher for the more agglomerated powder F (Figure 4.38).

A set of capsules for each powder was prepared and stored for 3 months (5 months from production) at ambient conditions but protected from light. E and F showed an opposite behavior with respect to the Emitted Fraction: compared to time zero after production, E reported an increase of mannitol EF, while for F it decreased, in both cases the change was

around 10%. MMAD was unvaried, although RF increased for both powders (83.25% and 69.41% for E and F, respectively). Surprisingly better performance was achieved after storage, possibly due to a partial loss of residual humidity, which improved the powder deagglomeration process after aerosolization. However, a higher amount of mannitol deposited in the IP with powder F. Powders were, then, checked for antigen content through SDS-PAGE. The bands intensity was comparable to the one expected for both of them (Figure 4.39).

Table 4.11. Composition (% by weight of the solute) and pH of the feed solution and production yield (%) of the spray dried powders for the animal study.

Powder	Antigen	Mannitol	GLA	KP buffer (% v/v)	pH	Yield (%)
E	2.00	97.83	0.17	1.00	7.75	65.00
F*	2.00	97.83	0.17	1.00	9.44	71.39

* containing an updated version of the antigen (*Pf*Trx HPV 16 L2 OVX313).

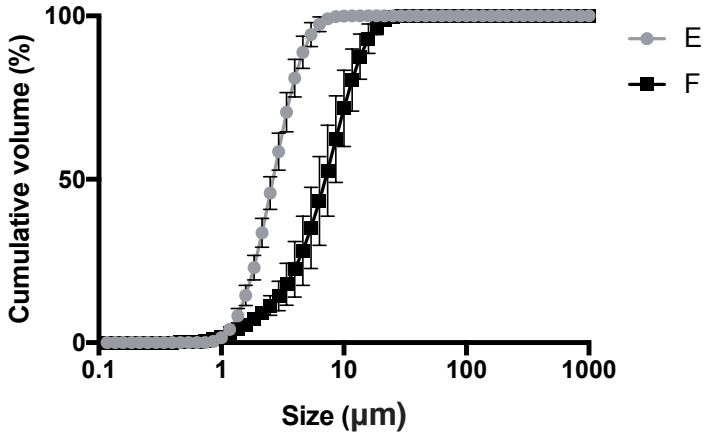

Figure 4.35. Particle cumulative undersize distribution evaluated by laser light diffraction of powders E containing 2.00% w/w of *Pf*Trx HPV16 L2 antigen and F containing 2.00% w/w of *Pf*Trx HPV16 L2 OVX313 antigen. The bars represent the standard deviation (n=3).

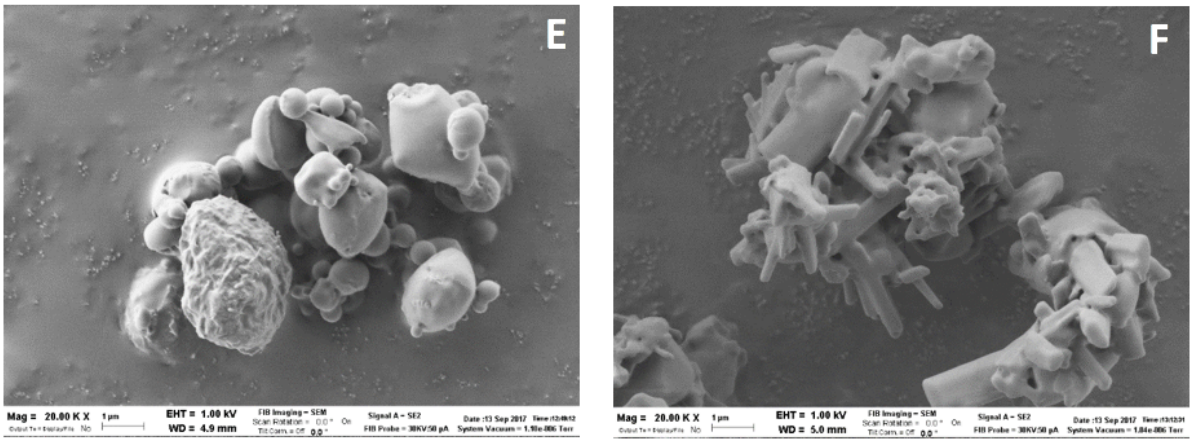

Figure 4.36. SEM images of powder E containing 2.00% w/w of *Pf*Trx HPV16 L2 antigen and powder F containing 2.00% w/w of *Pf*Trx HPV16 L2 OVX313 antigen. Magnification 20.000x.

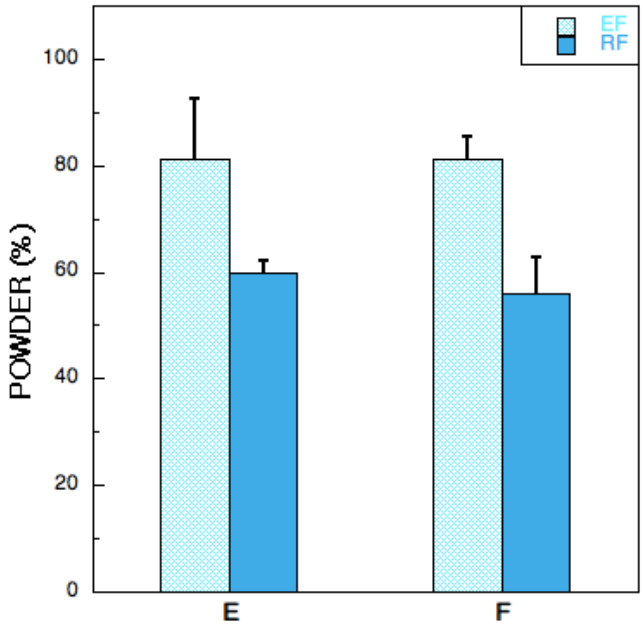

Figure 4.37. Emitted (EF) and Fine Particle Fraction (FPF), of powders E containing 2.00% w/w of *Pf*Trx HPV16 L2 antigen and F containing 2.00% w/w of *Pf*Trx HPV16 L2 OVX313 antigen (n=3, the bars represent the standard deviation).

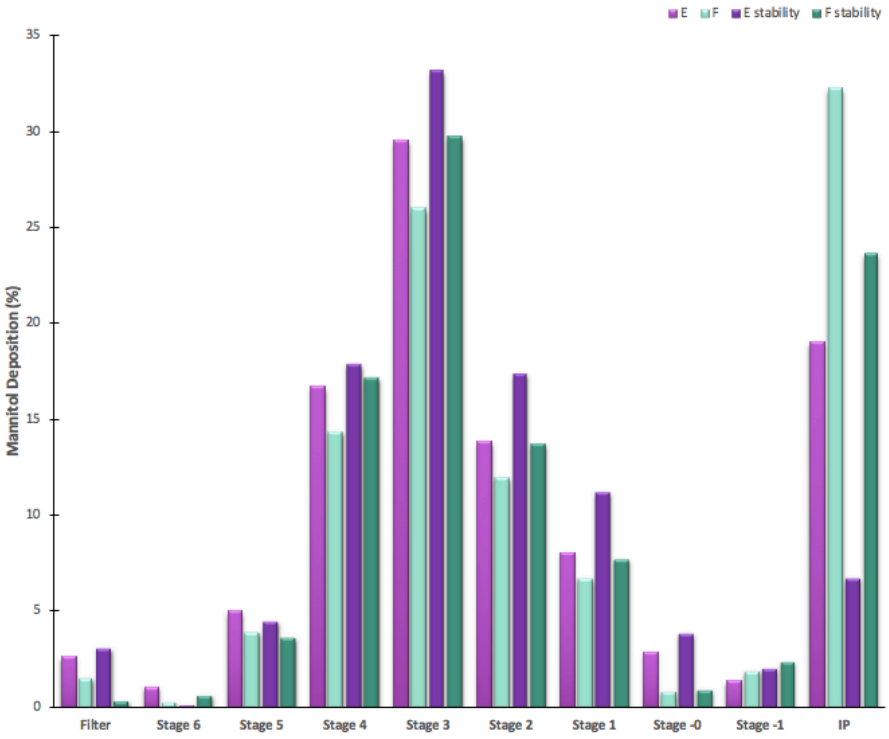

Figure 4.38. Mannitol percentage distribution in the ACI (from Induction Port, IP, to Filter) for powder E containing 2.00% w/w of *Pf*Trx HPV16 L2 antigen, powder F containing 2.00% w/w of *Pf*Trx HPV16 L2 OVX313 antigen, at time zero and after storage for 3 months at ambient conditions.

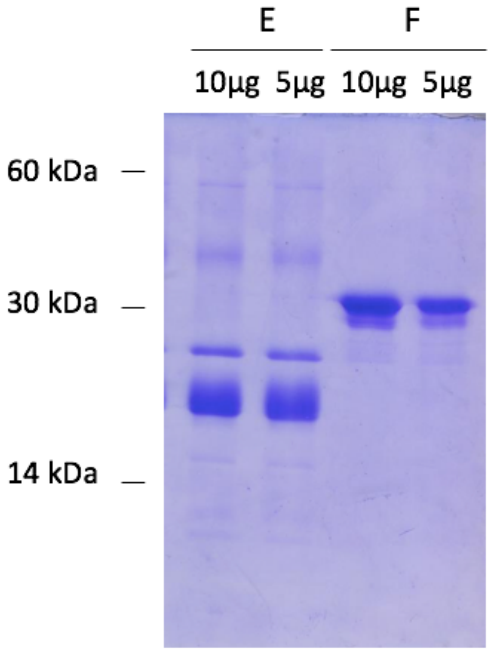

Figure 4.39. Antigens content in the powders E and F, evaluated solubilizing in buffer two different amount of powder (10 or 5 µg). *Pf*Trx HPV16 L2 antigen molecular weight was 18 kDa, while for *Pf*Trx HPV16 L2 OVX313 antigen it was 25 kDa.

These formulations were, finally, used for an *in vivo* immunization study.

The study protocol implied 5 different groups:

- 3S (7 mice): receiving a subcutaneous administration of a saline solution containing *Pf*Trx HPV16 L2 + Alum (50 μg) + GLA (10 μg), (positive control);

- 4S (7 mice): subcutaneous administration of powder E, containing *Pf*Trx HPV16 L2 and GLA, solubilized in PBS;

- 5S (5 mice): subcutaneous administration of a blank spray dried powder, containing only mannitol and GLA, solubilized in PBS;

- 1T (7 mice): intratracheal administration of powder E, containing *Pf*Trx HPV16 L2 and GLA;

- 2T (13 mice): intratracheal administration of powder F, containing *Pf*Trx HPV16 L2 OVX313 and GLA.

From the sera collected after the sacrifice (day 28) it was possible to identify the presence of specific antibodies anti-L2 and evaluate their titer (Figures 4.40 and 4.41), through GST-ELISA. The titers obtained were not significantly different among all groups, except for negative control (5S), where no anti-L2 antibodies were produced. The vaccine DPIs, intratracheally administered, showed the same level of immune response of the control (3S, already studied [24]. It has to be noticed that one mouse of the group 1T did not present any anti-L2 antibodies (Figure 4.41): this point can be considered an outlier, possibly due to a problem during the intratracheal administration, which determined the failure to reach the target.

The values of the obtained titers were not so high compared to those usually obtained in similar experiments [60]. This can be explained by considering the short time of the type of protocol adopted [60,90,91].

Nevertheless, this amount of antibodies produced might be enough to determine protection.

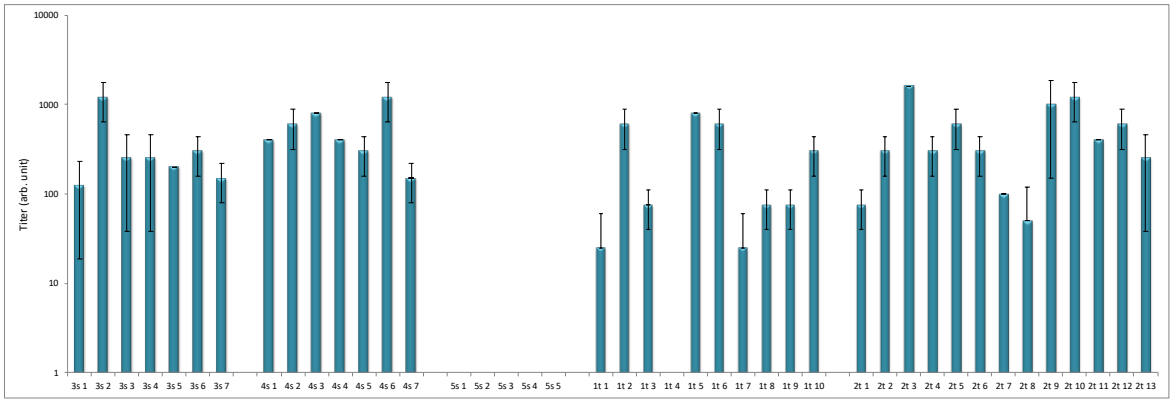

Figure 4.40. Titers of the antibodies anti-L2 in the sera of the different groups, bonded to glutathione (GST) attached to the ELISA plate. Representation one.

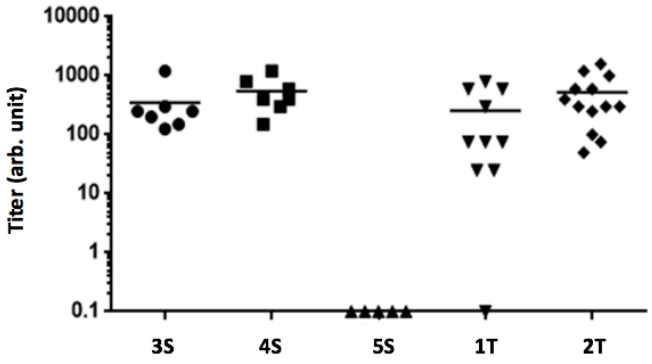

Figure 4.41. Titers of the antibodies anti-L2 in the sera of the different groups, bonded to glutathione (GST) attached to the ELISA plate. Representation two. Lines represent the mean value.

A final test on the sera was carried out to evaluate the different isotyping of the antibodies produced. Figure 4.42 shows that there was no difference in the type of antibodies produced between the groups, with a major production of IgG, that are those determining longer and wider protection [92].

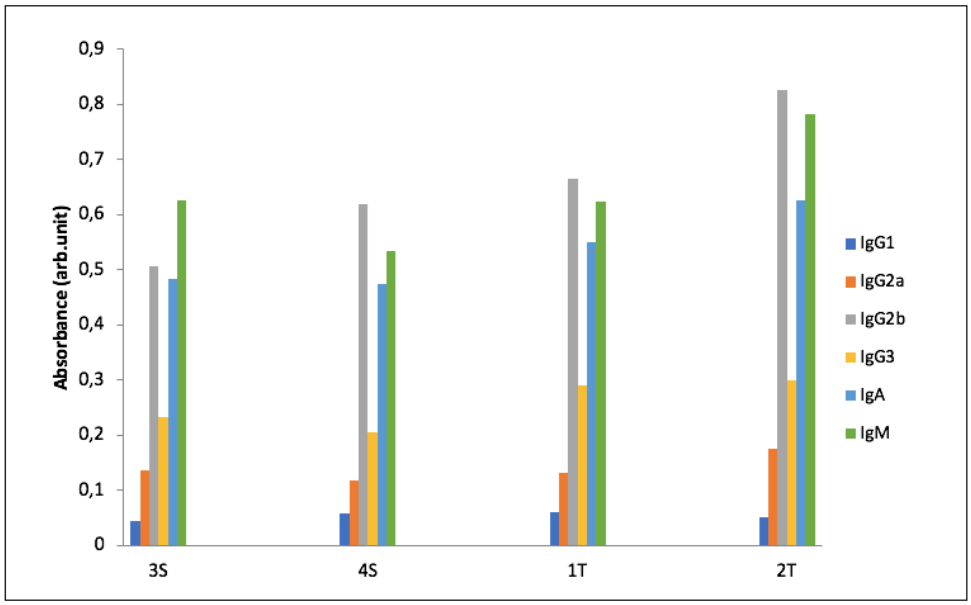

Figure 4.42. Isotyping of the antibodies produced by the four responding groups.

4.9 Technological and solid-state characterization of the produced powders

4.9.1 Bulk and tapped density

For DPIs, bulk density is an important parameter with an opposite meaning for powders characteristics of aerosolization and flowability. A low value of bulk density is beneficial for powder aerosolization; while, at the same time, a higher value improves powder flow properties [93,94]. Spray dried powders produced with sodium stearate or GLA (powders B and D, respectively), were also characterized in terms of bulk and tapped density. Bulk (poured) density was lower for powder with GLA (0.15 g/cm^3) compared to 0.29 g/cm3 calculated for the sodium stearate-containing formulation.

Density, after mechanical tapping, showed an increase for both formulations: 0.23 and 0.39 g/cm^3 for powders B and D, respectively. Powder D reported a lower bulk and tapped density and, as result, it showed a better aerodynamic performance, in terms of RF, compared to powder B. However, the measured values remained below 0.4 g/cm^3, that has been reported in many works as cutoff for determining good aerodynamic characteristics ("aerodynamically light particles") [93].

4.9.2 Powders Flow

Dynamic angle of repose for formulation B and D was determined in order to characterize the powders flow, following what reported in Ph. Eur. 9th ed. The two DPIs presented completely different values: 18.74° ± 1.48 and 46.60° ± 0.60 for powder D and B respectively. Flow properties, based on Carr classification, identified excellent flow properties for powder with GLA and poor properties for powder with sodium stearate. It is always important to recall the use of a higher volume of KP buffer (8% v/v of feed solution) for the production of powder B; this put into evidence that salts may influence negatively the flow properties of this formulation.

4.9.3 Thermal behavior

Solid-state characteristics of powders B and D were assessed by differential scanning calorimetry (DSC). All spray dried powders presented a single thermal event in the temperature range considered; This was an endothermic peak around 166 °C, corresponding to the melting temperature of the beta form of mannitol, the most abundant component in the powders. This data indicates that the spray dry process, afforded the thermodynamically stable form of the bulking agent [95]. Since the surfactant and the antigen were present in very low percentage in the powder no signal ascribable to their thermal behavior could be detected due to the insufficient instrumental sensitivity. For all powders produced a thermogravimetric analysis (TGA) was performed; the obtained values of weight loss as a function of heating were, in all the cases, very close to zero, indicating a very small percentage of residual water in the powders. This data was not surprising considering that, as reported in literature, mannitol usually does not absorb moisture and does not presents high residual humidity values [96]. To confirm this data, a short stability study was performed for powders B and D employing dynamic vapor sorption (DVS) at 25 and 40°C with a cycle of relative humidity (RH) from 0 to 95%, i.e. the powders were exposed to increasing RH up to 95%, then the RH was progressively reduced down to 0 RH. Figure 4.43 displays isothermal curves obtained from the powders analyzed (B and D). In all the experiments, powders absorbed a relatively small amount of moisture. As expected, lower value of absorbed moisture was recorded at 40°C.

Overall, all curves come back to the starting weight at the end of the experiment, further indicating their physical stability.

The powders collected after DVS experiments were analyzed by DSC, to evaluate if the starting crystalline structure was maintained after exposure to humidity (Figure 4.44). Both powders were still crystalline, mannitol melting peaks overlapped with those recorded before exposure to humidity. However, exposure to the 0-95% RH cycle afforded a change in the aerosolization performance for both powders. In fact, while the emitted percentage from the device was always

comparable to the powders performance after production (Figure 4.45), a major drop of the RF after DVS cycle at 40°C was observed (values ≤ 10%).

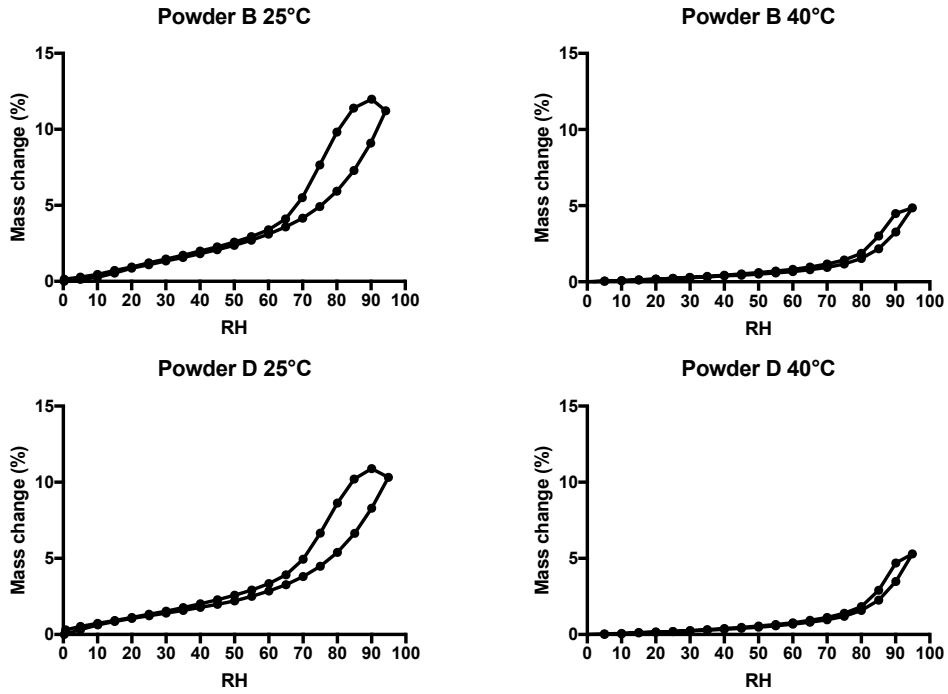

Figure 4.43. Isothermal curves of mass change (%) at as a function of RH (0-95%) recorded for powders B and D studied at 25 and 40°C.

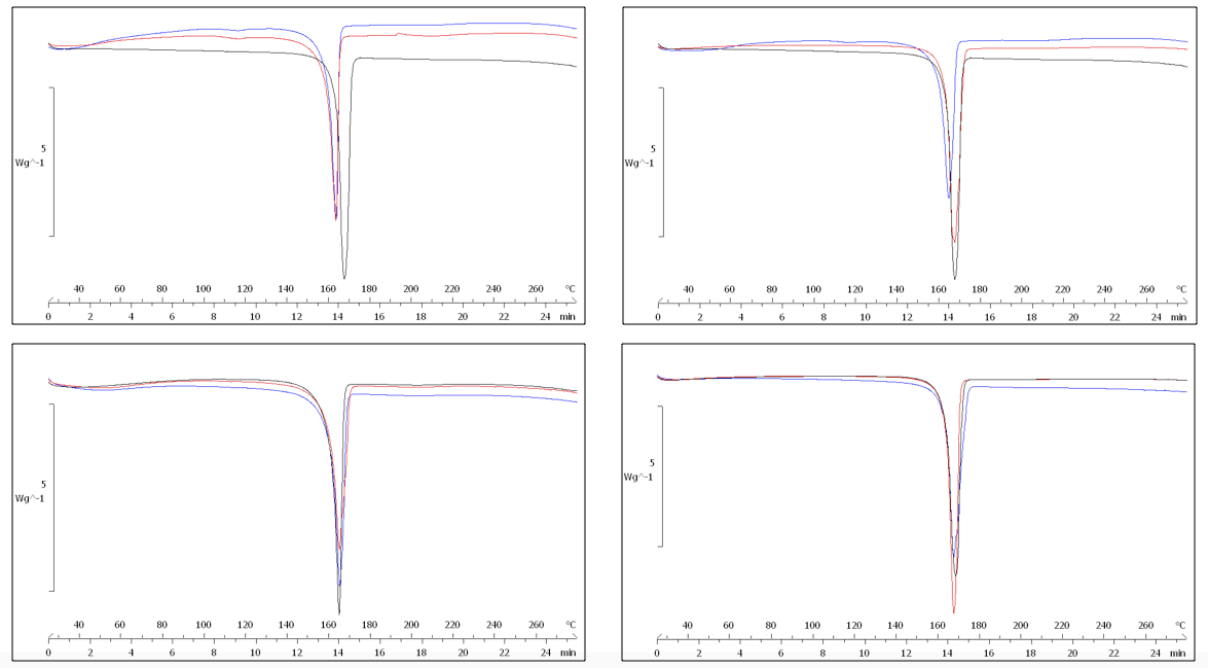

Figure 4.44. DSC traces for samples collected after DVS study. On the top, powder B samples: on the left-hand side samples from study at 25°C and on the right-hand side samples from 40°C study. On the bottom, powder D samples: on the left-hand side samples from study at 25°C and on the right-hand side samples from 40°C study. For all the panels, reference (powder before DVS study) is displayed as the black curve, DVS samples as the red and blue curves.

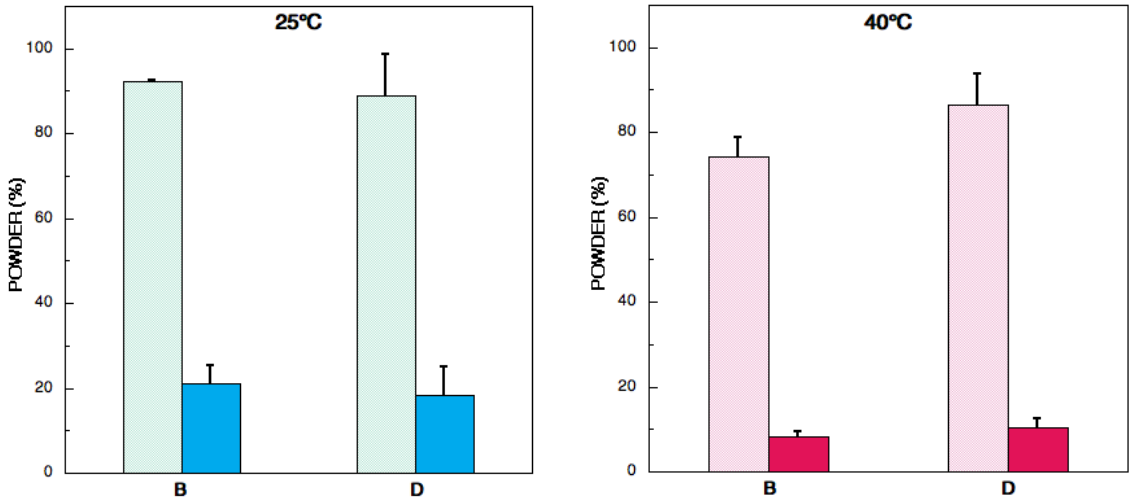

Figure 4.45. Aerodynamic characterization of powders after DVS study. Panel on the left-hand side shows Emitted Fraction (light blue) and Respirable Fraction (blue) for powders B and D after isothermal DVS cycle at 25°C. Panel on the right-hand side displays Emitted Fraction (pink) and Respirable Fraction (red) for powders B and D after isothermal DVS cycle at 40°C. Bars represent the standard deviation (n=3).

4.9.4 Crystallinity

Crystallinity was also investigated for powders E and F, that contained different antigens employing X-ray powder diffraction (PXRD) and DSC. Figure 4.46 displays the X-ray intensity in counts per second (cps) observed for each angle 2θ for the two spray dried formulations compared to mannitol raw material (Pearlitol SD 200). Spray dried powders maintained the crystalline structure with the same peaks of Pearlitol SD 200. The only observed difference was a small shift in peak position that was ascribed to the different particle size of the spray dried powders and Perlitol SD 200.

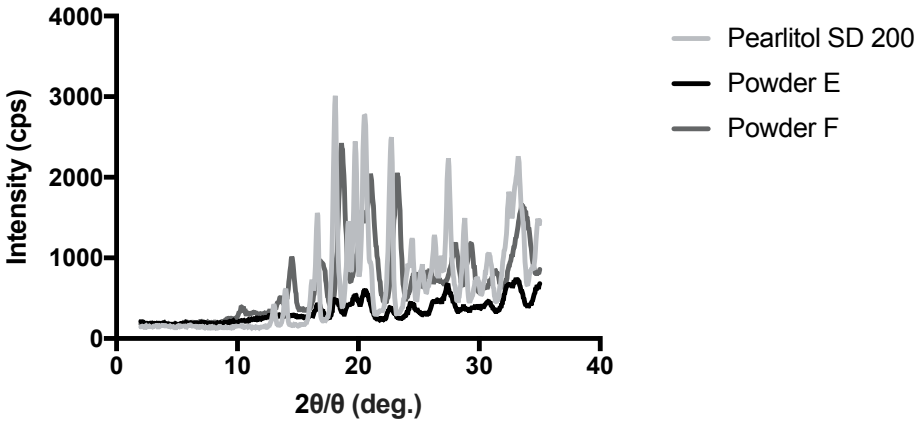

Figure 4.46. X-ray diffraction patterns of spray dried powders E and F and mannitol raw material (Pearlitol SD 200).

The crystalline state of the two vaccine containing powders prepared for the *in vivo* immunization study was also confirmed by the presence of the endothermic peak at 166 °C, ascribed to the melting of mannitol (Figure 4.47).

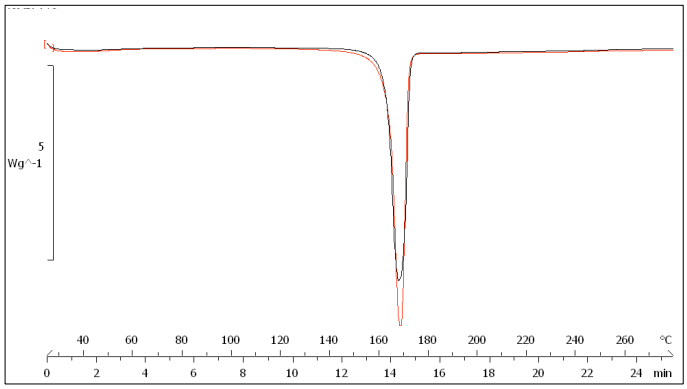

Figure 4.47. DSC traces for powders E and F.

PART II

5. AIM

According to the World Health Organization (WHO), Tuberculosis (TB) is a major communicable infectious disease. In the same time nontuberculous mycobacteria are increasingly recognized worldwide, as cause of superinfections in immunocompromised patients [97]. As already explained in the Chapter 1, Bacillus Calmette–Guérin (BCG) vaccine is the only one currently approved. This vaccine, however, presents many limits, especially in covering against all TB strains, including drug resistant TB [31] and NTM, towards HIV-infected people and connected to its partial and variable protective effects against pulmonary TB [32]. Said limits are strongly prompting the scientific community toward the development of an efficient vaccine against TB.

Beside the availability of a better performing agent determining an immune response against mycobacteria, from the point of view of the delivery, a significant step toward a novel vaccine would imply the development of a platform for the efficient targeting of the vaccine to alveolar macrophages as primary site for eliciting a suitable immune response in the organ that represent the principal way of colonization for these pathogens.

As a first step toward this approach in the aim of the second part of the present work was to develop a novel platform for pulmonary administration of two first-line antimycobacterial drugs with specific targeting to alveolar macrophages. As a matter of facts, TB and nontuberculous mycobacteria (NTM) infections treatment with antibiotics are very challenging, because of the difficult accessibility to the pharmacological target inside alveolar macrophages (AMs) and the peculiar capability of Mycobacterium tuberculosis (Mtb) to slow-down its metabolism and survive in a dormant state [35]. NTM are, to some extent, similar to Mtb, as they can infect alveolar macrophages. Hence, for the above reasons and because the lungs are the primary entrance for mycobacteria, an efficient pulmonary delivery of antibiotics has been largely investigated during the last decade [42]. Many studies reported different antibiotics

delivery strategies targeting AMs [98] to increase the efficacy of antibiotics, reduce resistance and, at the same time, lower the dose of drugs in blood, and, consequently the side effects.

Few studies reported that low molecular weight hyaluronic acid sodium salt (HA) can promote the targeting infected AMs through CD44 binding [52]. Other studies have shown that particles with a size distribution between 200-550 nm are more subjected to AMs internalization [99]. Moreover, the association of efflux pump inhibitor has been introduced as a new approach for increasing the intracellular antibiotic concentration [100].

Considering this scenario, the specific aim of this section was to develop an innovative dry powder for inhalation (DPI) in the form of respirable microparticles consisting of HA nanoparticle agglomerates for AMs phagocytosis loaded with two different antibiotics, rifampicin and isoniazid, and one efflux pump inhibitors, verapamil hydrochloride.

6. MATERIALS AND METHODS

6.1 Materials

Isoniazid (INH) and rifampicin (RIF), were obtained by Alfa Aesar GmbH & Co. KG (Germany) and Sanofi-Aventis S.p.a. (Italy) respectively. Verapamil hydrochloride (VER) was bought by Hangzhou Dayangchem Co. Ltd. (China). Low molecular weight HA (PrymalHyal 50, average MW= 29.5 kDa) was obtained from Soliance (France). High molecular weight HA (MW= 750-1000 kDa) was purchased by Contipro Biotech sro, Czech Republic. For dissolution experiments phosphate buffer saline (PBS) at pH 7.4 was prepared according to Eur. Ph. 9th ed., using monobasic potassium phosphate and sodium hydroxide (ACEF, Italy), while dialysis membranes (cut-off 14 kDa) were acquired from Sigma-Aldrich (USA). All solvents used were at analytical grade and ultrapure water (0.055 μS/cm, TOC 1 ppb) was obtained by reverse osmosis (Purelab Pulse + Flex ultrapure water, Elga-Veolia, Italy).

6.2 Methods

6.2.1 Powders production by spray drying

A powder (P1) containing sodium hyaluronate (HA) at low molecular weight and the three drugs, i.e. rifampicin, isoniazid and verapamil, was produced employing a mini spray dryer B-290 (BÜCHI, Switzerland) starting from a nanosuspension (0.59 w/v) obtained with antisolvent process (Figure 6.1) according to the method described by Martinelli (F. Martinelli, Ph.D. Thesis “Particle engineering for the production of respirable dry powder formulations”, 2016) [101].

The drying parameters were set as follow: inlet temperature (90°C), drying air flow rate (750 L/h), aspiration (35 m^3/h), solution feed rate (3.0 mL/min) and nozzle diameter 0.7 mm [102].

To produce 100 mL of the starting nanosuspension, low molecular weight HA (35.04 g) and isoniazid (18.12 g) were dissolved in 30 mL of purified water, while rifampicin (35.18 g) and verapamil HCl (11.66 g) in 70 mL of ethanol. The latter solution was added to the aqueous one under continuous magnetic stirring, at 200 rpm, and contemporary homogenization with Ultra-Turrax® TP 18/10 at 10,000 rpm for 15 min (IKA Werke GmbH & Co, Germany).

The same production process was adopted to prepare other three powders, for comparison purposes:

- P2: as P1, but without verapamil HCl;
- P3: as P1, but with high molecular weight HA instead of low molecular weight HA;
- P4: as P3, but without verapamil HCl.

A physical mixture of the three drugs (raw materials) in the same weight ratio was also produced by blending all components with a Turbula® mixer (type T2A, WAB, Switzerland) at 25 rpm for 15 min.

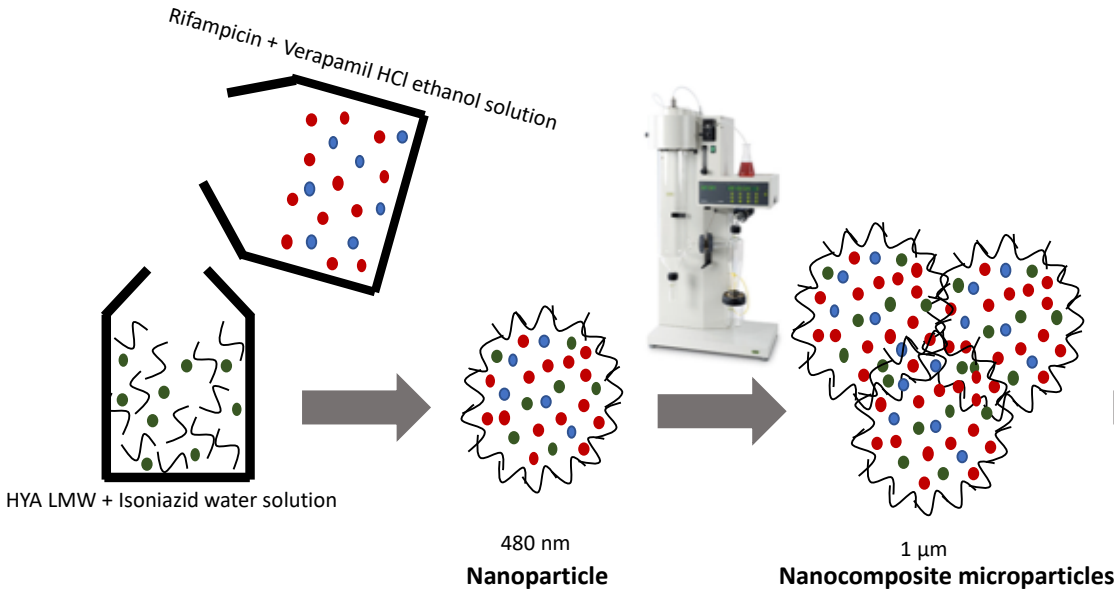

Figure 6.1. Schematic of the proposed nanoparticle formation with antisolvent process and successively aggregation of nanoparticles to form a microparticle during spray drying.

6.2.2 Loading efficiency in the nanosuspension and in the spray dried powder

The amount of the drugs loaded in the nanoparticles was evaluated in the dried powder P1 as well as by difference of the amount remaining in the starting nanosuspension. About 30 mg of powder were accurately weighed, dispersed in 5 mL of ultrapure water and exposed to ultrasound application for 7 min in order to obtain a homogenous suspension. Samples of 500 µL of both starting nanosuspension and suspension obtained from the powder, were filtered using Vivaspin® 500 centrifugal concentrators (Sartorius, Germany) following the instructions of the manufacturer using a centrifuge (Model D3024, Scilogex, Connecticut, USA) operated at 19,980 g for 15 min. The obtained filtrates, which contained the drugs in solution and hence not entrapped in the nanoparticles, were analyzed by HPLC.

6.2.3 Drugs content in the spray dried powders

The total drugs content in the spray dried powders was evaluated by dissolving 5 mg of powder in 100 mL of a solution water: acetonitrile 50:50 v/v. The obtained solutions were analyzed by HPLC.

6.2.4 HPLC analysis

A specific high performance liquid chromatography with UV-detection (HPLC-UV) method for the contemporary quantification of isoniazid, rifampicin and verapamil HCl was developed modifying the method reported by Chan et al [38]. An Agilent 1200 Series HPLC-UV (Agilent Technologies, USA) equipped a C18 µBondapak, 10 µm, 3.9x300 mm column (Waters Chromatography Ltd, Ireland) was used as stationary phase.

Standard and samples were prepared in water:acetonitrile 50:50 v/v. Mobile phase was pumped in gradient elution using: A) 0.05 M potassium phosphate buffer (KH_2PO_4) (KPB) adjusted to

pH 3 with diluted phosphoric acid (10% v/v); B) methanol; C) ultrapure water and D) acetonitrile. The adopted gradient is reported in Table 6.1. The injection volume was set at 10 µL, while the flow rate and wavelength were modified during the analysis as reported in Table 6.1 in order to detect the three drugs. Retention time was 3.5 min for isoniazid, 20 min for rifampicin and 40.5 min for verapamil HCl. Linearity of the responses (Figure 6.2) was assessed between 0.001 and 0.1 mg/mL (R^2= 0.999) for each drug. The limit of detection (LOD) and the limit of quantification (LOQ) were between 1-2 and 3-4 µg/mL respectively for all drugs.

Table 6.1 Mobile phase gradient and flow as well as wavelengths of the UV detector used to quantify the three drugs by HPLC: KPB (A), methanol (B), ultrapure water (C) and acetonitrile (D).

Time (min)	**A (%)**	**B (%)**	**C (%)**	**D (%)**	**Flow rate (mL/min)**	**Wavelength (nm)**
0-7	90	10			1.0	261
7-8		5	95			
8-10			90	10	1.2	
10-12			80	20		278
12-34			63	37	1.5	
34-35	60			40	1.2	
35-52	50			50	1.0	254
52-55	90	10				261

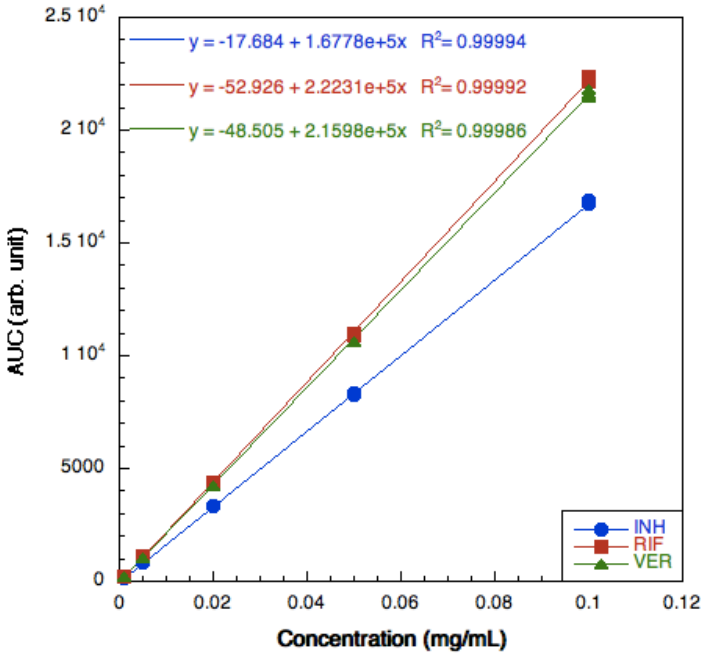

Figure 6.2. Responses of the UVC detector as a function of concentration of solutions containing the three drugs between 0.001 mg/mL and 0.1 mg/mL. Circle, isoniazid; square, rifampicin and triangle verapamil HCl.

6.2.5 Particle size distribution

Dynamic Light Scattering (DLS, ZetaPALS®, Brookhaven, USA) was used to measure the average particle size of the nanosuspension at 25 °C before spray drying and to investigate the de-aggregation kinetics of the spray dried powder when dispersed in ultrapure water under two different conditions: upon ultrasound application for 1, 5, 10 and 15 min (Ultrasonic Bath, USC-T, VWR, USA), or simply by magnetic stirring (200 rpm) at room temperature for 30, 50, 60, 75 min.

The spray dried powder and the physical mixture of raw materials were characterized in terms of particle size distribution by laser diffraction (Spraytec®, Malvern, UK). About 5 mg of powder were suspended in 5 mL of isopropanol and sonicated for 5 min. Obscuration threshold was around 5%. Data were expressed as volume diameter of 10^{th} ($D_{v,10}$), 50^{th} ($D_{v,50}$) and 90^{th} ($D_{v,90}$) percentile of the particle population and as Span value $[(D_{v,90}-D_{v,10})/D_{v,50}]$.

All particle size measurements were carried out in triplicate.

6.2.6 Solid state characterization and thermal analysis

Thermogravimetric analysis (TGA/DSC1 STARe System, Mettler Toledo, Italy) was carried out by placing about 5 mg of powder samples in a 70 μL alumina pans with a pierced cover. Samples were heated under a flux of dry nitrogen (100 mL/min) at 10 °C min^{-1} in the 25–150 °C temperature range. Each analysis was performed in triplicate.

Differential Scanning Calorimetry (DSC) was adopted to evaluate the solid-state of raw materials and of the dried powder. Measurements were performed on an Indium calibrated (onset of melting T_m = 157.1°C, enthalpy of melting ΔH_m = 27.84 J g^{-1}) Mettler DSC 821e (Mettler Toledo, Italy) operated using STARe software (Mettler Toledo, Italy). DSC traces were recorded by placing accurately weighed quantities (5–11 mg) in a 40 μL aluminum pan which was then sealed and double pierced. Scans were performed between 25 and 250 °C at heating rate of 5°C min^{-1} under a flux of dried nitrogen (100 mL/min). Each powder sample was analyzed at least in duplicate. Data relevant to the observed thermal events were reported as onset and peak temperatures.

Crystalline state was also assessed by Powder X-Ray Diffraction (Miniflex, Rigaku, Japan). The powder sample (about 300 mg) was placed in a sample holder and flattened using a glass slide. Radiation CuKα of 30 kV, scan speed of 0.05°/min and a range of scan between 2° and 35° were used.

6.2.7 Microscopy

Microparticles and nanoparticles morphology were studied by Scanning Electron Microscopy, SEM (SUPRA 40, Carl Zeiss NTS GmbH, Germany), and Transmission Electron Microscopy, TEM (JEM 2200-FS microscope, JEOL Ltd., Japan) respectively.

For SEM analysis, powders were deposited on adhesive black carbon tabs pre-mounted on aluminum stubs and exposed to a gold metallization process to deposit a gold film of 60 nm.

The microscope was operated after 30 min of depressurization under high vacuum conditions ($1.33x10^{-2}$ Pa) with an accelerating voltage of 1.5 kV.

The morphological analysis of the nanoparticles was carried out using TEM operated at 80 kV. Nanoparticles were recovered from the dried powder P1 and dispersed in ultrapure water (1 mg/mL) put in an ultrasonic bath for 5 min. For sample preparation, a drop of the suspension was deposed on formvar/carbon coated copper grids (300 Mesh, Electron Microscopy Sciences, USA). After 10 min the excess sample was gently dried with filter paper and the grid was stained using a drop of UranyLess (Electron Microscopy Sciences, USA) for 90 s. Then, the grid was rapidly dipped in particle free ultrapure water to remove excess staining.

6.2.8 Aerodynamic performance

The aerodynamic performance of the powders was investigated using a Fast Screening Impactor (FSI, Copley scientific Ltd, UK). 5 mg of powder were loaded manually in a hypromellose Quali-V-I capsule size 3 (Qualicaps®, Spain) and aerosolized using two different devices: RS01® (RPC, Plastiape, Italy) and Turbospin® (PH&T, Italy). A single capsule was discharged inside the impactor for each test. The entire system was connected to a vacuum pump (Mod. 1000, Erweka GmbH, Germany) which created the air flow to aerosolize the powder and distribute it in the FSI. The flow rate used during each test was adjusted, according to current USP monograph, with a Critical Flow Controller TPK (Copley Scientific, Nottingham, UK) in order to produce a pressure drop of 4 kPa over the inhaler. Thus, flow rates of 60 L/min for RS01® and of 65 L/min for Turbospin® were set before each experiment using a Flow Meter DFM 2000 (Copley Scientific, Nottingham, UK). The device was activated and the vacuum applied for 4 s for RS01® and for 3.7 s for Turbospin®, so that a total volume of 4 L of air was drawn through the inhaler during the experiment.

The aerodynamic performance was tested in triplicate and the samples collected using water-acetonitrile mixture 50:50 v/v. The residual amount of the drugs still present in the capsule and

in the device after aerosolization as well as the powder deposited in the rubber adaptor and in the induction port, were solubilized in 50 mL of the same solvent mixture. Ten mL of solvent mixture were put in the CFC insert before the aerosolization; thereafter another 20 mL were used to collect the powder inside CFC. Finally, the filter in the FFC was transferred in a glass crystallizer and washed with 20 mL of the solvent mixture; the crystallizer was then put in an ultrasonic bath for 5 min, in order to allow complete dissolution of the powder deposited on the filter. Filter and device plus capsule samples were filtered with 0.45 μm cellulose acetate syringe filters (Labservice Analytica Srl, Italy). The amount of the drugs in the obtained solutions was quantified by HPLC.

The quantification of the drugs deposited in the impactor allowed for the calculation of the following aerodynamic parameters: the emitted dose (ED) was the amount of each drug which was emitted from the device namely, the amount of drug collected from the induction port (IP) to the filter (F). The emitted fraction (EF), calculated as the ratio between the ED and the amount of powder loaded in the capsule. The fine particle dose (FPD) was the mass of each drug with aerodynamic diameter lower than 5 μm, i.e. the amount found in the FFC filter; the fine particle fraction (FPF) was calculated as the ratio between FPD and ED.

6.2.9 Stability

Stability of the spray dried powder P1 was assessed by measuring the drugs content and aerodynamic performance (RS01®) after storing about 100 mg of the powder in a 20 mL amber vial sealed with a clamped elastomeric stopper both for 1 month under ambient conditions and for 24 hours at 50 °C.

6.2.10 Dissolution

The dissolution rate of the drugs from both the spray-dried powder P1 and the physical mixture of the three drugs was investigated with a Franz type cell (surface 60 mm^2) with a dialysis

membrane (cut-off 14 kDa) placed between the donor and the receptor compartments. The dissolution was carried out using 4.7 mL of phosphate buffer at pH 7.4 (Ph. Eur. 9th ed.), for 40 hours at 37 °C, under continuous magnetic stirring (350 rpm). In detail, the receptor was loaded with 4.2 mL of phosphate buffer and the dialysis membrane was put between the donor and receptor compartments. Then, 0.1 mL of phosphate buffer were added to wet the upper side of the membrane in the donor. The assembled system was equilibrated for 1 hour at 37 °C. Successively, 5 mg of powder were carefully spread onto the dialysis membrane in the donor and 0.4 mL of phosphate buffer were added to wet the deposited powder. Samples (0.7 mL) were withdrawn from the receptor at fixed time. After each sampling the volume of the solution withdrawn was replaced with the same volume of fresh buffer, in order to keep the total volume of buffer inside the receptor unvaried. The amount of the three drugs dissolved were quantified by HPLC using the method described above.

6.2.11 *In vitro* cytotoxicity

Cell culture and differentiation

The human monocytic cell line THP-1 cells (ATCC, Manassas, VA, USA) was cultured in RPMI 1640 medium (high glucose with L-Glutamine with HEPES, ATCC, Manassas, VA, USA) supplemented with 10% v/v of fetal bovine serum (Corning, Manassas, VA, USA) and 0.05 mM of 2-mercaptoethanol (Sigma-Aldrich, USA) at 37 °C with 5% CO_2 in a humidified incubator. THP-1 cells were differentiated just prior to experimentation by centrifuging and resuspending the cells in fresh media containing 20 nM of phorbol myristate acetate (PMA, Sigma Aldrich, Missouri, USA) for 24 hours.

Cell Viability Tests

The XTT cell proliferation assay (Thermo Fisher Scientific, USA) was used to determine cytotoxicity on THP- 1 cells, following the manufacturer's instructions; the absorbance was

read at λ 450 nm. The four formulations were tested in THP-1 cells by incubating in 96-well plates for 24 or 48 hours with six different concentrations (between 1.0-0.0125 mg/mL). The formulations were previously prepared by uniformly suspending the powders in RPMI 1640 medium and applying a brief sonication for 10 min. Cell viability was expressed as a percentage of the control group.

6.2.12 Bactericidal activity

The efficacy of the dried powders against *Mycobacterium smegmatis* (*M. smeg*) was tested *in vitro* after 24 and 48 hours of incubation at 37°C shaking at 220 rpm. The two time points were chosen based on the *in vitro* drug release data. Different concentrations (1.0-0.0125 mg/mL) of the powders P1 and P2 were prepared in Middlebrook 7H9 broth medium (Sigma Aldrich, USA) and added to $4x10^5$ CFU/mL of *M. smeg* culture, prepared resuspending a small amount of bacteria from a steak plate in 3 mL of fresh 7H9 broth medium and incubating for 24 hours at 37°C shaking at 220 rpm. Optical density at λ 600 nm was, then, measured (Biophotometer D30, Eppendorf, Germany) for the calculation of the concentration of bacteria (1 absorbance value = $3x10^8$ CFU/mL). The *M. smeg* concentration (CFU) was chosen based on preliminary studies of *in vitro* infection of macrophages, where it was showed that the best multiplicity of infection (MOI) was 1 ($4x10^5$ cells/mL cells confluency in a 12 well plate). After 24/48 hours 100 µL were transferred in a 96 well-plate and diluted 4 times 1:10 with PBS. The 4 serial dilutions were, then, plated on 7H10 (Sigma Aldrich, USA) agar petri plates and incubated for 3 days at 37°C. Bacteria grown was, finally, count and plot. Single raw materials were also assessed, as control, at the same percentage w/w as in 0.5 mg/mL suspension of P1 and P2. Moreover, kanamycin at minimum inhibitory concentration (MIC, 25 µg/mL) was tested as negative control and growth baseline was determined by bacteria only.

6.2.13 Intracellular killing of *M. smeg.* in macrophages

An *in vitro* infection and treatment was performed on THP-1 cells differentiated into macrophages. Macrophages were infected for 3 hours (MOI 1) with a *M. smeg.* culture prepared as reported in 5.2.12. Wells were washed three-times with PBS to remove extracellular *M. smeg*, as validated in preliminary studies of *in vitro* infection. P1 and P2 formulations were resuspended in RPMI medium and sonicated for 10 min to achieve a homogenous suspension. Suspensions were added to the infected macrophages.

Different powders concentrations were tested for three times of incubation (24, 48 and 96 hours) with respect to the minimum inhibitory concentration (MIC) of RIF reported for *M. smeg.* (31.8 μg/mL) [103]:

- 24 hours experiment: one concentration higher (0.125 mg/mL, corresponding to 0.36 mg/mL of RIF) and two lower (0.05 mg/mL, corresponding to 0.017 mg/mL of RIF and 0.025 mg/mL, corresponding to 0.009 mg/mL of RIF) RIF concentration, considering its content (% w/w) in the powders;
- 48 hours: two concentrations higher (0.5 mg/mL and 0.125 mg/mL) and one lower (0.05 mg/mL) RIF concentration, considering its content (% w/w) in the powders;
- 96 hours: two concentrations higher (0.5 mg/mL and 0.125 mg/mL) and two lower (0.05 mg/mL and 0.025 mg/mL) RIF concentration, considering its content (% w/w) in the powders.

After incubation, wells were washed three-times with PBS and 500 μL of sterile lysin solution (0.05% w/v Sodium Dodecyl Sulphate in ultrapure water). Plates were incubated at room temperature for 5 minutes, 100 μL were transferred in a 96 well-plate and diluted 4 time 1:10 with PBS. The 4 serial dilutions were, then, plated on 7H10 agar petri plates and incubated for 3 days at 37°C. Bacteria grown were, finally, count and plot.

Powders 3 and 4 were, also, tested, following the same protocol of 3 hours of infection and 48 hours of incubation with formulations at 0.5 mg/mL, 0.125 mg/mL and 0.05 mg/mL.

To better investigate the different efficacy of P1 and P2 in inhibit *M. smeg.* growth, others infection experiments were performed. THP-1 cells differentiated into macrophages were infected for 24, 48 and 96 hours (MOI 1) and incubated with powders suspensions (0.5 mg/mL, 0.125 mg/mL and 0.05 mg/mL) for 48 hours. As negative control infected cells were treated with Kanamycin at MIC and not infected cells, whereas as positive control not treated infected cells were used.

6.2.14 Confocal microscopy

Confocal microscopy was employed to investigate the uptake of nanoparticles from macrophages.

In this experiment two new spray dried powders of composition similar to P2 and P4, but containing 5% w/w fluorescein sodium salt (Polichimica srl, Italy) were used.

$2x10^5$ THP-1 cells were differentiated to make them adherent in an 8 well-plate for microscopy (LAB-TEK Chambered Coverglass, Thermo Scientific, Massachusetts, USA). A suspension at the concentration 0.25 mg/mL in RPMI of P2 or P4, was added to macrophages and plates were incubated for 24 hours at 37°C. Wells were, then, washed two times with PBS and, to fix cells, 200 µL of para-formaldehyde (PFA) solution in PBS (4% v/v) was added for 15 minutes at room temperature. PFA solution was removed, wells were washed with PBS other two times and plates were stored at 4 °C overnight. Thereafter, wells were treated for 15 minutes at room temperature and protected from light with 200 µL of a PBS solution containing 2 drops/mL of a dye for nuclear stain (NucRed Live 647, Invitrogen, California, USA). After three washes with PBS, plates were covered with an aluminium foil and images were taken through an Axiovert 100M microscope (Carl Zeiss, Germany); Z-stack acquisition was also performed. Control wells with cells not treated were taken as control.

6.2.15 Statistical analysis

Values were expressed as mean ± standard deviation. Statistical significance of differences was examined using two-tailed unpaired t-test with significance level fixed at p-value ≤ 0.05. Statistical analysis was performed with Microsoft Excel version 16.18 (Microsoft Corporation, Washington, USA) and Prism 7 software version 7.0d (GraphPad Software, California, USA).

7. RESULTS AND DISCUSSION

7.1 Spray dried powders production

Low molecular weight sodium hyaluronate (LMW HA) (0.83% w/v) was dissolved in purified water (30% v/v) and then, ethanol (antisolvent agent, 70% v/v) was added dropwise to produce a stable colloidal nanosuspension of about 400 nm [102]. The same method could not be applied to the production of a nanosuspension with high molecular weight sodium hyaluronate (HMW HA), probably due to the higher viscosity of the HA water solution, which determined a separation between the aqueous and alcohol phases, with slow ethanol diffusion in the aqueous solution of HA and consequently precipitation of HA in form of large aggregates instead of nanoparticles.

Nevertheless, in order to efficiently load these LMW HA nanoparticles with two antibiotics (isoniazid, INH, and rifampicin, RIF) and an efflux pump inhibitor (verapamil HCl, VER), a preliminary formulation study was carried out to optimize the starting suspension in terms of total solid concentration and components ratio. This study was done employing first of all laser light diffraction and, successively, dynamic light scattering to determine the size of the LMW HA particles precipitated by ethanol addition.

The first suspension (number 1) was prepared starting from a water (30% v/v) solution of HA low molecular weight (0.83% w/v), based on the solution/suspension equilibrium plot reported by Martinelli [101] and what reported by Martinelli et al. [102] to spray dry LMW HA nanoparticles. First of all, the four solutes (HA, INH RIF, VER) were added at the same amount. The suspension obtained was composed by different particle populations (Span = 24.26) (Figure 7.1).

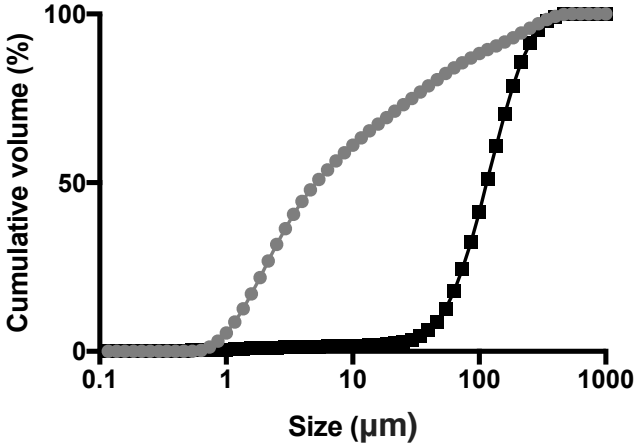

Figure 7.1. Particle size cumulative undersize distribution evaluated by laser light diffraction of suspension number 1 (circle) and of suspension number 2 (square).

Considering the results obtained, successively, components ratio was changed based on Chan et al. and Parumasivam et al. publications [38,104]. A new formulation was produced employing always 0.83% w/v of LMW HA, a ratio 1:3 between antibiotics (RIF+INH, that were in ratio 1:2 to each other) and VER. Rifampicin solubility was the major issue to address; thus, after the determination of its solubility in the ethanol fraction (70% v/v), a concentration of 4 mg/mL was selected.

The monomodal cumulative undersize distribution of the particles of this second suspension (number 2), obtained after 30 minutes of Ultra-Turrax® mixing, is reported in Figure 7.1. The value of mean volume diameter was around 100 µm, still too high. For this reason, in the third suspension tested the LMW HA was reduced to a concentration of 0.2% w/v, while the same ratios were maintained between the other components. After 30 minutes of mixing with Ultra-Turrax®, the suspension was analyzed by laser light diffraction and no size distribution could be observed, suggesting that the particle diameter was lower than the lower detection limit of the Spraytec®. Thus, the measurement was repeated with DLS and a mean diameter of 405.1 ± 5.35 nm was obtained.

The nanosuspension with the same ratios was prepared again and nanoparticles with average diameter of 480 ± 150 nm were obtained. The encapsulation efficiency data on this nanosuspension reported an entrapment efficiently higher than 50% for all the drugs. In particular, for RIF 84.57 ± 3.47% of the leaded dose was associated with nanoparticles and in the case of VER, the whole dose was encapsulated in the nanoparticles (100.00 ± 0.00%). INH showed the lowest encapsulation value (53.93 ± 0.82%). This different behavior was attributed to the hydrophilic nature of INH (solubility in water 140 mg/mL) and the production method of the nanosuspension. Indeed, INH was dissolved in the water fraction together with the polymer; so, during the formation of the polymer nanoparticles, the drug tended to remain into the aqueous phase, resulting in a relatively low entrapment percentage.

This last nanosuspension was spray dried (Powder 1, P1) with a total solid concentration of 0.59 w/v; the theoretical composition percent is reported in Table 7.1 The yield of the spray drying process was 50.1%.

After the spray drying process, the encapsulation percentages decreased for all the drugs: 48.75% ± 4.32 for INH; 77.52% ± 0.11 for RIF and 80.45% ± 4.80 for VER. These values were slightly lower than the encapsulation efficiencies reported in other formulations using HA [105,106], but equal, and in some cases even higher, to the data published for nanoparticles prepared using the same drugs separately and a different type of polymers, e.g. chitosan [107-110].

Finally, other three powders were produced, keeping constant total solid content at 0.59% w/v, in order to be used as comparison in different experiments (Table 7.1). Powder 2 (P2) and powder 4 (P4) comprised fluorescein sodium salt, because they were both thought to be used for macrophages uptake imaging employing confocal microscope (see 7.13). Powder 3 (P3) and P4, were produced with high molecular weight sodium hyaluronate (HMW HA). All these powders were produced with the same spray drying parameters used for producing P1. Yields were comprised in a range from 58.23% for P2 to 81.31% for P4. Higher yields were obtained

with HMW HA (70-80%).

Table 7.1 Nominal composition of spray dried powders (% w/w).

Powder	HA	INH	RIF	VER	Fluorescein sodium salt
P1	LMW 35.0	18.1	35.2	11.7	-
P2	LMW 37.0	21.0	37.0	-	5.0
P3	HMW 35.0	18.1	35.2	11.7	-
P4	HMW 37.0	21.0	37.0	-	5.0

The drug content after the production reflected the nominal values (Table 7.2) for all formulations with a relative standard deviation ≤ 0.04% indicating an even drug distribution in the powders.

Table 7.2 Actual drug content expressed as % of the nominal value for the four powders produced. Mean values and standard deviations in parenthesis (n=3).

	Assay (% of the nominal value)			
Powder	**HA (%)**	**INH (%)**	**RIF (%)**	**VER (%)**
P1	-	98.4 (0.03)	100 (0.03)	100 (0.02)
P2	-	100 (0.04)	99.3 (0.01)	-
P3	-	98.1 (0.01)	98.6 (0.03)	98.7 (0.02)
P4	-	100 (0.01)	98.6 (0.04)	-

7.2 Solid state characterization of the reference Powder 1

After the spray drying process, most of the powder remained adhered to the glass surfaces of cyclone and collector; this phenomenon could be attributed to the high residual water content of the powder (6.3% w/w), evaluated through TGA and ascribed to the hydrophilic nature of HA that tends to entrap water in its structure [111].

This characteristic was also confirmed by the DSC trace of P1 (Figure 7.2), which presented a broad endothermic event between 25 and 130°C, reasonably due to the evaporation of residual water bonded to the polymer. This phenomenon was followed by an exothermic peak at high temperature (210-285 °C) ascribable to the thermal degradation of one or more components of the powder (likely HA). Solid state of P1 was also investigated by PXRD. Despite all the raw materials were crystalline, the powder collected after the spray drying process displayed the typical halo of an amorphous substance. Figure 7.3 shows the X-ray intensity in counts per second (cps) observed for each angle 2θ. From the diffraction pattern is clear that the crystalline nature of the three drugs was completely lost after the spray drying process.

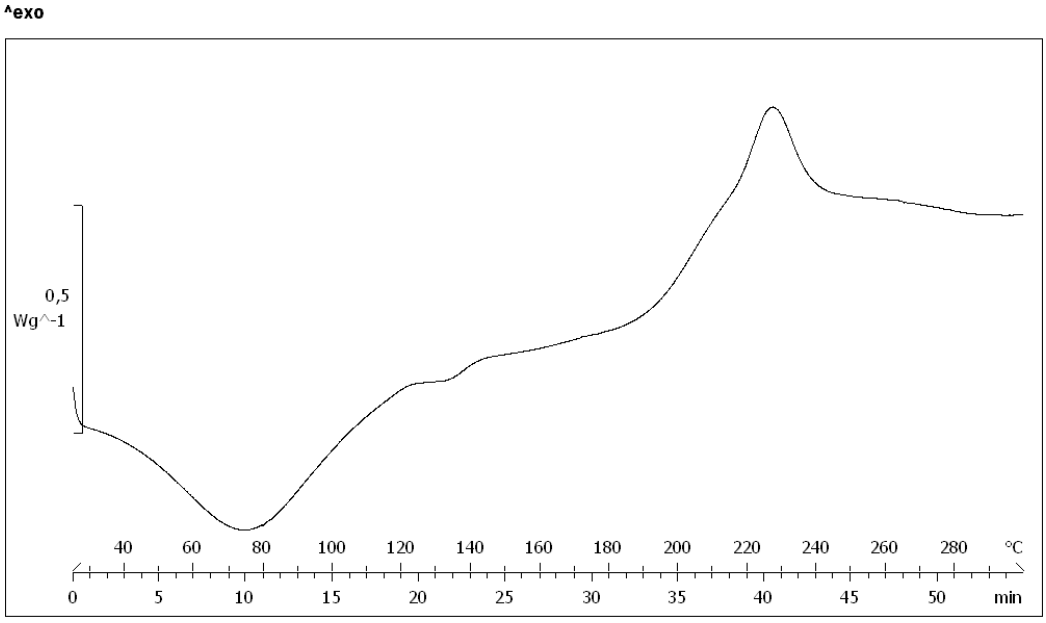

Figure 7.2. DSC thermograms of the spray dried powder 1.

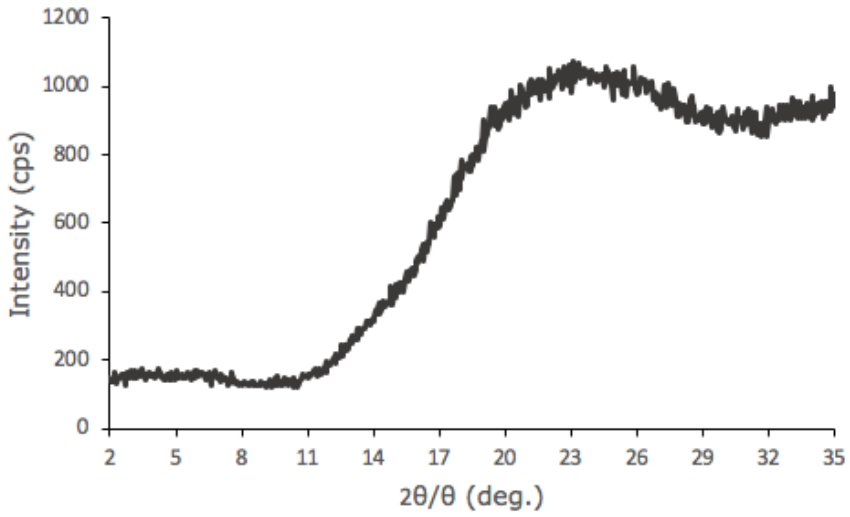

Figure 7.3. X-ray plot of the spray dried powder.

7.3 Particle size distribution of all powders

The spray dried powders were further investigated in terms of particle size distribution by laser diffraction. P1 and P2 proved to be composed of microparticles with a very small median volume diameter ($D_{v,50}$) of 0.94 ± 0.15 μm for P1 and 1.96 ± 0.38 μm for P2, and a very narrow monomodal distribution (Figure 7.4) as indicated by span value 1.79 ± 0.17 and 1.62 ± 0.15 for P1 and P2, respectively. Powders containing HMW HA reported larger and multimodal particle distributions (span value 6.53 ± 1.22 for P3 and 3.57 ± 0.11 for P4), likely to the above mentioned precipitation of the HMW HA during the spray drying process and the impossibility to obtain a stable nanosuspension. Even though $D_{v,50}$ for P3 was lower than P2 (1.21 ± 0.54 μm), $D_{v,90}$ for this formulation was the highest. Particle size distribution was completely shifted to the right for P4. Although these diameters were geometric rather than aerodynamic, these data suggested that especially P1, but also P2, may be particularly suitable for inhalation and deposition in the deep alveolar region, if compared with the particle size distribution of the physical mixture of the three drugs raw materials that presented median volume diameter of 11.67 ± 0.64 μm as displayed in Figure 7.5.

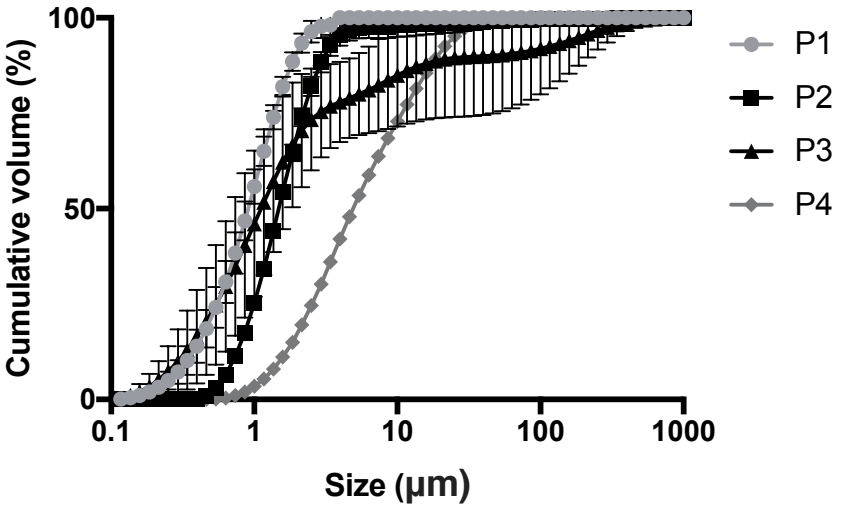

Figure 7.4. Cumulative undersize particle distribution evaluated by laser light diffraction of the spray dried powders P1 (gray circle), P2 (black square), P3 (black triangle) and P4 (gray rhombus). The bars represent the standard deviation (n=3).

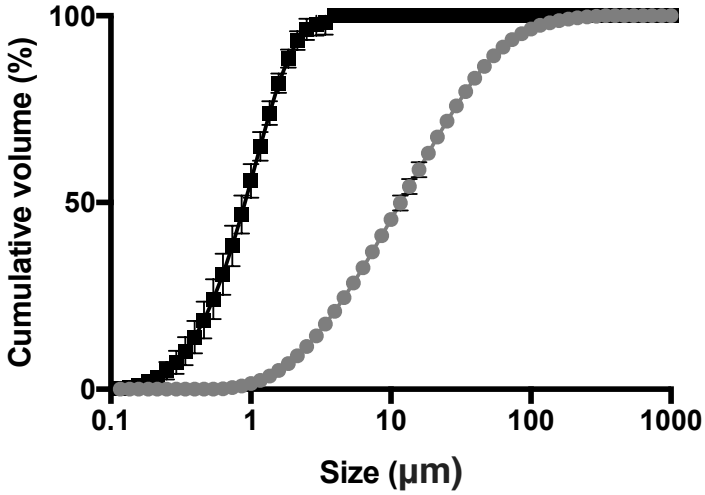

Figure 7.5. Cumulative undersize particle distribution evaluated by laser light diffraction of the reference spray dried powder P1 (square) and of the physical mixture of the drugs (circle). The bars represent the standard deviation (n=3).

7.4 Aerodynamic performance of the main spray dried Powder 1

The aerodynamic performance of the main powder was evaluated with two different devices (RS01® and Turbospin®) using the Fast Screening Impactor (FSI). Figure 7.6 represents the percentage distribution relevant to the sum of the percentages of each of the three drugs. With both devices, the highest percentage of drugs was found in the Fine Fraction Collector, where the particles with an aerodynamic diameter < 5 µm are collected. However, Turbospin® was

more efficient in emitting the powder when compared to RS01®. Indeed, the total emitted dose of the three drugs with the Turbospin® device was 2.24 ± 0.42 mg, corresponding 74.25 ± 8.20% of the loaded dose versus 1.62 ± 0.49 mg with RS01®, i.e. 50.40 ± 15.83% of the loaded dose. Furthermore, the deposition in the FFC was higher for Turbospin®. The better aerodynamic performance with the latter device can be explained taking into consideration the relatively high stickiness of the powder stemming from the high moisture content. With such a powder, the emission mechanism of the Turbospin®, which implied a reduced contact between the powder and the plastic parts of the device resulted in a higher emitted dose [112]. Nevertheless, it is worth noting that the powder emitted from the RS01® deposited almost entirely in the FFC (more than 90% of the ED for each drug was *vs* around 73% for the Turbospin®).

Table 7.3 summarizes the aerosolization performance of the three drugs with the two devices. In all cases the respirability was high, with FPF greater than 70% for all the drugs relative to the emitted dose). The Fine Particle Dose of the powder aerosolized with the two devices was not statistically different ($p \geq 0.5$), indicating that both devices presented the same de-aggregation efficiency despite the powder was constituted by very small particles, $D_{v,50} < 1$ μm, and contained a significant amount of residual moisture.

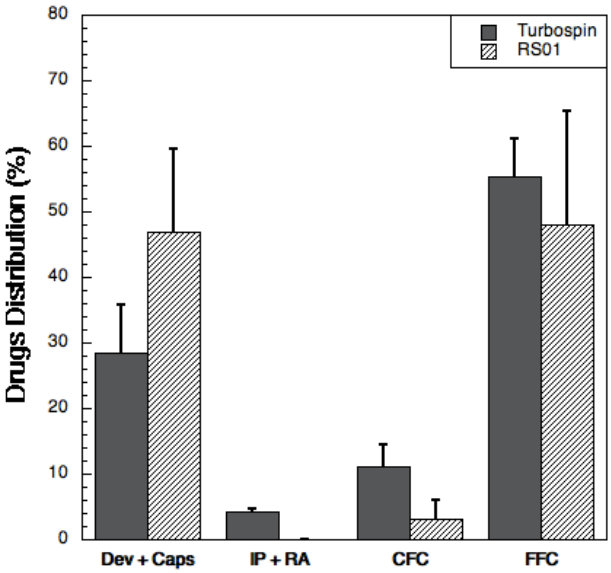

Figure 7.6 Drug distribution (% of the loaded amount) of the three drugs (sum of them) upon aerosolization with RS01® and Turbospin® in the Fast screening impactor. Data are expressed as mean of the values obtained for each drug in each analysis; the bars represent the standard deviation (n=3).

Table 7.3 Emitted Dose (ED), Emitted Fraction (EF), Fine Particle Dose (FPD) and Fine Particle Fraction (FPF) obtained upon aerosolization with the two devices, referred to the single drugs; mean values and standard deviation in parenthesis (n=3).

	RS01®				**Turbospin®**			
	ED (mg)	**EF (%)**	**FPD (mg)**	**FPF (%)**	**ED (mg)**	**EF (%)**	**FPD (mg)**	**FPF (%)**
INH	0.44 (0.14)	49.35 (15.32)	0.40 (0.16)	90.62 (8.15)	0.63 (0.17)	88.72 (3.35)	0.47 (0.10)	76.88 (7.48)
RIF	0.87 (0.26)	47.86 (14.19)	0.83 (0.29)	93.55 (5.69)	1.23 (0.20)	74.75 (6.23)	0.96 (0.15)	77.68 (4.87)
VER	0.31 (0.10)	50.89 (16.16)	0.30 (0.11)	93.89 (5.72)	0.37 (0.04)	68.43 (3.14)	0.30 (0.05)	80.54 (5.01)

7.5 Aerodynamic performance of the P2, P3 and P4 spray dried powders

Aerodynamic performance was studied also for spray dried powders produced as comparison of the main powder P1 (Figure 7.7). Turbospin® was employed as device, due to the better emission values obtained with P1.

Emitted fraction was also for these powders about 70%. FPFs of P3 and P4, were similar to that of P1 whereas the value obtained for P2 was significantly lower. Thus, also powders prepared with HMW HA proved to be respirable.

In any case, the idea behind this project was to produce a highly respirable HA-based dry powder for the efficient deliver to the lungs, but also to increase macrophages uptake. Therefore, powder P1 should be considered, in principle, the most appropriate DPI as it should be constituted of nanoparticles of diameter suitable for AMs uptake, exploiting the capability of LMW HA to bind CD44 receptors; this characteristic is in fact reported to be dependent by HA molecular weight.

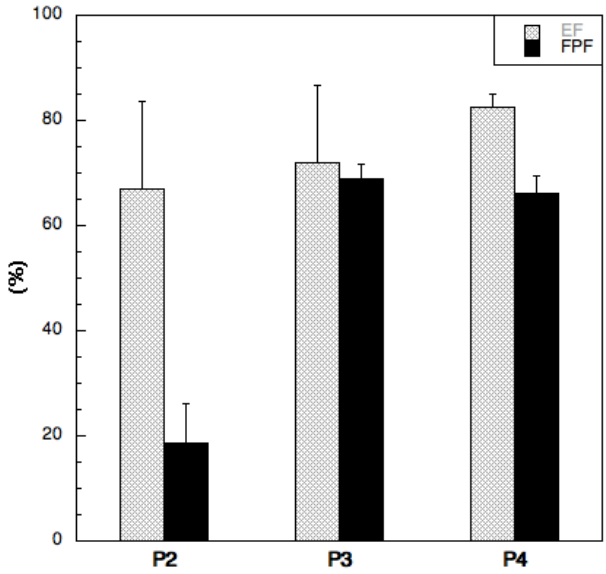

Figure 7.7 Emitted Fractions (EF) and Fine Particle Fractions (FPF) of powders P2, P3 and P4 aerosolized with Turbospin® in the Fast screening impactor. Data are expressed as mean of the values obtained for each drug in each analysis; the bars represent the standard deviation (n=3).

7.6 P1 spray dried microparticles de-agglomeration study by dynamic light scattering

Taking into account the above reported considerations, the demonstration of the correctness of rationale beyond the production of a respirable powder (P1) starting from a nanosuspension implies the verification of the reconstitution of the parent nanoparticles once the microparticles get in contact with the biological fluids. Because of their size and composition, the nanoparticles would therefore be more prone to be captured and internalized by AMs (Figure 7.8). The de-aggregation kinetics of the microparticles was investigated by DLS. Figure 7.9 reports the time-dependent value of diameter of the particles in suspension obtained when the spray dried particles are re-suspended in ultrapure water. After 75 minutes of simple magnetic stirring, the average particle size of the dispersed particles reached a value comparable to that of the initial nanosuspension. As expected, this time was considerably lower (15 minutes) when the re-suspended particles were submitted to ultrasounds. These data, suggest that once inhaled, these microparticles could be able to de-agglomerate progressively with a linear slow rate in about one or two hours, giving rise to particles with suitable a diameter for AMs phagocytosis [41,99].

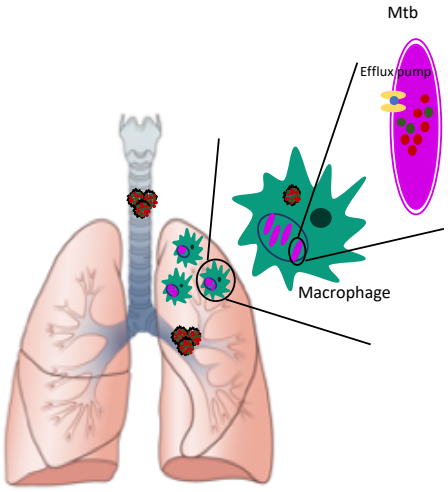

Figure 7.8. Schematic of the rationale beyond the production of a respirable powder starting from a nanosuspension comprising LMW HA, two first-line antibiotics and an efflux pump inhibitor.

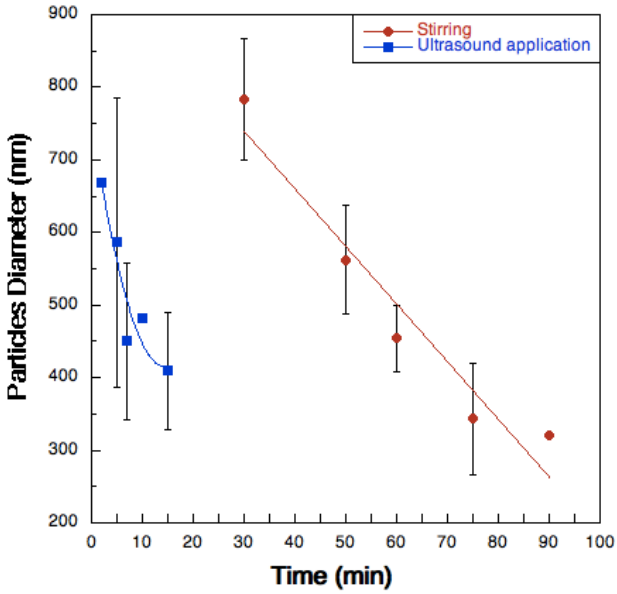

Figure 7.9. Diameter value as a function of time of the microparticles suspended in two difference test conditions: magnetic stirring (red circles) and ultrasound application (blue squares).

7.7 Morphology of particles constituting P1

The morphology of the micro- and nanoparticles was studied by SEM and TEM, respectively. SEM pictures (Figure 7.10 panel A) show the generally uniform shape of the particles that presented a slightly rough surface. The powder was re-dispersed in water and put in an ultrasonic bath for 15 min in order to allow de-aggregation. Figure 7.10 panel B shows the typical structure of the obtained assembly that clearly evidenced the presence of nanoparticles starting detaching to each other.

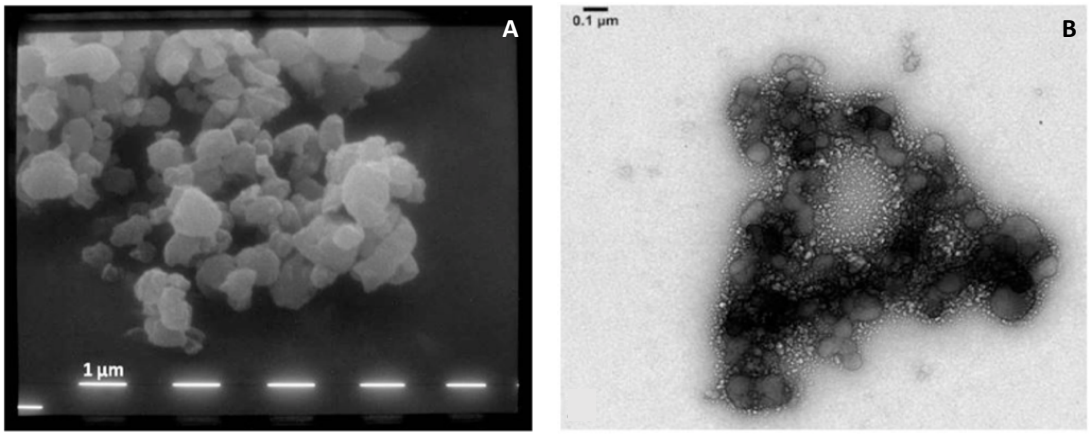

Figure 7.10. SEM (A) of the microparticles constituting the powder and TEM (B) pictures of the nanoparticles agglomerated to form the microparticles.

7.8 Drugs release from P1

The amount of antibiotics taken by AMs depends by particles size and composition. In this respect, drugs release from particles has to be consider as a key feature for achieving an optimal efficacy since the drugs should not be release significantly before the particle uptake from the AMs. The time for AMs uptake has been reported to occur within 1-6 hours [113].

The dissolution test was carried out by comparing the drugs release rate from powder P1 in comparison to the physical mixture of the drugs. Figure 7.11 panel A shows the release rate of the three drugs from the spray dried powder. Isoniazid was completely released in 24 hours: after 20 hours, the amount dissolved was already 80%. The release rate of rifampicin and verapamil was lower due to their relatively low solubility in water (2.5 mg/mL and 83 mg/mL respectively) [114,115]. The maximum levels reached after 40 hours were 70 and 60% of the dose for verapamil and for rifampicin, respectively. For these two drugs the release kinetics was more linear compared to isoniazid, that showed the typical release profile of a hydrophilic drug from a hydrophilic polymeric matrix. It is worth underlying that the relative release rate of the three drugs mirrors the relevant solubility in water as well as their degree of encapsulation.

The release rates from the physical blend of the three drugs (Figure 7.11 panel B) were slower for rifampicin and verapamil that released 50 and 60% of the nominal dose in 40 hours. The observed difference can be explained by considering the crystalline solid state of raw materials compared to the amorphous state of the spray dried powder. In addition, the higher particle size of the powder blend contributed to slow down the dissolution rate due to the lower surface area available for the contact with the dissolution medium. On the other hand, the release of isoniazid was similar for both the tested powders, because of the high solubility in water of this drug as well as because of the fact that in P1 less than 50% of the nominal isoniazid dose was encapsulated in the HA particles.

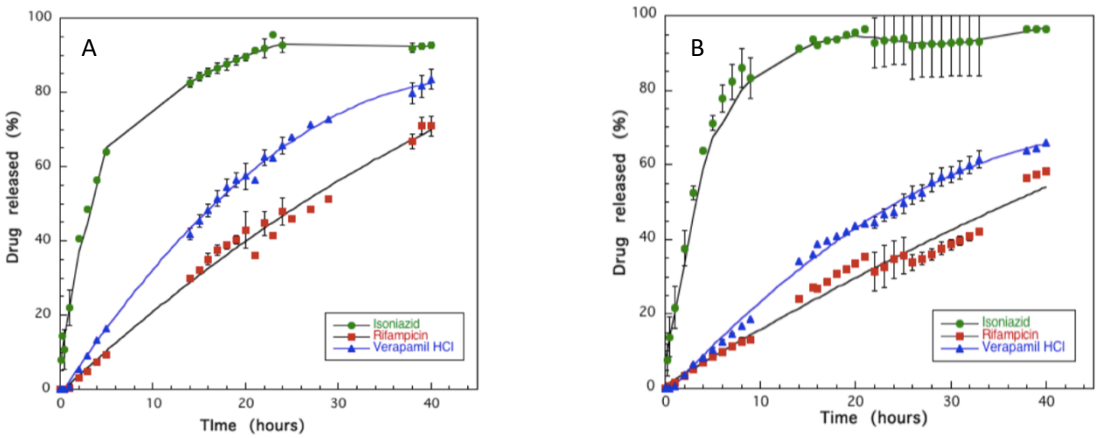

Figure 7.11. Release rate profiles of the drugs from P1 (panel A) and from the physical mixture of the three drugs (B)

7.9 Stability study of the main formulation P1

Powder 1 was stored for 1 month at not controlled temperature and for 24 hours at 50°C, in order to evaluate its stability in different conditions. Stability after storage was assessed measuring the drugs content and evaluating the aerodynamic performance. As to the drug content, Table 7.4 reports drugs content expressed as % versus the nominal value. The results observed after one month of storage at 25 °C were similar to the ones collected just after the powder production, whereas, when the powder was stored at 50 °C for 24 hours, isoniazid content significantly decreased, while only a slight degradation (well below 5%) was observed for rifampicin. Verapamil proved to be stable in all conditions tested.

Table 7.4 Actual drugs content, expressed as % versus the nominal value, upon storage in different conditions: 1 month under not controlled temperature and 24 hours at 50°C. Mean values standard deviations in parenthesis (n=3).

	Assay (% of the nominal value)	
	Month 1/ not controlled	**24 h/50°C**
HA LMW	-	-
INH	90.4 (0.02)	81.3 (0.02)
RIF	100 (0.01)	96.9 (0.03)
VER	100 (0.01)	99.2 (0.04)

The other parameter investigated for stability was the aerodynamic performance. The measurement was repeated, in this case, with RS01® device, because, although the emitted dose was not the highest, the respirable dose was close to 100% of the amount emitted. The powder resulted very stable at room temperature with values of ED and FPD (Table 7.5) similar ($p > 0.2$) to those obtained with the same inhaler just after the production. On the contrary, the storage at high temperature caused a statistically significant ($p < 0.02$) decrease of the emitted and respirable dose (Table 7.5) compared to the values obtained from the fresh powder.

Rifampicin was the drug reporting the major reduction in terms of respirable fraction (84% after 24h at 50°C and 90% after 1 month at not controlled temperature). This result suggest that the product would need a packaging (capsule and blister) capable to efficiently protect the powder content from the environmental humidity.

Table 7.5 Emitted Dose (ED), Emitted Fraction (EF), Fine Particle Dose (FPD) and Fine Particle Fraction (FPF) of powder aerosolized by RS01®, after storage for 1 month at not controlled temperature or 24 hours under accelerated stability condition (50°C); mean values and standard deviation in parenthesis (n=3).

RS01®

	Month 1/ not controlled				**24 h/50°C**			
	ED (mg)	**EF (%)**	**FPD (mg)**	**FPF (%)**	**ED (mg)**	**EF (%)**	**FPD (mg)**	**FPF (%)**
INH	0.50 (0.05)	61.99 (5.92)	0.46 (0.04)	92.34 (1.28)	0.42 (0.01)	58.75 (1.96)	0.37 (0.01)	87.95 (0.57)
RIF	1.03 (0.11)	58.56 (6.07)	0.93 (0.08)	90.81 (1.21)	0.95 (0.06)	55.81 (3.11)	0.80 (0.05)	83.62 (0.83)
VER	0.37 (0.03)	62.83 (5.35)	0.34 (0.03)	92.26 (0.85)	0.35 (0.02)	59.54 (4.24)	0.31 (0.03)	7.81 (1.33)

7.10 Biocompatibility of powders with THP-1/macrophages

The cellular viability after exposure to the four formulations are shown in Figure 7.12. The THP-1 viability after exposure to Powder 1 and 3 remained at 100% after 24 and 48 hours for powder concentrations ≤ 0.125 mg/mL (RIF=43.75 µg/mL; INH=22.5 µg/mL; VER=15 µg/mL; HA=43.75 µg/mL). This indicates that the amount of each component at the above concentrations was not toxic to the cells. However, formulation 1 and 3 were toxic for THP-1 cells at concentrations 0.5 mg/mL or above, with the cells losing 50% viability at both 24 and 48 hours. Moreover, there was no significant difference in cell viability after 24 and 48 hours for P1 and P3, except for the 0.5 mg/mL concentration for Powder 3 ($p > 0.05$); after 48 hours the viability was of 10% less than that registered after 24 hours.

The cell toxicity from powders 2 and 4 was lower, even though they comprised fluorescein sodium salt, when observed at 1 mg/mL after exposure for 24 hours. However, higher toxicity for both powders after 48h exposure was observed; Powders E and F (0.5 mg/mL) decreased cell viability to 54% and 75%, respectively ($p < 0.05$). It is possible to speculate that this differential toxicity for formulations 2 and 4 could be due to the absence of verapamil in these formulations compared to 1 and 3. Verapamil could be toxic for macrophages > 15 μg/mL, which corresponds to the concentration of verapamil in 0.125 mg/mL of powders 1 and 3.

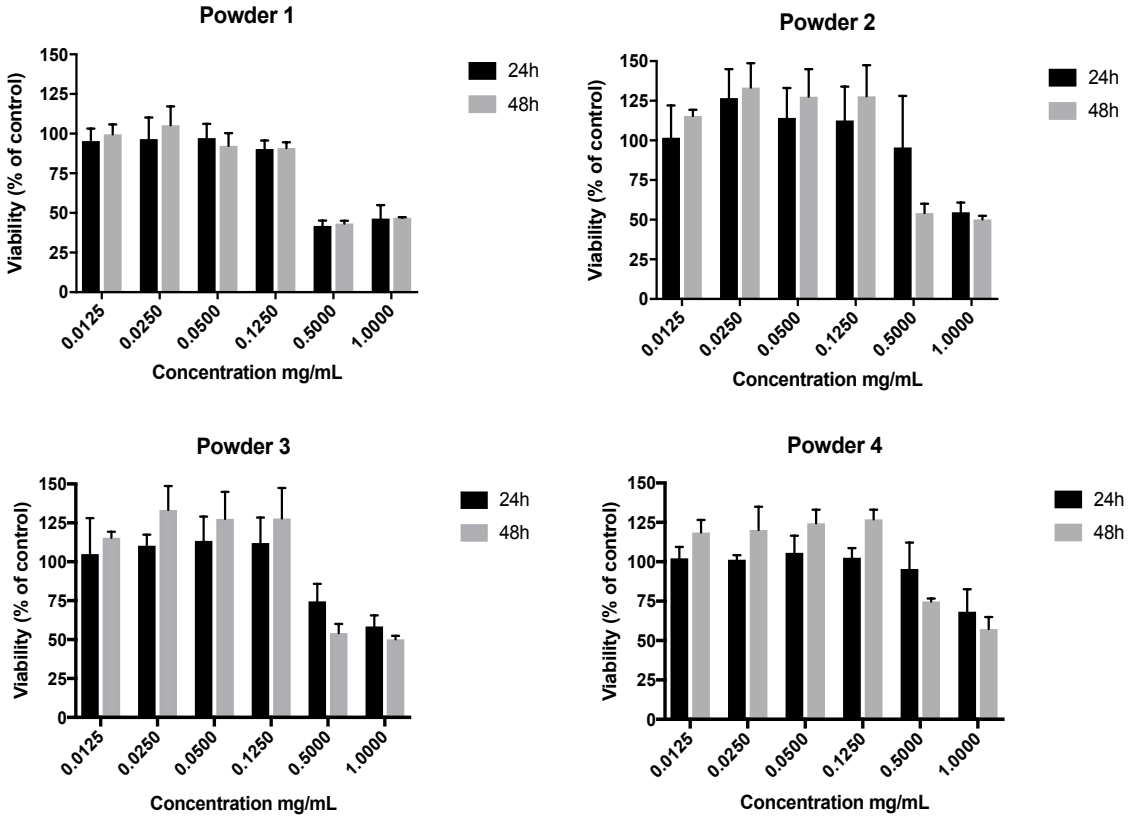

Figure 7.12. Biocompatibility of powders with THP-1 cells/macrophages using the XTT assay for cells viability. Six different concentrations for each formulation were tested at two time points, 24 and 48 hours. Mean values; the bars represent the standard deviation (n=3).

7.11 *In vitro* efficacy of spray dried powders 1 and 2 in inhibit *Mycobacterium smegmatis* growth

The experiments relevant to the *in vitro* efficacy of P1 and P2 against *Mycobacterium smegmatis* (*M. smeg.*), taken as model for nontuberculous mycobacteria (NTM), showed

superior activity for P1 in inhibiting *M. smeg.* growth; a concentration of 0.05 mg/mL was able to suppress bacterial growth after 48 hours of incubation in culture medium (Figure 7.13). In figure 7.13 values are reported as ratio between the amounts of bacteria grown for each powder concentration tested and the amount of bacteria in the control (not treated). The standard deviation of the replicate was, in some cases high because the tests were carried out from different bacteria cultures with probably different growth rate. This analysis was conducted in order to evaluate which was the smallest powder concentration able to inhibit *M. smeg.* growth for both the powders and whether they presented a variation in the responses. It is worth underlying that pure VER toxic concentration on *M. smeg*. was measured *in vitro* and corresponded to 0.12 mg/mL, namely the concentration of VER in 1 mg/mL of P1. In addition, this investigation was important to evaluate the ability of the antibiotics to kill *M. smeg.*, since previous studies have reported resistance for this NTM against the antibiotics used in the present study [116].

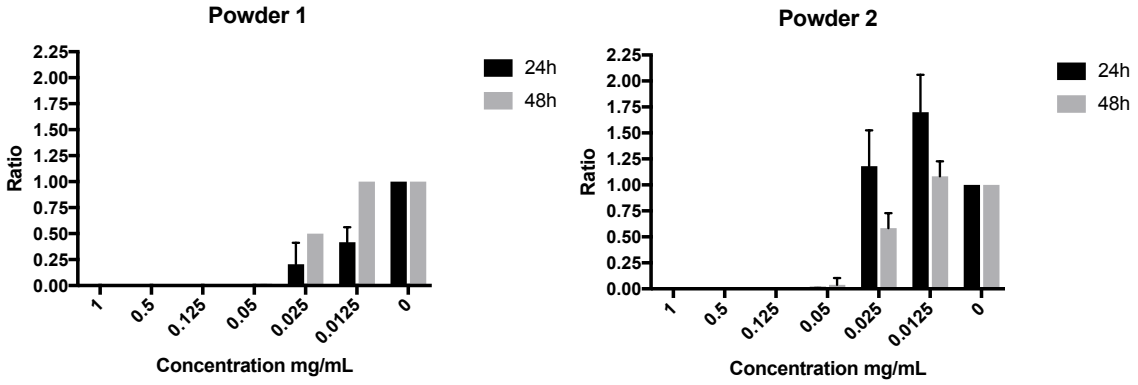

Figure 7.13. *In vitro* efficacy of dried powders in inhibit *M. smeg.* growth after 24 or 48 hours of incubation (mean value, bars represent standard deviation, n=3). Data are expressed as ratio between the mean value (CFU/mL) found for each powder concentration studied and the amounts of bacteria (CFU/mL) growing in the positive control without any formulation added (0 mg/mL).

7.12 *In vitro* infection of macrophages with *Mycobacterium smegmatis* and consecutive treatment with spray dried powders

Macrophages infected *in vitro* with *M. smeg.* for 3 hours were then, treated with powders 1 and 2 for three different times (24, 48 and 96 hours), in order to evaluate the growth inhibition of

intracellular bacteria. Figure 7.14 displays the results collected. Powders concentrations were chosen based on the results obtained with the *in vitro* efficacy test (Figure 7.13), considering only the biocompatible ones. After 24 hours of treatment (panel A), growth remained unvaried compared to the not treated control, likely because of the slow release of drugs from powders or of too low concentrations. Taking into account these data, for the 48 hours treatment the lowest concentration (0.025 mg/mL) was replaced with a higher (0.5 mg/mL), even though this one was cytotoxic for both the powders under testing. Indeed, this P1 concentration completely inhibited bacteria, whereas this was not the case for P2 (panel B). Furthermore, the growth reduction obtained with P1 at 0.125 mg/mL after 48 hours (ratio of bacteria growth/control < 10^2) and 96 hours (ratio of bacteria growth/control < 10^4) has to be highlighted; this was not observed for P2. After 96 hours (panel C), even the smallest concentration tested, 0.025 mg/mL, afforded a significant reduction (ratio of bacteria growth/control < 10). The bacteria growing decreased with increasing the treatment time; this may be connected to the slow release rate of drugs from the tested powders as shown in Figure 7.11.

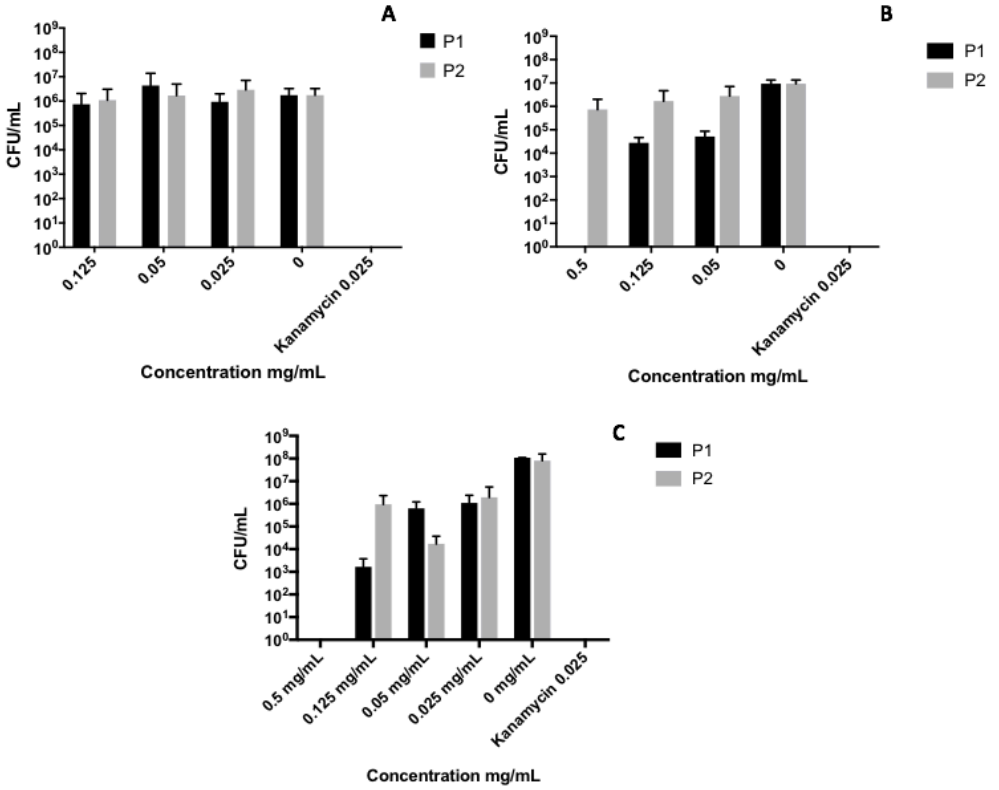

Figure 7.14. *In vitro* infection of macrophages with *M. smeg.* and consecutive treatment with the two powders (P1 and P2) for 24 (panel A), 48 (panel B) or 96 (panel C) hours. Data are expressed as the amounts of bacteria growing (CFU/mL) for each powder concentration studied (n=3 ± standard deviation). Kanamycin at MIC was used as a negative control.

Macrophages infected for 3 hours were also treated with powders 3 and 4 for 24 or 48 hours (Figure 7.15). For these formulations, compared to the previous ones, a difference between bacteria grown in the three concentrations tested and control was observed after 24 hours (ratio of bacteria growth/control < 10). These results may be explained with a faster release rate for the powders containing HMW HA, associated with the higher particle size distribution (Figure 7.4) as well as with the lack of a nano-structure in the microparticles. Indeed, as previously stated, the turbidimetric analysis carried out for both HA MWs, indicated that for HMW it was not possible to achieve a nanosuspension.

Moreover, P3, similarly to P1, at concentration 0.5 mg/mL which proved to be a toxic concentration also for macrophages, after 48 hours reported no bacteria growth. Colonies formed after P3 treatment were always less than after P4, treatment; however; the difference was less evident by decreasing the powder concentration.

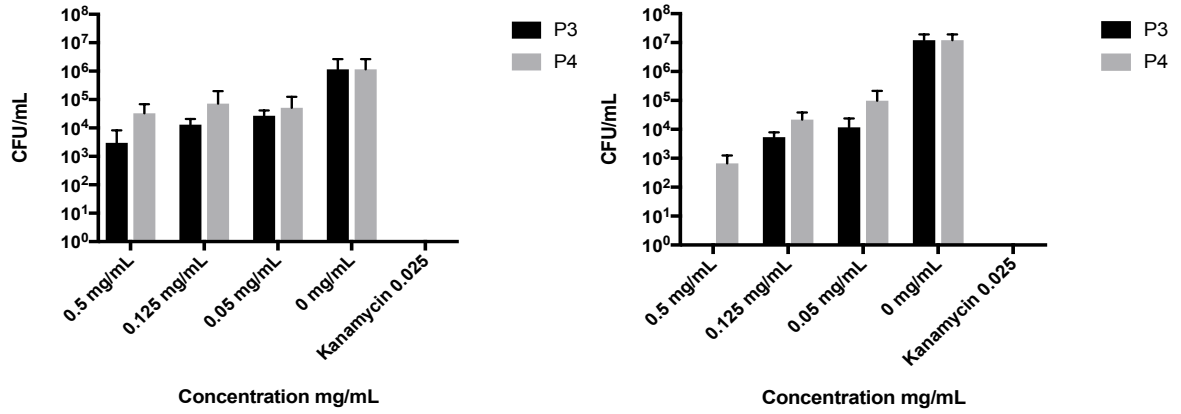

Figure 7.15. *In vitro* infection of macrophages with *M. smeg.* and consecutive treatment with the two powders (P3 and P4) for 24 (left-hand side) or 48 (right-hand side) hours. Data are expressed as the amount of bacteria growing (CFU/mL) for each powder concentration studied (n=3 ± standard deviation). Kanamycin at MIC was used as a negative control.

In order to see whether it was possible to induce antibiotics tolerance in *M. smeg.*, following what reported by Adams et al. for Mtb [117], a different type of infection experiments was performed. Macrophages were infected for 24 or 96 hours; thereafter powders 1 and 2 were added for 48 hours, which was the more appropriate and feasible interval time based on the previous results. Figures 7.16 displays the results collected along with those obtained from the infection time 3 hours. Statistical analysis found most of the results collected for each concentration significant. In details, P1 showed a slightly higher efficacy to inhibit bacteria growth, especially for 0.5 mg/mL concentration: with 3 hours of infection, growth was completely inhibited, while for the other two times points difference between P1 and P2 was not so highlighted, likely due to the too high colonies number formed during longer infection times; this was clear at 96 hours, where also in the negative control afforded bacteria growth. However, for smaller powder concentration (0.125 and 0.05 mg/mL) P1 was 10 times more effective in inhibiting *M. smeg.* colony formation compared to P2.

These data demonstrate a better bactericidal activity of the formulation comprising verapamil for longer infection times, even though it is not possible to certainly affirm that antibiotic tolerant *M. smeg.* strain, presenting more efflux pumps, was induced (a real time PCR may be needed), or perhaps that only the total amount of bacteria was increased.

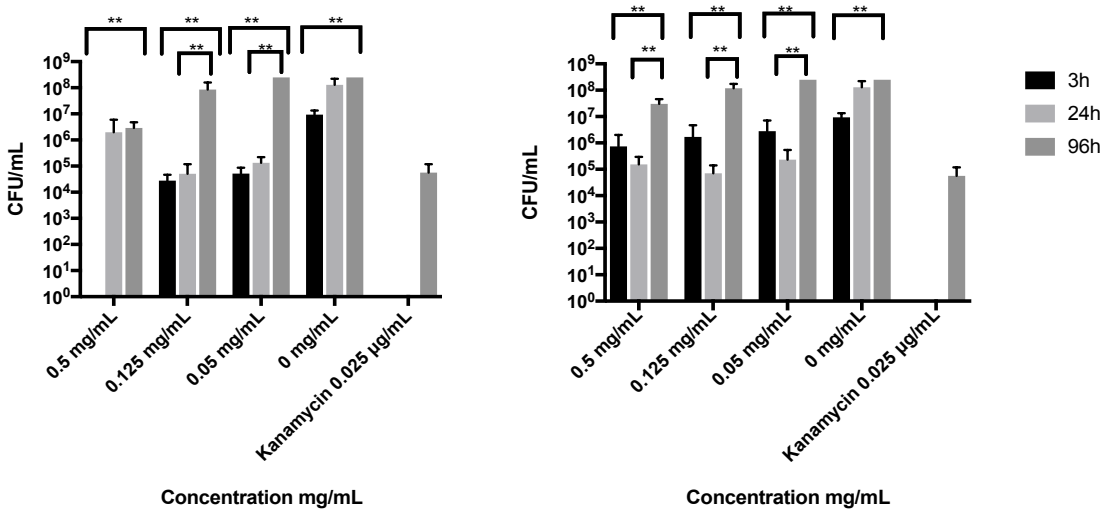

Figure 7.16. *In vitro* infection of macrophages for 3, 24 or 96 hours with *M. smeg.* and consecutive treatment with powder 1 (on the top) and powder 2 (on the bottom) for 48 hours. Data are expressed as the amounts of bacteria growing (CFU/mL) for each powder concentration studied (± standard deviation) (n=3). Kanamycin at MIC was used as a negative control.
** $p < 0.05$.

7.13 Confocal microscope imaging

Powders 2 and 4 containing fluorescein sodium salt were employed for confocal microscope imaging, in order to evaluate the AMs uptake with the different MW HA. Figure 7.17 illustrates the images obtained for the two powders, after staining macrophages nucleus with a dye. Panels C display the different uptake of the two powders by macrophages: for P4 the amount of fluorescent powder remained in the well after washes with PBS (shown also in panels A), was less and not clearly inside AMs. Whereas for P2 higher presence of green fluorescence, determined by fluorescein sodium salt, was present closer to cell nucleus. Moreover, Z-stack images acquisition was performed to evaluate where fluorescent particles were located inside the macrophages, at which level of Z axis. Figure 7.17 (panels C) reports the image at the central point of Z axis obtained from Z-stack analysis. This analysis highlighted that fluorescent particles, for both powders, where located at the center of the cells, at the same level of nucleus, the point on Z axis where they are more clearly visible. Therefore, P2, containing LMW HA formulated in a λ 480 nm system, was more engulfed by AMs compared to the particles with same composition by prepared with HMW HA.

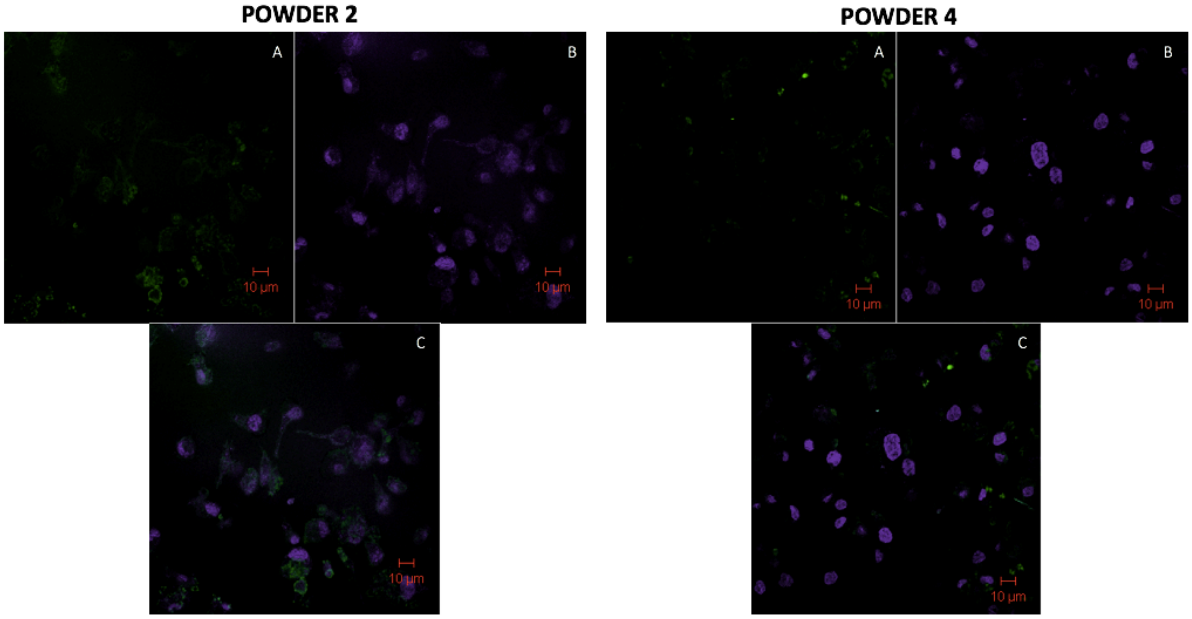

Figure 7.17 Confocal microscope images of macrophages treated with powder 2 and 4. For each sequence of pictures on the top left-hand side treated cells without nucleus dye, on the top right-hand side cells not treated with nucleus dye and on bottom cells treated with nuclear stain.

8. CONCLUSIONS

The first part of this project was focused on the develop of a platform for pulmonary administration of a vaccine. In this respect, a dry powder for inhalation was designed, produced and characterized. Spray drying was found as a suitable method to produce highly respirable powders for inhalation comprising an antigen which kept its structure and activity, by employing molecular deposition of an amphiphilic molecule.

This process is suitable for protein thermally stable and susceptible to degradation in organic solvents such as ethanol.

Mannitol proved to be the best balking agent to produce the DPI vaccine.

The powder respirable fraction increases with the antigen concentration and decreases with the buffer concentration in the spray drying feed solution. KP buffer proved to be more effective than Tris-buffered saline to get more respirable powders.

This work afforded an inventive step consisting in the discovery that the coating lubricant can be replaced with an adjuvant amphiphilic in nature, that permits to obtain powers with technological properties (flow, de-aggregation, respirability) similar to those obtained with sodium stearate, but possessing the capability to boost the immune response.

Finally, *in vivo* experiments evidenced the preferential deposition of the powder in the lungs, when administered intratracheally, and its efficacy in the determining an immune response comparable to the injected vaccine.

These last data emphasize the rationale beside the use of dry powder vaccines as a great alternative to available formulations.

The second part of the project was focused on the development and characterization of a new platform for lung delivery of antibiotics aiming at efficiently treating mycobacterial infections and tackling the multidrug resistance phenomenon.

In the case of TB, the efficient administration of antibiotics to the lung implies the capability to reach the alveolar region with particles of suitable aerodynamic diameter as well as to deliver the drugs into the AMs where the Mtb resides. These issues were addressed by exploiting the peculiar characteristic of HA sodium salt in aqueous solution to produce, upon treatment with an antisolvent such as ethanol, nanoparticles with size suitable for AMs uptake. An HA low molecular weight to further improve the AMs recognition and engulfment was selected. The drying by nebulization of the nanosuspension affords a powder constituted of microparticles with a mean volume diameter of 1 μm, ideal for a deep lung deposition. These microparticles are constituted of agglomerates of nanoparticles, that restore their original nanosize upon contact with an aqueous medium and release their drug content in a sustained manner.

To further improve the drug efficacy, the particles contain also an efflux inhibitor to maintain the suitable concentration of the drug into both the macrophages and Mtb.

The powder shows an *in vitro* bactericidal activity inhibiting *Mycobacterium smegmatis* growth, even against intracellular bacteria at sub-MIC concentration of the antibiotics encapsulated in the microparticles.

Finally, it is worth underlying that, besides the mycobacteria *per se,* the formulation developed targets AMs and includes an efflux pump inhibitor to further increase the concentration of the antibiotics inside the mycobacteria. For these reasons, the approach is expected to be effective regardless the extent of bacterial resistance and the mycobacterium species.

In conclusion, the system developed, capable to target and be uptake by alveolar macrophages, cells of the immune system, may be a promising platform for pulmonary delivery of a novel and more effective TB vaccine.

Acknowledgments

First of all, I would like to thank Prof. Ruggero Bettini (Food and Drug Department, University of Parma) to have guided me during every single step of this project and Prof. Francesca Buttini (Food and Drug Department, University of Parma), who always collaborated with prompt and important suggestions. Thank Prof. Fabio Sonvico (Food and Drug Department, University of Parma) to have been always ready to listen and give essential advice.

I would like to acknowledge particularly Dr. Fabio Stellari (Chiesi Farmaceutici Spa) to have carried out the *in vivo* imaging and immunization experiments; Prof. Simone Ottonello and, especially, Dr. Gloria Spagnoli (Department of Chemistry, Life Sciences and Environmental Sustainability, University of Parma) to have provided the antigens and to have carried out all the biochemicals characterization as well as the *in vivo* immunization experiments.

A very special thank goes also to Prof. Pavan Muttil (College of Pharmacy, Department of Pharmaceutical Sciences, University of New Mexico, NM, USA) to have received me and have permitted to conduct *in vitro* experiments on infected macrophages.

Finally, it is really worth to remember the undergraduate students who contributed to this work: Eride Quarta, Filippo Affaticati, Marta Pasquale.

9. REFERENCES

[1] N. Carlone, Microbiologia Farmaceutica, 2009.

[2] T.G. Parslow, D.P. Stites, A.I. Terr, J.B. Imboden, Medical Immunology, 2001.

[3] https://edition.cnn.com/2017/06/06/health/vaccine-uptake-incentives/index.html, September 29th,2018.

[4] http://www.who.int/news-room/fact-sheets/detail/measles, September 14th, 2018.

[5] https://www.who.int/immunization/diseases/hpv/en/, September 14th, 2018.

[6] A.N. Glazer, H. Nikaido, Microbial Biotechnology: Fundamentals of Applied Microbiology, 2007.

[7] M.G. Carstens, Opportunities and challenges in vaccine delivery, Eur. J. of Pharm. Sci. 36 (2009) 605–608.

[8] T. Sou, E.N. Meeusen, M. de Veer, D.A.V. Morton, L.M. Kaminskas, M.P. McIntosh, New developments in dry powder pulmonary vaccine delivery, Trends Biotechnol. 29 (2011) 191–198.

[9] I. Saleem, K. Petkar, S. Somavarapu, Rationale for Pulmonary Vaccine Delivery: Formulation and Device Considerations, 2017.

[10] W.F. Tonnis, G.F. Kersten, H.W. Frijlink, W.L.J. Hinrichs, A.H. de Boer, J.-P. Amorij, Pulmonary Vaccine Delivery: A Realistic Approach? J. Aerosol Med. Pulm. Drug. Deliv. 25 (2012) 249–260.

[11] W.H. Lin, D.E. Griffin, P.A. Rota, M. Papania, S.P. Cape, D. Bennett, B. Quinn, R.E. Sievers, C. Shermer, K. Powell, R.J. Adams, S. Godin, S. Winston, Successful respiratory immunization with dry powder live-attenuated measles virus vaccine in rhesus macaques, Pnas. 108 (2011) 2987–2992.

[12] N.K. Kunda, I.M. Alfagih, I.Y. Saleem, G.A. Hutcheon, Polymer-based delivery systems for the pulmonary delivery of biopharmaceuticals, Pulmonary Drug Delivery. (2015) 301–320.

[13] J.P. Amorij, J. Meulenaar, W.L.J. Hinrichs, T. Stegmann, A. Huckriede, F. Coenen, H.W. Frijlink, Rational design of an influenza subunit vaccine powder with sugar glass technology: Preventing conformational changes of haemagglutinin during freezing and freeze-drying, Vaccine. 25 (2007) 6447–6457.

[14] D. McAdams, D. Chen, D. Kristensen, Spray drying and vaccine stabilization, Expert Rev. Vaccines. 11 (2014) 1211–1219

[15] H.P. Patil, S. Murugappan, J. de Vries-Idema, T. Meijerhof, A. de Haan, H.W. Frijlink, J. Wilschut, W.L.J. Hinrichs, A. Huckriede, Comparison of adjuvants for a spray freeze-dried whole inactivated virus influenza vaccine for pulmonary administration, Eur. J. Pharm. Biopharm. 93 (2015) 231–241.

[16] J. Huang, R.J. Garmise, T.M. Crowder, K. Mar, C.R. Hwang, A.J. Hickey, J.A. Mikszta, V.J. Sullivan, A novel dry powder influenza vaccine and intranasal delivery technology: induction of systemic and mucosal immune responses in rats, Vaccine. 23 (2004) 794–801.

[17] R.J. Garmise, H.F. Staats, A.J. Hickey, Novel dry powder preparations of whole inactivated influenza virus for nasal vaccination, AAPS Pharm. Sci.Tech. 8 (2007) 2–10.

[18] P. Muttil, C. Prego, L. Garcia Contreras, B. Pulliam, J.K. Fallon, C. Wang, A.J. Hickey, D. Edwards, Immunization of guinea pigs with novel hepatitis B antigen as nanoparticle aggregate powders administered by the pulmonary route, AAPS J. 12 (2010) 330–337.

[19] L. Garcia Contreras, Y.-L. Wong, P. Muttil, D. Padilla, J. Sadoff, J. DeRousse, W.A. Germishuizen, S. Goonesekera, K. Elbert, B.R. Bloom, R. Miller, P.B. Fourie, A.J. Hickey, D. Edwards, Immunization by a bacterial aerosol, Proc. Natl. Acad. Sci. U.S.A. 105 (2008) 4656–4660.

[20] N.K. Kunda, D. Wafula, M. Tram, T.H. Wu, P. Muttil, A stable live bacterial vaccine, Eur. J. Pharm. Biopharm. 103 (2016) 109–117.

[21] AACR Cancer Progress Report, 2017.

[22] D. Nardellihaefliger, F. Lurati, D. Wirthner, F. Spertini, J. Schiller, D. Lowy, F. Ponci, P. De Grandi, Immune responses induced by lower airway mucosal immunisation with a human papillomavirus type 16 virus-like particle vaccine, Vaccine. 23 (2005) 3634–3641.

[23] H. Seitz, L. Ribeiro-Müller, E. Canali, A. Bolchi, M. Tommasino, S. Ottonello, M. Müller, Robust in vitro and in vivo neutralization against multiple high-risk hpv types induced by a thermostable thioredoxin-l2 vaccine, Cancer Prev. Res. (Phila). 8 (2015) 932–941.

[24] E. Canali, A. Bolchi, G. Spagnoli, H. Seitz, I. Rubio, T.A. Pertinhez, M. Müller, S. Ottonello, A high-performance thioredoxin-based scaffold for peptide immunogen construction: proof-of-concept testing with a human papillomavirus epitope, Sci. Rep. 4 (2014) 4729.

[25] E. Tumban, P. Muttil, C.A.A. Escobar, J. Peabody, D. Wafula, D.S. Peabody, B. Chackerian, Preclinical refinements of a broadly protective VLP-based HPV vaccine targeting the minor capsid protein, L2, Vaccine. 33 (2015) 3346–3353.

[26] S. Saboo, E. Tumban, J. Peabody, D. Wafula, D.S. Peabody, B. Chackerian, P. Muttil, optimized formulation of a thermostable spray-dried virus-like particle vaccine against human papillomavirus, Molecular Pharmaceutics. 13 (2016) 1646–1655.

[27] J. Peabody, P. Muttil, B. Chackerian, E. Tumban, Characterization of a spray-dried candidate HPV L2-VLP vaccine stored for multiple years at room temperature, Papillomavirus Research. 3 (2017) 116–120.

[28] Global Tuberculosis Report, 2017.

[29] http://www.who.int/vaccine_safety/committee/topics/bcg/June_2017/en/, September 30th, 2018.

[30] Y.L. Wong, S. Sampson, W.A. Germishuizen, S. Goonesekera, G. Caponetti, J. Sadoff, B.R. Bloom, D. Edwards, Drying a tuberculosis vaccine without freezing, Proc. Natl. Acad. Sci. U.S.A. 104 (2007) 2591–2595.

[31] A.C. Vasconcelos-Junior, J.A. de Araújo-Filho, E.B. de Silva, E.M. de Sousa, A. Kipnis, A.P. Junqueira-Kipnis, Limitations of the BCG vaccine and new prophylaxis strategies against human tuberculosis, Einstein. 7 (2009) 383–389.

[32] K.C. Chang, C.C. Leung, BCG Immunization: Efficacy, Limitations, and Future Needs, in: Handbook of Global Tuberculosis Control, 4th ed., (2017) 343–357.

[33] I. Abubakar, L. Pimpin, C. Ariti, R. Beynon, P. Mangtani, J.A.C. Sterne, P.E.M. Fine, P.G. Smith, M. Lipman, D. Elliman, J.M. Watson, L.N. Drumright, P.F. Whiting, E. Vynncycky, L.C. Rodrigues, Systematic review and meta-analysis of the current evidence on the duration of protection by bacillus Calmette-Guérin vaccination against tuberculosis, Health Technol. Assess. 17 (2013) 1–372.

[34] E.D. Chan, X. Bai, M. Kartalija, I.M. Orme, D.J. Ordway, Host immune response to rapidly growing mycobacteria, an emerging cause of chronic lung disease, Am. J. Respir. Cell Mol. Biol. 43 (2010) 387–393.

[35] P. Muttil, C. Wang, A.J. Hickey, Inhaled drug delivery for tuberculosis therapy, Pharm. Res. 26 (2009) 2401–2416.

[36] K. Makino, T. Nakajima, M. Shikamura, F. Ito, S. Ando, C. Kochi, et al., Efficient intracellular delivery of rifampicin to alveolar macrophages using rifampicin-loaded

PLGA microspheres: effects of molecular weight and composition of PLGA on release of rifampicin, Colloids Surf. B. 36 (2004) 35–42.

[37] S.C. Das, J. Luu, D. Morton, P.J. Stewart, A novel approach to develop high dose drug alone inhaler, Drug Delivery to the Lung Conference, Edinburgh International Conference Center, UK. (2013) 1–4.

[38] J.G.Y. Chan, H.-K. Chan, C.A. Prestidge, J.A. Denman, P.M. Young, D. Traini, A novel dry powder inhalable formulation incorporating three first-line anti-tubercular antibiotics, Eur. J. Pharm. Biopharm. 83 (2013) 285–292.

[39] C. Parlati, P. Colombo, F. Buttini, P.M. Young, H. Adi, A.J. Ammit, D. Traini, Pulmonary spray dried powders of tobramycin containing sodium stearate to improve aerosolization efficiency, Pharm. Res. 26 (2009) 1084–1092.

[40] I.M. El-Sherbiny, N.M. El-Baz, M.H. Yacoub, Inhaled nano- and microparticles for drug delivery, Glob Cardiol Sci Pract. 2015 (2015) 2.

[41] S. Vyas, S. Quraishi, S. Gupta, K. Jaganathan, Aerosolized liposome-based delivery of amphotericin B to alveolar macrophages, Int. J. Pharm. 296 (2005) 12–25.

[42] A.J. Hickey, A. Misra, P.B. Fourie, Dry powder antibiotic aerosol product development: inhaled therapy for tuberculosis, J. Pharm. Sci. 102 (2013) 3900–3907.

[43] K. Hirota, T. Hasegawa, H. Hinata, F. Ito, H. Inagawa, C. Kochi, G. Soma, K. Makino, H. Terada, Optimum conditions for efficient phagocytosis of rifampicin-loaded PLGA microspheres by alveolar macrophages, J. Control. Release. 119 (2007) 69–76.

[44] E. Maretti, T. Rossi, M. Bondi, M.A. Croce, M. Hanuskova, E. Leo, F. Sachetti, V. Iannuccelli, Inhaled solid lipid microparticles to target alveolar macrophages for tuberculosis, Int. J. Pharm. 462 (2014) 74-82.

[45] E. Maretti, L. Costantino, C. Rustichelli, E. Leo, M.A. Croce, F. Buttini, E. Truzzi, V. Iannuccelli, Surface engineering of solid lipid nanoparticle assemblies by methyl α-d-mannopyranoside for the active targeting to macrophages in anti-tuberculosis inhalation therapy, Int. J. Pharm. 528 (2017) 440-451.

[46] A. Bhardwaj, L. Kumar, R.K. Narang, R.S.R. Murthy, Development and characterization of ligand- appended liposomes for multiple drug therapy for pulmonary tuberculosis, Artif. Cells Nanomed. Biotechnol. 41 (2013) 52-59.

[47] S. Rodrigues, A.D. Alves, J.S. Cavaco, J.F. Pontes, F. Guerreiro, A.M. da Costa, F. Buttini, A. Grenha, Dual antibiotherapy of tuberculosis mediated by inhalable locust bean gum microparticles, 529 (2017) 433-441.

[48] S. Ganguly, V. Moolchandani, J.A. Roche, P.S. Shapiro, S. Somaraju, N.D. Eddington, R.N. Dalby, Phospholipid-induced in vivo particle migration to enhance pulmonary deposition, J. Aerosol Med. Pulm. Drug. Deliv. 21 (2008) 343–350.

[49] T. Ellis, M. Chiappi, A. García-Trenco, M. Al-Ejji, S. Sarkar, T.K. Georgiou, M.S.P. Shaffer, T.D. Tetley, S. Schwander, M.P. Ryan, A.E. Porter, Multimetallic microparticles increase the potency of rifampicin against intracellular mycobacterium tuberculosis, ACS Nano. 12 (2018) 5228–5240.

[50] L. Cunha, S. Rodrigues, A. Rosa da Costa, M. Faleiro, F. Buttini, A. Grenha, Inhalable fucoidan microparticles combining two antitubercular drugs with potential application in pulmonary tuberculosis therapy, Polymers. 10 (2018) 636.

[51] J. Lesley, V.C. Hascall, M. Tammi, R. Hyman, Hyaluronan binding by cell surface CD44, J. Biol. Chem. 275 (2000) 26967–26975.

[52] S. Ghosh, S.A. Hoselton, G.P. Dorsam, J.M. Schuh, Hyaluronan fragments as mediators of inflammation in allergic pulmonary disease, Immunobiology. 220 (2015) 575–588.

[53] Y. Gao, M.K. Sarfraz, S.-D. Clas, W. Roa, R. Löbenberg, Hyaluronic Acid-Tocopherol Succinate-Based Self-Assembling Micelles for Targeted Delivery of Rifampicin to Alveolar Macrophages, J Biomed Nanotechnol. 11 (2015) 1312–1329.

[54] W. Rojanarat, N. Changsan, E. Thawithong, S. Pinsuwan, H. Chan, T. Srichana, Isoniazid proliposome powders for inhalation- preparation, characterization an cell culture studies, Int. J. Mol. Sci. 12 (2011) 4414-4431.

[55] A. Patil-Gadhe, V. Pokharkar, Single step spray drying method to develop proliposomes for inhalation: a systematic study based on quality by design approach, Pulm. Pharmacol. Ther. 27 (2014) 197–207.

[56] S.N.M. Hanif, L. Garcia Contreras, Pharmaceutical aerosols for the treatment and prevention of tuberculosis, Front. Cell. Infect. Microbiol. 2 (2012) 118.

[57] G.E. Louw, R.M. Warren, N.C. Gey van Pittius, C.R.E. McEvoy, P.D. Van Helden, T.C. Victor, A balancing act: efflux/influx in mycobacterial drug resistance, Antimicrob. Agents Chemother. 53 (2009) 3181–3189

[58] T. Parumasivam, J.G.Y. Chan, A. Pang, D.H. Quan, J.A. Triccas, W.J. Britton, H.K. Chan, In vitro evaluation of novel inhalable dry powders consisting of thioridazine and rifapentine for rapid tuberculosis treatment, Eur. J. Pharm. Biopharm. 107 (2016) 205–214.

[59] D. Machado, I. Couto, J. Perdigão, L. Rodrigues, I. Portugal, P. Baptista, B. Veigas, L. Amaral, M. Viveiros, Contribution of efflux to the emergence of isoniazid and multidrug resistance in Mycobacterium tuberculosis, PLoS ONE. 7 (2012) e34538.

[60] G. Spagnoli, S. Pouyanfard, D. Cavazzini, E. Canali, S. Maggi, M. Tommasino, A. Bolchi, M. Müller, S. Ottonello, Broadly neutralizing antiviral responses induced by a single-molecule HPV vaccine based on thermostable thioredoxin-L2 multiepitope nanoparticles, Sci. Rep. 7 (2017) 18000.

[61] R. Shotton, K. Ridgway, Physical Pharmaceutics, Oxford, Claredon Press.

[62] S.W. Harder, D.A. Zuck, J.A. Wood, Characterization of tablet surfaces by their critical surface-tension values, J. Pharm. Sci. 59 (1970) 1787–1792.

[63] A.B.D. Cassie, S. Baxter, Wettability of porous surfaces, Transactions of the Faraday Society. 40 (1944) 546–551.

[64] F. Ruscitti, F. Ravanetti, G. Donofrio, Y. Ridwan, P. van Heijningen, J. Essers, G. Villetti, A. Cacchioli, W. Vos, F.F. Stellari, A multimodal imaging approach based on micro-ct and fluorescence molecular tomography for longitudinal assessment of bleomycin-induced lung fibrosis in mice, J Vis Exp. (2018).

[65] G. Bergamini, F. Stellari, A. Sandri, M. M Lleo, G. Donofrio, F. Ruscitti, F. Boschi, A. Sbarbati, G. Villetti, P. Melotti, C. Sorio, An IL-8 transiently transgenized mouse model for the in vivo long-term monitoring of inflammatory responses, J. Vis. Exp. (2017) e55499–e55499.

[66] G. Lee, Spray-drying of proteins, Pharm. Biotechnol. 13 (2002) 135–158.

[67] M. Ameri, Y.F. Maa, Spray drying of biopharmaceuticals: stability and process considerations, drying technology. 24 (2007) 763–768.

[68] R.L. Strack, B. Hein, D. Bhattacharyya, S.W. Hell, R.J. Keenan, B.S. Glick, A rapidly maturing far-red derivative of DsRed-Express2 for whole-cell labeling, Biochemistry. 48 (2009) 8279–8281.

[69] https://pubchem.ncbi.nlm.nih.gov/compound/sodium_stearate#section=Computed-Properties, October 4th, 2018.

[70] K. Kramek-Romanowska, M. Odziomek, T.R. Sosnowski, L. Gradoń, Effects of process variables on the properties of spray-dried mannitol and mannitol/disodium cromoglycate powders suitable for drug delivery by inhalation, Ind. Eng. Chem. Res. 50 (2011) 13922–13931.

[71] I. Rubio, H. Seitz, E. Canali, P. Sehr, A. Bolchi, M. Tommasino, S. Ottonello, M. Müller, The N-terminal region of the human papillomavirus L2 protein contains overlapping binding sites for neutralizing, cross-neutralizing and non-neutralizing antibodies, Virology. 409 (2011) 348–359.

[72] S. Jagu, K. Kwak, B. Karanam, W.K. Huh, V. Damotharan, S.V. Chivukula, R.B.S. Roden, Optimization of multimeric human papillomavirus L2 vaccines, PLoS ONE. 8 (2013) e55538.

[73] W.H. Wu, E. Gersch, K. Kwak, S. Jagu, B. Karanam, W.K. Huh, R.L. Garcea, R.B.S. Roden, Capsomer vaccines protect mice from vaginal challenge with human papillomavirus, PLoS ONE. 6 (2011) e27141.

[74] C. Schellenbacher, K. Kwak, D. Fink, S. Shafti-Keramat, B. Huber, C. Jindra, H. Faust, J. Dillner, R.B.S. Roden, R. Kirnbauer, Efficacy of RG1-VLP vaccination against infections with genital and cutaneous human papillomaviruses, J. Invest. Dermatol. 133 (2013) 2706–2713.

[75] M. McGrath, G.K. de Villiers, E. Shephard, I.I. Hitzeroth, E.P. Rybicki, Development of human papillomavirus chimaeric L1/L2 candidate vaccines, Arch. Virol. 158 (2013) 2079–2088.

[76] K. Nieto, M. Weghofer, P. Sehr, M. Ritter, S. Sedlmeier, B. Karanam, H. Seitz, M. Müller, M. Kellner, M. Hörer, U. Michaelis, R.S. Roden, L. Gissmann, J.A. Kleinschmidt, Development of AAVLP(HPV16/31L2) particles as broadly protective HPV vaccine candidate, PLoS ONE. 7 (2012) e39741.

[77] S.W. Yoon, T.Y. Lee, S.J. Kim, I.H. Lee, M.H. Sung, J.S. Park, H. Poo, Oral administration of HPV-16 L2 displayed on Lactobacillus casei induces systematic and mucosal cross-neutralizing effects in Balb/c mice, Vaccine. 30 (2012) 3286–3294.

[78] E. Tumban, J. Peabody, D.S. Peabody, B. Chackerian, A Pan-HPV Vaccine Based on Bacteriophage PP7 VLPs Displaying Broadly Cross-Neutralizing Epitopes from the HPV Minor Capsid Protein, L2, PLoS ONE. 6 (2011) e23310.

[79] A. Micsonai, F. Wien, L. Kernya, Y.-H. Lee, Y. Goto, M. Réfrégiers, J. Kardos, Accurate secondary structure prediction and fold recognition for circular dichroism spectroscopy, Proc. Natl. Acad. Sci. U.S.A. 112 (2015) E3095–E3103.

[80] A. Breda, N.F. Valadares, O.N. de Souza, Protein Structure, Modelling and Applications, Bioinformatics in Tropical Disease Research. (2016) 1–41.

[81] K. Talley, E. Alexov, On the pH-optimum of activity and stability of proteins, Proteins. 8 (2010).

[82] F. Buttini, A.G. Balducci, G. Colombo, F. Sonvico, S. Montanari, G. Pisi, A. Rossi, P. Colombo, R. Bettini, Dose administration maneuvers and patient care in tobramycin dry powder inhalation therapy, Int. J. Pharm. 548 (2018) 182–191.

[83] M. Quilaqueo, J.M. Aguilera, Crystallization of NaCl by fast evaporation of water in droplets of NaCl solutions, Food Res. Int. 84 (2016) 143–149.

[84] H.Y. Cho, B. Kim, J.Y. Chun, M.J. Choi, Effect of spray-drying process on physical properties of sodium chloride/maltodextrin complexes, Powder Technology. 277 (2015) 141–146.

[85] R. Vehring, Pharmaceutical particle engineering via spray drying, Pharm. Res. 25 (2008) 999–1022.

[86] K. Mosén, K. Bäckström, K. Thalberg, T. Schaefer, H.G. Kristensen, A. Axelsson, Particle formation and capture during spray drying of inhalable particles, Pharm. Dev. Technol. 9 (2004) 409–417.

[87] https://www.niaid.nih.gov/research/vaccine-adjuvants, October 20th, 2018.

[88] S. Lousada-Dietrich, P.S. Jogdand, S. Jepsen, V.V. Pinto, S.B. Ditlev, M. Christiansen, S.O. Larsen, C.B. Fox, V.S. Raman, R.F. Howard, T.S. Vedvick, G. Ireton, D. Carten, S.G. Reed, M. Theisen, A synthetic TLR4 agonist formulated in an emulsion enhances humoral and Type 1 cellular immune responses against GMZ2--a GLURP-MSP3 fusion protein malaria vaccine candidate, Vaccine. 29 (2011) 3284–3292.

[89] S. Fukuoka, K. Brandenburg, M. Müller, B. Lindner, M.H. Koch, U. Seydel, Physico-chemical analysis of lipid A fractions of lipopolysaccharide from Erwinia carotovora in relation to bioactivity, Biochim. Biophys. Acta. 1510 (2001) 185–197.

[90] P.M. Day, R.C. Kines, C.D. Thompson, S. Jagu, R.B. Roden, D.R. Lowy, J.T. Schiller, In Vivo Mechanisms of Vaccine-Induced Protection against HPV Infection, Cell Host & Microbe. 8 (2010) 260–270.

[91] D.M. Herrin, E.E. Coates, P.J. Costner, T.J. Kemp, M.C. Nason, K.K. Saharia, Y. Pan, U.N. Sarwar, L. Holman, G. Yamshchikov, R.A. Koup, Y.Y. Pang, R.A. Seder, J.T. Schiller, B.S. Graham, L.A. Pinto, J.E. Ledgerwood, Comparison of adaptive and innate immune responses induced by licensed vaccines for Human Papillomavirus, Hum. Vaccin. Immunother. 10 (2014) 3446–3454.

[92] E.T.S. Ben-Ahmeida, C.W. Potter, G. Gregoriadis, C. Adithan, R. Jennings, IgG subclass response and protection against challenge following immunisation of mice with various influenza A vaccines, J. Med. Microbiol. 40 (1994) 261–269.

[93] M.B. Chougule, B.K. Padhi, K.A. Jinturkar, A. Misra, Development of dry powder inhalers, Recent. Pat. Drug. Deliv. Formul. 1 (2007) 11-21.

[94] A.J. Hickey, H.M. Mansour, M.J. Telko, Z. Xu, H.D.C. Smyth, T. Mulder, R. Mclean, J. Langridge, D. Papadopoulos, Physical characterization of component particles included in dry powder inhalers. II. Dynamic characterization, J. Pharm. Sci. 95 (2007) 1302-1319.

[95] H.M. Berman, G.A. Jeffrey, R.D. Rosenstein, The crystal structures of the alpha and beta forms of D-mannitol, Acta. Crystallogr. B. 24 (1968) 442-449.

[96] C.A. Browne, Moisture absorptive powder of different sugars and carbo-hydrates under varying conditions of atmospheric humidity, J. Ind. Eng. Chem. 14 (1922) 712-713.

[97] M.M. Johnson, J.A. Odell, Nontuberculous mycobacterial pulmonary infections, J. Thorac. Dis. 6 (2014) 210–220.

[98] S. Das, I. Tucker, P. Stewart, Inhaled Dry Powder Formulations for Treating Tuberculosis, Curr. Drug Deliv. 12 (2015) 26–39.

[99] M. Geiser, Update on macrophage clearance of inhaled micro- and nanoparticles, J Aerosol Med Pulm Drug Deliv. 23 (2010) 207–217.

[100] K.N. Adams, J.D. Szumowski, L. Ramakrishnan, Verapamil, and its metabolite norverapamil, inhibit macrophage-induced, bacterial efflux pump-mediated tolerance to multiple anti-tubercular drugs, J. Infect. Dis. 210 (2014) 456–466.

[101] http://dspace-unipr.cineca.it/handle/1889/3118, October 29th, 2018.

[102] F. Martinelli, A.G. Balducci, A. Kumar, F. Sonvico, B. Forbes, R. Bettini, F. Buttini, Engineered sodium hyaluronate respirable dry powders for pulmonary drug delivery, Int. J. Pharm. 517 (2017) 286–295.

[103] K. Gupta, S. Singh, M.L. van Hoek, Short, synthetic cationic peptides have antibacterial activity against mycobacterium smegmatis by forming pores in membrane and synergizing with antibiotics, Antibiotics (Basel). 4 (2015) 358–378.

[104] T. Parumasivam, J.G.Y. Chan, A. Pang, D.H. Quan, J.A. Triccas, W.J. Britton, H.K. Chan, In vitro evaluation of inhalable verapamil-rifapentine particles for tuberculosis therapy, Mol. Pharm. 13 (2016) 979–989.

[105] G.G. Pereira, C.B. Detoni, A.G. Balducci, V. Rondelli, P. Colombo, S.S. Guterres, F. Sonvico, Hyaluronate nanoparticles included in polymer films for the prolonged release of vitamin E for the management of skin wounds, Eur. J. Pharm. Sci. 83 (2016) 203–211.

[106] W.H. Wei, X.-M. Dong, C.G. Liu, In vitro investigation of self-assembled nanoparticles based on hyaluronic acid-deoxycholic acid conjugates for controlled release doxorubicin: effect of degree of substitution of deoxycholic acid, Int. J. Mol. Sci. 16 (2015) 7195–7209.

[107] T. Rawal, R. Parmar, R.K. Tyagi, S. Butani, Rifampicin loaded chitosan nanoparticle dry powder presents an improved therapeutic approach for alveolar tuberculosis, Colloids Surf. B. 154 (2017) 321–330.

[108] Z. Ge, R. Ma, G. Xu, Z. Chen, D. Zhang, Q. Wang, L. Hei, W. Ma, Development and in vitro release of isoniazid and rifampicin-loaded bovine serum albumin nanoparticles, Med. Sci. Monit. 24 (2018) 473–478.

[109] H. Qin, C.M. Wang, Q.Q. Dong, L. Zhang, X. Zhang, Z.Y. Ma, Q.R. Han, Preparation and characterization of magnetic Fe_3O_4–chitosan nanoparticles loaded with isoniazid, J. Magn. Magn. Mater. 381 (2015) 120–126.

[110] Z. Nagheh, S. Irani, R. Mirfakhraie, R. Dinarvand, SN38-PEG-PLGA-verapamil nanoparticles inhibit proliferation and downregulate drug transporter ABCG2 gene expression in colorectal cancer cells, Progress in Biomaterials. 6 (2017) 137–145.

[111] J. Necas, L. Bartosikova, P. Brauner, J. Kolar, Hyaluronic acid (hyaluronan): a review, Veterinární Medicína. 53 (2008) 397–411.

[112] F. Martinelli, A.G. Balducci, A. Rossi, F. Sonvico, P. Colombo, F. Buttini, "Pierce and inhale" design in capsule based dry powder inhalers: Effect of capsule piercing and motion on aerodynamic performance of drugs, Int. J. Pharm. 487 (2015) 197–204.

[113] J.H. Park, N. Oh, Endocytosis and exocytosis of nanoparticles in mammalian cells, Int. J. Nanomed. 9 (2014) 51–63.

[114] O.S. Kluin, H.J. Busscher, D. Neut, H.C. van der Mei, Poly(trimethylene carbonate) as a carrier for rifampicin and vancomycin to target therapy-recalcitrant staphylococcal biofilms, J. Orthop. Res. 34 (2016) 1828–1837.

[115] M.I. Yoshida, E.C.L. Gomes, C.D.V. Soares, A.F. Cunha, M.A. Oliveira, Thermal analysis applied to verapamil hydrochloride characterization in pharmaceutical formulations, Molecules. 15 (2010) 2439–2452.

[116] R. Teng, T. Dick, Isoniazid resistance of exponentially growing Mycobacterium smegmatis biofilm culture, FEMS Microbiol. Lett. 227 (2003) 171–174.

[117] K.N. Adams, K. Takaki, L.E. Connolly, H. Wiedenhoft, K. Winglee, O. Humbert, P.H. Edelstein, C.L. Cosma, L. Ramakrishnan, Drug tolerance in replicating mycobacteria mediated by a macrophage-induced efflux mechanism, Cell. 145 (2011) 39–53.